The Dissertation Committee for Columbia Mishra Certifies that this is the approved version of the following dissertation:

Volume Averaged Phonon Boltzmann Transport Equation for Simulation of Heat Transport in Composites

Committee:

Li Shi, Supervisor

Jayathi Y. Murthy, Co-Supervisor

Ofodike A. Ezekoye

Roger T. Bonnecaze

Deji Akinwande

Yaguo Wang

Volume Averaged Phonon Boltzmann Transport Equation for Simulation of Heat Transport in Composites

by

Columbia Mishra, B.M.E.; M.S.

Dissertation

Presented to the Faculty of the Graduate School of

The University of Texas at Austin

in Partial Fulfillment

of the Requirements

for the Degree of

Doctor of Philosophy

The University of Texas at Austin

December 2016

Dedication

To my parents Jai Prakash and Minati

&

My brothers Challenger and Chandragupta

Acknowledgements

I sincerely thank my advisor, Dr. Jayathi Murthy, for her extraordinary guidance and support throughout my time in her research group. I am grateful that she took me on as her student and prepared me extensively for my dissertation research. I have learned many things from her over the years and for that I will remain forever grateful. She is without doubt the best mentor and guide anyone could have. I am thankful that I was presented this opportunity to learn from the best. I am also thankful to Dr. Murthy for being supportive in my endeavors outside research. Her thoughtful mentorship has been the reason I was able to pursue these interests.

I want to thank my Ph.D. committee members Dr. Li Shi, Dr. Roger Bonnecaze, Dr. Yaguo Wang, Dr. Ofodike Ezekoye, and Dr. Deji Akinwande for taking the time to review my work and give feedback that enriched this dissertation. I am especially thankful to Dr. Shi for taking on the role of my supervisor after Dr. Murthy's transition to UCLA earlier this year. I am very thankful to Dr. Bonnecaze for his valuable perspective on my work. Thanks to Dr. Akinwande for all the wonderful discussions. I cannot thank Dr. Ezekoye enough for his unwavering confidence, support, and encouragement since the early days of my graduate school.

I am very thankful to Dr. David Bogard for his incredible patience, words of wisdom, and advising throughout my time at UT Austin. I am thankful to Dr. Janet Ellzey for the countless hours she spent on making my transition between dissertation topics

smooth and later on mentoring me on my leadership roles on campus. I am thankful to Dr. Robert Moser for introducing me to my advisor.

I am thankful to Dr. Rodney Ruoff for giving me the opportunity to work on the cutting edge graphene technology and contributing to several successful grants including the Keck Foundation. I am grateful for his support and for everything I learned during my time in his research group. During my work on RF induction system for graphene growth in the Ruoff group, I found a great mentor and friend in Dr. Richard Piner. Richard is a brilliant experimentalist and I am fortunate to have learnt from him.

Thanks to Dr. Michael Webber for his mentorship and giving me the opportunity to be a teaching assistant for his signature entrepreneurship course. Thanks to Dr. Thomas Kiehne for being a wonderful professor to work with during my time as a teaching assistant for the heat transfer laboratory. I am thankful to the Department of Mechanical Engineering, the past and present administrative leadership, who helped me through appointments and all the paperwork over the years. I am thankful to Sarah Parker, Jenny Kondo, Prabhu Khalsa, David Justh, Dustin, Lori, Cindy, Diana, Danielle, and Debbie Matthews for all the support. I am thankful to the staff members at Texas Advanced Computing Center for their availability and technical support.

My time at UT was enriched with the opportunity to be an active member of the UT Austin campus community. I am grateful to the Graduate Engineering Council and the Graduate Student Assembly for giving me the opportunity to participate in the graduate student community and building friendships. I am very thankful to Dr. Gerald Speitel for his guidance as the Graduate Engineering Council faculty advisor. I enjoyed

our time working together on various GEC initiatives including the Graduate and Industry Networking (GAIN) event. I am thankful to Michael Powell for his nurturing mentorship and counseling over the years, initially for the GEC programs and later on as a part of my support system in Austin. There are not enough words to express my gratitude. I am thankful to the UT administration for allowing me the wonderful opportunity to work with and learn: Dr. Gage Paine, Dr. Soncia Reagins-Lilly, Dr. Gregory Fenves, Dr. Judith Langlois, and Dr. William Powers. I am especially thankful to Dr. Paine for her mentorship during GSA and later on for actively taking an interest in my progress through the graduate program.

My time at UT Austin would not have been the same without my amazing labmates and friends. I have found lifelong friendships in my labmates: Prabhakar, Ajay, James, Dan, Yu, Brad, Anil, and Shankhadeep for whom I am grateful. I am especially thankful to Prabhakar for being there whether it was to discuss research, to run a campaign for elections, or simply explore Austin. I am thankful to Annie Weathers and Katie Carpenter for our Gorgeous Grads workout group, all those dinners we had and the unconditional friendship. Thanks to Randall Williams for being there for me through every major academic and non-academic hurdle, most importantly coaching me as a Texan and finally inducting me as an honorary Texan. I am grateful for my friends Srinivas Bajjuri, Abhishek Saha, Shubobrata Palit, Souma, Sheshu, David Ottesen, Jorge Vazquez, Matt Charlton, Swagata Das, Ravi Singh, Rehan Rafui, Matt Kincaid, Paras, and several others who made me feel at home while being so far away from home. Thanks for being there for me always. All my time and efforts would not have meant

much without the fun-filled, loving, thought-provoking, challenging, motivating, and rock-solid partnership with Deepjyoti Deka. Thank you Deep for standing by me for all these years.

Finally, I am thankful for the support of my parents and my brothers throughout this journey. It would not have been possible without their constant encouragement and belief in me. I am especially thankful to Challenger for visiting me whenever possible and for those Skype calls discussing research whenever I came across challenges. Thanks to my little nephew Arya for bringing such joy through our Skype visits.

Volume Averaged Phonon Boltzmann Transport Equation for Simulation of Heat Transport in Composites

Columbia Mishra, Ph.D.

The University of Texas at Austin, 2016

Supervisors: Li Shi, Jayathi Murthy

Heat transfer in nano-composites is of great importance in a variety of applications, including in thermoelectric materials, thermal interface and thermal management materials, and in metamaterials for emerging microelectronics. In the past, two distinct approaches have been taken to predict the effective thermal conductivity of composites. The first of these is the class of effective medium theories, which employs Fourier conduction as the basis for thermal conductivity prediction. These correlate composite behavior directly to volume fraction, and do not account for inclusion structure, acoustic mismatch, and sub-continuum effects important in nanocomposites. More recently, direct numerical simulations of nanoscale phonon transport in composites have been developed. Here the geometry of the inclusion or the particulate phase is represented in an idealized way, and the phonon Boltzmann Transport Equation (BTE) solved directly on this idealized geometry. This is computationally intensive, particularly if realistic particle composites are to be simulated.

Here, we develop, for the first time, a volume-averaged formulation for the phonon BTE for nanocomposites, accounting for the complex particle-matrix geometry. The formulation is developed for a nanoporous domain as a first step and then a nanocomposite domain is considered. The phonon BTE is written on a representative elemental volume (REV) and integrated formally over the REV using the laws of volume averaging. Extra integral terms resulting from the averaging procedure are approximated to yield extra scattering terms due to the presence of inclusions or holes in the REV. The result is a phonon BTE written in terms of the volume-averaged phonon energy density, and involving volumetric scattering terms resulting from both bulk scattering and scattering at the interfaces of the inclusions in the REV. These volumetric scattering terms involve two types of relaxation times: a volume-averaged bulk scattering relaxation time $\overline{\tau}$ resulting from phonon scattering in the bulk matrix material, and an interface scattering relaxation time τ_B resulting from volume-averaging scattering due to interfaces within the REV. These relaxation times are determined by calibration to direct numerical simulations (DNS) of the particle or pore-resolved geometry using the phonon BTE.

The additional terms resulting from the volume-averaging are modeled as in-scattering and out-scattering terms. The scattering terms are written as a function of a scattering phase function, $\Phi_{\mathbf{KK'}}$, and the interface scattering relaxation time, τ_B. The scattering phase function represents the redistribution of phonon energy upon scattering at the interface. Both τ_B and $\Phi_{\mathbf{KK'}}$ are functions of the interface geometry and the phonon wave vector space. The scattering phase function in the model is evaluated in the geometric optics limit using ray tracing techniques and validated against available

analytical results for spherical inclusions. The volume-averaged bulk scattering relaxation time, $\bar{\tau}$ takes in to consideration the effects of the pores on the effective thermal conductivity of the composite. It is calibrated using a Fourier limit solution of the nanoporous domain.

The resulting governing equations are then solved using a finite volume discretization and the coupled ordinates method (COMET). In the gray limit, the model is applied to nanporous geometries with either cylindrical or spherical pores. It is demonstrated to predict effective thermal conductivity across a range of Knudsen numbers. It is also demonstrated to be much less computationally intensive than the DNS.

This model is extended to include non-gray effects through the consideration of both polarization and dispersion effects. For non-gray transport, the bulk and interface scattering relaxation times are now wave-vector dependent. Two different models are proposed for determining the interface scattering relaxation times, one assuming a constant value of interface scattering relaxation time, and another which accounts for variation with wave vector. As before both bulk and interface relaxation times are calibrated with the DNS solution in the Fourier and ballistic limits. The scattering phase function developed for gray transport in the geometric limit is expanded to consider the appropriate energy exchanges between different phonon modes assuming elastic scattering. The non-gray volume-averaged BTE is compared to the DNS for a range of porosities at the limits of bulk average Knudsen number and for intermediate average Knudsen numbers. The model with variable interface scattering relaxation times is found

to better predict the variation of effective thermal conductivity with wave vector, though both models for interface scattering are less accurate than the gray model.

Further, the volume-averaged BTE is extended for two material composites. We solve the volume-averaged BTE model for particle sizes comparable to the phonon wavelength in the composite matrix. We employ analytical scattering phase functions in the Mie scattering limit for particles to include wave effects. The calibration of model relaxation time parameters is conducted similar to that in the gray volume-averaged BTE model for nanoporous materials. The composite domain is solved in the Fourier limit to calibrate the volume-averaged bulk relaxation time. This relaxation time parameter considers the material properties of both the host material and particle. For small particle sizes, calibration in the ballistic limit is conducted using a nanoporous domain. This is possible as the interface scattering relaxation time is driven primarily by the travel time of the phonons between particles, and not by the residence time inside the particle. The scattering phase function is computed considering properties of both the host material and the particle scatterers. We solve the volume-averaged BTE for the two-material composite for a silicon host matrix with spherical germanium particles. We demonstrate the gray two-material composite domain for varying porosities over a range of Knudsen numbers.

The present work creates a pathway to model thermal transport in nanocomposites using volume-averaging which can be used in arbitrary geometries, accounting for both bulk scattering and boundary scattering effects across a range of transport conditions. The model accounts not only for the volume fraction of particulates and inclusions, but also

their specific shape and spacing. It also accounts for sub-continuum effects. Furthermore, the volume-averaging method also allows inclusion of wave effect through the scattering phase function so that particles on the order of the phonon wavelength or smaller can be considered. The formulation is also generalizable to the limit when the particles are large compared to the wavelength; in this limit, geometric optics may be employed to compute the scattering phase function. Overall, the volume averaging approach offers a computationally inexpensive pathway to including composite microstructure and subcontinuum effects in modeling nanoporous materials and composites.

Table of Contents

List of Tables

List of Figures

Chapter 1: Introduction

1.1 Motivation and Background

Nanocomposites are of great scientific interest due to their applications in thermal-management, thermal generation and energy storage. Recent focus in nanocomposites has been on the manipulation of their thermal and electronic transport properties through the use of different material combinations and engineered nanostructures [1-4]. In order to design and fabricate engineered nanocomposites for thermal applications, it is essential to understand sub-continuum thermal transport in these materials. There are limitations and challenges in both the experimental as well as theoretical understanding of nanomaterials. The added structural complexities in nanoporous materials and nanocomposites introduce further challenges in modeling irregular geometries and predicting interface effects accurately.

Thermal transport in many nanocrystalline solids is through quantized modes of vibration in the atomic lattices. These quantized vibrations, also known as phonons, determine many of the physical properties of the material, such as heat capacity and thermal conductivity. Phonons demonstrate wave-particle duality when analyzed using quantum mechanics and, therefore, are quasi-particles [5]. If the length scale of the nanostructure, L, is large compared to the phonon wavelength λ, coherence effects can be neglected and phonons may be treated as semi-classical particles. In this particle viewpoint, the mean free path Λ of the phonon is the average distance travelled by the phonon before it experiences a collision. These collisions can be due to a variety of interactions: phonon-phonon, phonon-electron, phonon-boundary, phonon-interface or

phonon-impurity, among others. Phonon-interface or boundary scattering is elastic and phase information is not lost. Phonon-phonon scattering or bulk scattering is central to the determination of thermal conductivity, and is inelastic in nature [6]. For typical composites of interest, phonon mean free paths are in the range of tens to a few hundred nanometers, while wavelengths may be of the order of a few nanometers. Thus, a particle treatment is expected to suffice for most nanocomposites of interest.

When are sub-continuum effects important?

For simplicity let us consider a nanoporous material of length scale L_D composed of unit cells or modules of length scale L as shown in Figure 1. Within each module are pores of length scale L_P separated by distance d, so that $L_P \sim (L-d)$.

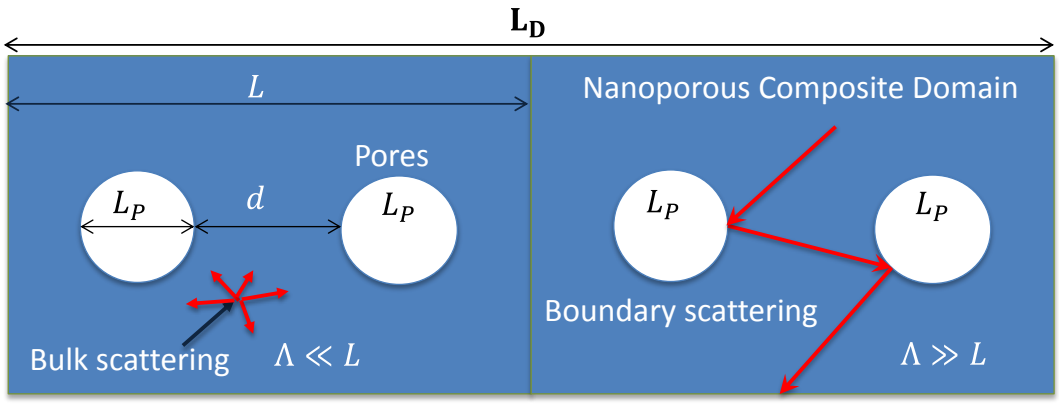

Figure 1: Schematic of bulk and boundary scattering mechanisms in a nanoporous composite domain

Let us assume that $d/\lambda >> 1$ so that coherence effects may be neglected. Phonons traveling through the module undergo ~ $O(L/\Lambda)$ number of scattering events in the matrix material

due to phonon-phonon, phonon-carrier and phonon-impurity scattering. The corresponding time scale,.i.e., the bulk relaxation time τ_{bulk}, is given by

$$\tau_{bulk} = \Lambda / v_g$$

Phonons scatter on interfaces as well as on carriers or impurities. The number of interface scattering events is of order L/d, and the interface scattering time scale is given by:

$$\tau_B = \mathrm{d}/v_g$$

An effective relaxation time, τ_{eff}, accounting for both bulk and boundary scattering is given by Matthiessen's rule [7]:

$$\frac{1}{\tau_{eff}} = \frac{1}{\tau_{bulk}} + \frac{1}{\tau_B}$$

We may define an effective Knudsen number Kn as:

$$\mathrm{Kn} = v_g \tau_{eff} / L$$

Kn is inversely proportional to the number of scattering events (bulk or interface or both) that occur over the module length scale L. If Kn<<1, there are sufficient numbers of scattering events that diffuse behavior obtains within the module. In this limit, it may be shown that the Fourier law is valid, and the effective thermal conductivity of the porous material is given approximately by

$$K_{bulk} \sim \frac{1}{3} C {v_g}^2 \tau_{eff}$$

where, C is the specific heat of the composite and v_g is the phonon group velocity in the composite. (A more detailed derivation accounting for material porosity and tortuosity is given in Chapter 2). It follows of course that if the density of interfaces is small (d/L~1) within the module,

$$\frac{1}{\tau_{eff}} \sim \frac{1}{\tau_{bulk}}$$

then the effective thermal conductivity of the porous material is given approximately by

$$K \sim \frac{1}{3} C v_g \Lambda \sim \frac{1}{3} C {v_g}^2 \tau_{bulk}$$

By the same token, if the density of interfaces is sufficiently high (d/L<<1), interface scattering would dominate bulk scattering and therefore

$$\frac{1}{\tau_{eff}} \sim \frac{1}{\tau_B}$$

In this limit, the porous material obeys Fourier diffusion and the effective thermal conductivity of the material is given approximately by:

$$K \sim \frac{1}{3} C v_g \mathrm{d} \sim \frac{1}{3} C {v_g}^2 \tau_B$$

If, on the other hand, $\mathrm{Kn} = v_g \tau_{eff}/L \geq 1$, there are relatively few scattering events within the module, either bulk or interface, and Fourier diffusion does not obtain. In this limit, it is important to consider sub-continuum effects within the module.

If sub-continuum effects are important within the module, but the material length scale $L_D >> L$, there are many modules or unit cells in the material. In this limit, bulk behavior will nevertheless obtain, but on the length scale L_D. The effective thermal conductivity of the bulk material will depend on the conductance of the individual modules; the latter must account for sub-continuum effects. If the material length scale L_D is of the order of the module length scale L, sub-continuum effects are again important, but a material property such as effective thermal conductivity cannot be

defined. Instead, thermal transport in the material will depend on the size and shape of the material, as well as boundary scattering on the boundaries of the material domain.

Now, instead of a nanoporous material, let us consider a composite consisting of the matrix material in which are embedded particles of a different material. Phonons traveling through the matrix material again undergo bulk scattering as before. Phonons impinging on the particle-matrix interface are partially reflected and partially transmitted; the fraction depends on the mismatch in spectral properties between the matrix material and the particle, as captured by, for example, the diffuse mismatch model [8]. The physics governing the reflected phonon energy are the same as for scattering in porous materials, and the discussion above applies. What is new, however, is transmission. Here, a fraction of the phonon energy impinging on the particle undergoes transmission into the particle, where, depending on particle size, it may encounter additional thermal resistance due to bulk scattering within the particle. However, in many composites of interest, the particle length scale L_P <<L, and phonons may be assumed to travel nearly ballistically within the particle, and to undergo multiple reflection and transmission events at particle-matrix interfaces. In such cases, the primary role played by the particle is to decrease the interface scattering time scale, and to re-arrange the directional distribution of phonon energy.

1.2 LITERATURE REVIEW

Researchers have modeled effective thermal conductivity of composite materials in the dilute limit. Hashin [9] developed a generalized self-consistent scheme to determine the rigorous bounds on effective conductivity of a two-phase material

supporting a particle view of the phonon transport and emphasizing interface scattering as the dominant phenomenon. The effective thermal conductivity of composites also requires a detailed resolution of phonon polarization and frequency. The mean free path of phonons in a material like silicon, for example, ranges over many orders of magnitude [10]. Thus, the transport of some phonons groups may be mediated primarily by scattering in the bulk matrix, while phonons with longer mean free paths may encounter scattering on the particle inclusions. Furthermore, the transmissivity of phonons across heterogeneous interfaces is a strong function of spectral signatures of the phonons in each material.

Over the years, significant effort has been made to better understand the temperature discontinuity at the interface between two dissimilar materials due to interface resistance. The earliest work in this area can be traced to Kurti, *et al.* [11] and Kapitza [12]. In 1941, a study by Kapitza [12] on thermal measurement of a solid submerged in liquid helium showed dissimilar temperatures at the interface of the two different materials in the experiment. In 1952, Khalatnikov [13] developed a model proposing the presence of a thermal boundary resistance (TBR) to explain the temperature jump at the interface. The TBR or Kapitza resistance is defined as the ratio of temperature discontinuity to the power flowing per unit area across the interface. This model was the early basis of the acoustic mismatch model (AMM). In 1959, Little [14] expanded the acoustic mismatch model to solid-solid boundaries by considering the mismatch in the sound velocity in the two media. Both Khalatnikov and Little adopted a harmonic model wherein a phonon interacts with a geometrically perfect interface and

experiences reflection or transmission that is elastic. The transmission and reflection coefficients are determined by the angle of incidence and the acoustic velocities of the phonons on either side of the interface.

Molecular dynamics (MD) simulations were compared with AMM by Schelling, Phillpot, and Keblinski [15] at a silicon-silicon interface with modified properties for one side. They found that there was a strong polarization dependence of the transmission of high frequency transverse acoustic phonons, allowing only specific phonon types to be transmitted across the interface. They could then calculate the transmission coefficients. Finally, they noted that the AMM and MD simulations agreed with each other for low frequency acoustic phonons, whereas at the high frequencies, AMM did not yield accurate results.

Another approach in modeling the interface, known as the Diffuse Mismatch Model (DMM), was proposed by Swartz and Pohl in 1987 [8]. Their model for an interface with sufficient roughness and high enough temperature predicted that the relative density of states of the two interface materials mattered more than the acoustic mismatch in the two materials in determining the interface transmission of the phonons. They assumed that the phonon was either reflected diffusely or transmitted, both elastically, from the rough interface. DMM assumes that a phonon would not know its origin once it impinges upon an interface, i.e., it “loses memory”. Consequently, we can say that the acoustic correlations at interfaces are assumed to be completely destroyed by diffuse scattering, which means that the transmission coefficient is determined solely based on the density of states on both sides and can be derived using the principle of

detailed balance [6]. Furthermore, the phonon transmission coefficient is found to be equal to the reflection coefficient for a phonon traversing the opposing direction.

The accuracy of DMM varies depending on the mismatch in the Debye temperature of the materials sharing the interface. The Debye temperature is a function of the maximum frequency. The errors in this model can be attributed to the elastic transmission assumption. In materials with a large Debye temperature mismatch, DMM underpredicts the thermal conductance. This error implies the presence of significant inelastic scattering at these interfaces [16-19].

Another approach to modeling interfaces is through the atomistic Green's function (AGF) [20-24]. Here anharmonicity is ignored at the interface and the Landauer formulation [25] of the energy transport is adopted. The system is decomposed into the device and two contacts and three different Green's function is computed for these sub-sections. This makes it possible to simulate the system response to a wave packet traveling through the system. AGF focuses on obtaining transmission functions for the phonon waves in a given crystal structure. It can handle the presence of boundaries, interfaces, defects and connections to bulk contacts by establishing interaction matrices between atoms and simulating the transport of plane lattice waves. While it is advantageous in capturing wave effects that may be present in phonon transport, AGF requires increased effort to incorporate anharmonic three-phonon scattering [26]. In cases where scattering is important and for system sizes which are significantly larger than the phonon wavelength, AGF is not suitable. This makes is unsuitable for studying thermal

conductivity itself [10], but it can be very useful in accounting for interface atomic structure in computing interface transmission functions.

We can identify two basic types of theoretical modeling approaches for phonon transport from the composite materials literature: (i) theories based on effective medium approximation (EMA) theory, and (ii) direct numerical simulations of a periodic idealized cell in the composite. The EMA is derived typically based on the Fourier conduction equations, and as we realize from our previous discussion, sub-continuum effects become important at the smaller length scales. Originally the EMA theory developed by Maxwell and Rayleigh [27], and numerous variants, including that by Maxwell-Garnett have been published [28].

An improvement to this classical work was made by Hasselman and Johnson (1987) [29] when they incorporated interfacial resistance in to this model for the first time. In 1991, Benveniste and Miloh [30] developed a model for effective thermal conductivity while incorporating thermal boundary resistance by averaging all relevant variables such as heat flux and intensity over the composite medium with a matrix and with inclusions being treated as a continuum. The Kaptiza resistance was corrected for in the EMA formulation by Every *et al.* [31]. They presented an asymmetric Bruggeman type model and solved it for high volume fraction of inclusions. A more general and significant EMA-based model was developed by Nan *et al.* in 1997 [32]. This analytical model gives a general form for computing effective thermal conductivity of arbitrary particulate composites. They consider the effect of particle size, shape, distribution, properties of the matrix and reinforcement and volume fraction in addition to interfacial

resistance, as the previous models. The expression for effective thermal conductivity k_{eff} of a composite in terms of the wire (k_{Si}) and matrix (k_{Ge}) thermal conductivities may be written as,

$$k_{eff} = \frac{k_{Ge}\left(\frac{k_{Si}}{k_{Ge}}(1+\alpha)+1+\phi\left(\frac{k_{Si}}{k_{Ge}}(1-\alpha)-1\right)\right)}{\frac{k_{Si}}{k_{Ge}}(1+\alpha)+1-\phi\left(\frac{k_{Si}}{k_{Ge}}(1-\alpha)-1\right)}$$

where $\alpha = 2k_{Ge}R/L_{Si}$, ϕ= volume fraction, and R is the interfacial thermal resistance which is a function of the phonon transmissivity and therefore, the geometry and wave vector space in the media. More recently, a modified EMA proposed by Minnich and Chen [33] takes into consideration size effects in each phase of the composite by modifying the bulk mean free path. This accounts for increased boundary scattering of phonons when the particle (wire) size and spacing are comparable to the mean free path of phonons. The reduced mean free path of phonons in the matrix (Ge) and wire (Si) based on the Matthiessen's rule is given by:

$$\frac{1}{\Lambda_{Ge}^{eff}} = \frac{1}{\Lambda_{Ge}^{bulk}} + \frac{1}{\Lambda_{coll}}$$

$$\frac{1}{\Lambda_{Si}^{eff}} = \frac{1}{\Lambda_{Si}^{bulk}} + \frac{1}{L_{Si}}$$

Here, Λ_{Ge}^{bulk} and Λ_{Si}^{bulk} are the bulk mean free paths of the phonon in the matrix (Ge) and wire, (Si), respectively. Λ_{coll} and L_{Si} represents the reduction in mean free path in the matrix and the wire due to diffuse boundary scattering. Λ_{coll} relates phonon boundary scattering to the density of nanowires within the matrix. For a square nanowire, Λ_{coll} =

φ/L_P, where L_P is the length of the periodic unit. The calculated effective mean free path of phonons in the matrix and the wire are used to compute the reduced thermal conductivity of each phase. The modified EMA model uses the reduced thermal conductivity to calculate the overall k_{eff}.

The effective medium approximation (EMA) has been successful in predicting effective properties of macrostructured composites but fails to make accurate predictions for nanocomposites [10]. This is not surprising given the complex nature of phonon transport not being supported by theories in the macroscopic limit. EMA theory severely overpredicts the effective thermal conductivity for small period lengths but shows closer predictions at micron sized nanocomposite unit cells with the inclusion of the interfacial thermal resistance. Despite accounting for boundary scattering, the modified EMA theory fails to provide accurate estimation of thermal conductivity in the ballistic limit of phonon transport. This range of transport in composites is governed by phonon transmission at the interface and view factors between scattering surfaces. In this range there is significant departure from the predictions of diffusive transport theory even if interfacial resistance due to scattering at interfaces is considered. Thus, EMA theory which is based on a diffusive transport theory is unable to predict accurately the effects that are dominated by surface view factors [32, 33].

We turn now to a brief review of numerical methods for the simulation of phonon transport. Over the last few years, molecular dynamics (MD) has increasingly come to be used to explore phonon transport. MD employs a time integration of Newton's second law of motion at the atomic level, where each atom is treated as a point particle

interacting with other particles through an interaction potential. The interaction potential may be derived through empirical models that fit specific bulk data [34-37]. Another approach is to use force constants based on density functional theory [DFT] [38]. Every atom is tracked for a set of discrete time steps over a span of a few nanoseconds and this data is analyzed to deliver transport parameters such as thermal conductivity. Both equilibrium MD (EMD) [39] employing the Green-Kubo formalism and non-equilibrium MD (NEMD) [40] have been employed. The dynamical and transport properties of solid crystals are obtained in EMD using the history of thermal fluctuations in the system, whereas NEMD directly determines the thermal conductance by imposing temperature gradients in the system. Both methods are consistent with each other and agree well with experiments [41]. MD simulations are inherently limited by the assumption of classical oscillators and results below the Debye temperature fail to recognize quantum effects. For silicon, the Debye temperature is 660 K, and consequently any solution below this limit cannot be considered accurate. Moreover, with current computational power, MD is not a realistic choice for simulating nanocomposites since a very large number of atoms would need to be used.

The semi-classical phonon BTE is capable of describing the quasi-particle nature of the phonons, especially at the length scales of our interest, where phonon mean free path may be of the order of the system size [6]. Typical solutions of the BTE make either a gray or a non-gray approximation to the phonon dispersion relation. A gray approximation means that we ascribe a single group velocity and relaxation time to all the phonon groups. Under the gray approximation, the group velocity v_g is chosen to reflect

the velocity of the dominant phonon groups at the temperature under consideration. Relaxation time, τ, is chosen such that we can recover the bulk thermal conductivity of $C_v v_g^2 \tau / 3$ corresponding to Fourier's law, for Kn << 1. Here C_v is the volumetric specific heat capacity of the solid. Non-gray models include the full **K**-space resolved phonon dispersion, the wave-vector and polarization dependence of phonon mean free paths and interface transmissivity and reflectivity values. Numerical solutions of the BTE employ computational schemes that have a basis in the thermal radiation and neutron transport literature [42]. One of the most commonly used solution techniques for the BTE is a finite volume based approach, where the physical domain is discretized in to control volumes. The Brillouin zone is also discretized into finite volumes. Conservation of phonon energy may be imposed by integrating the BTE over physical and wave vector space, and discretization and numerical solution carried out using standard linear solvers [43-45]. The discrete ordinates method is also widely used and is similar, with the quadrature in wave-vector space being based on well-established quadrature schemes [43, 46, 47].

Periodic nanocomposites have been studied using multiple methods described above, primarily due to their simplicity and significance in predicting effective properties and engineering new devices. In 1997 Chen [48] modeled effective thermal conductivity of periodic thin-film structures in the parallel direction. This model demonstrated that interface roughness causes reduction in thermal conductivity of superlattices. One of the findings of this BTE based model was that the non-gray approximation was more consistent with the experimental results as opposed to the gray approximation. The non-

gray model, however, came with an increase in the computational expense. In a separate study, Yang and Chen [49] modeled phonon transport in a two-dimensional composite with silicon nanowires embedded in a germanium matrix. The BTE based model assumed gray dispersion and diffuse scattering at the interface. They used the discrete ordinates method with double Gauss-Legendre quadratures for solution procedure. The study confirmed that temperature profile in nanocomposites were significantly different from the regular composites. It also demonstrated the effects of interface conditions, nanowire size and volume fraction of constituents on the thermal conductivity of the nanocomposite.

Monte Carlo methods have been developed for phonon transport in nanocomposite structures using a gray dispersion relation by Chen *et al.* and Yang *et al*. [50, 51]. In [50], a periodic boundary condition is implemented in the Monte Carlo simulation to study three-dimensional silicion/germanium nanocomposite periodic structures. The study shows that the thermal conductivity of nanocomposites can be lower than that of the minimum alloy value, which is important from thermoelectric energy conversion point of view. It was also found that randomly distributed nanoparticles in nanocomposites can yield a thermal conductivity similar to periodic aligned patterns when using the periodic boundary condition. In [51], Tian *et al*. used the same code to simulate compacted nanowire composites simplified as periodic units with nanowires embedded in a host matrix. This study showed that further reduction in thermal conductivity of nanocomposites was possible for compacted nanowires of the same characteristic size and atomic composition. Hseih and Yang [52] studied the effects

of nanowire shapes in periodic nanowire composites using a multiblock-structured grid based solver for phonon BTE. This study showed that a square approximation of circular nanowires overestimates the thermal conductivity. This is important as it shows that geometry effects cannot be ignored when phonon transport is in the ballistic limit.

Singh *et al*. [53] developed a finite volume based BTE solver to study the effects of phonon dispersion on silicon/germanium interfaces for two-dimensional domains. Results showed non-gray model of phonon transport leads to higher interfacial thermal resistance than that obtained using a gray model. This suggests that phonon frequency mismatch in the two materials is critical in determining interface resistance. Using a finite volume based BTE solver and an acceleration algorithm COMET, Loy [54] modeled phonon transport in silicon, germanium, a silicon/germanium composite with a single vertical interface and nanoporous silicon. This study used realistic nanoparticle composite geometries and non-gray phonon dispersion relations.

The above studies make significant assumptions on either the underlying phonon dispersion or about the geometry itself. The most commonly employed assumption is the gray approximation. Another common assumption is the use of idealized unit cell geometries. The extent and directionality of scattering depends on the specific orientation of inclusions, and the surface-to-volume ratio that they offer. If these are not represented correctly, the balance between interface and bulk scattering cannot be captured accurately. Ultimately, our intent is to create a model for nanocomposite transport which can be used in arbitrary geometries, accounting for both bulk scattering and boundary scattering effects across the range of Knudsen numbers.

The similarity between the BTE and the radiative transfer equation (RTE) has long been recognized. Further, a generalized equation for phonon radiative transport in a particulate media has been studied [55], which draws analogy between the RTE and phonon BTE. Thus, one may draw parallels between the development of volume-averaged models for phonon transport in nanocomposites and those for thermal radiation in porous media. In the radiation literature there have been studies on porous media where the governing equations (Maxwell's equations) of electrodynamics for heterogeneous media in the wave limit are used to derive volume averaged radiative transfer equations [56]. Consalvi *et al.* developed a volume-averaged formulation for multiphase radiative heat transfer equations while considering the various particle and phase effects such as particle-phase specific surface, gas scattering phase function and particle and wall emissivity [57]. The influence of interfaces on radiation intensity in a porous medium has been studied in packed beds, porous media composed of particles of different geometry, as well as different phases [58-62]. Anisotropic phase functions have been considered in [63]. For different particle sizes relative to the phonon wavelength, one needs to consider different scattering limits. Scattering from large reflecting spheres and cylinders in the geometric limit has been well studied [63]. In the geometric limit (analogous to the particle limit for the phonon BTE), ray tracing techniques can be employed wherever analytical expressions are unavailable, i.e., short cylinders or arbitrary geometries [64]. In the Rayleigh limit, i.e., for particle sizes much smaller than the phonon wavelength in the composite, scattering phase functions and transport cross sections for anisotropic scattering have been studied for longitudinal phonons [65]. For

particles comparable to the phonon wavelength, scattering phase functions and transport cross sections for anisotropic scattering have been developed for transverse phonons in the Mie limit [66].

These studies provide guidance on how we may develop a volume-averaged BTE and determine the scattering phase functions associated with them. Availability of experimental data for both nanoporous and nanocomposite domains makes the comparison process for developed models a possibility. Experimental data by Chen [67] on porous silicon shows significant departure from bulk properties. Additional experimental results are available for Si-Ge nanocomposites [68]. These composites have 20-80 nm silicon particle sizes in a germanium matrix. In the above studies, data on effective thermal conductivity of the domains are available for specific particle shapes and sizes.

Our primary objective is to develop the first volume-averaged model for BTE for nanoporous and nanocomposite materials. In the sections that follow, we outline the process of developing and solving the governing equations, the process for determiming model parameters, as well as validation.

1.3 DISSERTATION OBJECTIVES

The overall objective of this dissertation is to develop a volume-averaged model for thermal transport in nanoporous and nanocomposite materials, accounting for the full range of phonon Knudsen numbers and non-gray effects. The models will be implemented numerically in the MEMOSA software framework of Purdue's PRISM (Prediction of Reliability, Integrity and Survivability of Microsystems) center [69]. The

volume-averaged BTE is solved using a solver based on the finite volume method (FVM) employing the coupled ordinates method (COMET) [70]. Comparisons are made with direct numerical simulations of a geometrically-resolved composite, as well as with experimental data where available. The specific objectives and scope of the dissertation are discussed in details below.

1.3.1 Volume-Averaged Formulation for Nanoporous Materials with Gray Approximation

We will develop a volume-averaged formulation for nanoporous domains based on a formal averaging of the phonon BTE over a representative elemental volume (REV). As we show in the detailed derivation in chapter 2, this will result in an additional boundary scattering term which is a function of the interface geometry and the phonon wave vector space. A new relaxation-time like model parameter, τ_B, will be derived which is a function of the geometry of the representative elemental volume and varies in the phonon wave vector space; it represents interface scattering. We write the extra integrals as an in-scattering term using a scattering phase function computed from the specific shape of the inclusions and the phonon dispersion. The in-scattering term is multiplied by the interface scattering relaxation time parameter, τ_B, which is determined by calibration against a direct numerical simulation (DNS) of a periodic composite domain in the ballistic limit. We will develop a general ray tracing technique to evaluate the scattering phase function. The scattering phase function in the model is evaluated in the geometric optics limit and validated against available analytical results. We will use this technique to investigate scattering phase functions for both spherical and cylindrical

inclusions. Volume-averaging the bullk scattering term in the phonon BTE results in an average bulk scattering relaxation time, $\bar{\tau}$. This is determined by calibration against a Fourier solution in the periodic domain, and accounts for tortuosity of the thermal pathways due to pores and inclusions, in addition to the intrinsic thermal conductivity of the bulk matrix material.

This framework will be first implemented for gray phonon dispersion. We will solve the developed equations within the MEMOSA framework utilizing the COMET algorithm. The gray volume-averaged model for nanoporous composites is used for predictions for the full range of phonon transport by varying the Knudsen number. The method is used to compute the effective thermal conductivity of nanoporous materials and comparisons with DNS of the same material are provided. The model is demonstrated to predict effective thermal conductivity for spherical and cylindrical inclusions. We will investigate the effects of porosity using cylindrical pores. We compare the obtained effective thermal properties. We further make a direct comparison of the heat rate contributions of different phonon modes obtained from the volume-averaged BTE with that of the DNS and demonstrate that good agreement is obtained.

1.3.2 Volume-Averaged Formulation for Nanoporous Materials with Non-Gray Phonon Dispersions

In this work, we will consider non-gray phonon dispersions and implement a non-gray version of the volume-averaged model developed above. While the model development remains the same, the objective is to ensure anisotropic scattering from the inclusion interfaces is determined accurately. For non-gray transport, discretization of the

Brillouin zone results in a large number of phonon BTEs to be solved, one for each discrete K point. Thus, there are a corresponding number of boundary scattering relaxation times $\tau_{B,i}$ to be determined, along with a number of bulk relaxation times, τ_i. The scattering phase function matrix,$\Phi_{KK'}$, will be computed from the specific shape of the inclusions and the phonon dispersion. The general ray tracing technique developed above will be expanded to the non-gray case assuming elastic scattering. This model addresses anisotropic scattering from inclusion interfaces and considers realistic non-gray phonon dispersion accounting for phonon polarization. The resulting governing equations are then solved using a finite volume discretization and the coupled ordinates method (COMET). Relaxation times related to the interface scattering are geometry-specific and are determined by calibration to a DNS of the periodic geometry. The calibration is performed while accounting for the complete phonon dispersion in the non-gray limit. The calibration of $\tau_{B,i}$ at the ballistic limit is implemented using an iterative Newton-Rhapson method. Post-calibration, the heat rate contributions of different phonon modes are compared with those from the fully-resolved BTE. The predictions are compared with experimental data available for cylindrical inclusions for silicon nanoporous films [71]. We compare both accuracy and numerical speed-ups obtained using the volume-averaged model for non-gray phonon transport with respect to direct numerical simulation of the BTE.

1.3.3 Volume-Averaged Formulation for Two-Material Composites

We will extend our nanoporous formulation to consider two-material composites. We consider a nanocomposite domain with particles of a second material embedded in

the matrix. The phonon BTE is integrated on a representative elemental volume (REV) as earlier. The presence of composite particles in the matrix of the REV is modeled using the extra integral terms resulting from the averaging procedure and are approximated to yield additional scattering terms. The scattering at the inclusions is modeled using an in-scattering term, a scattering phase function determined using the specific shape of the particle, and a relaxation time like parameter, τ_B.

As discussed previously, relaxation times related to the interface scattering are dependent on the particle geometry. The relaxation-time like parameter, τ_B, obtained from the volume-averaged formulation, will be calibrated to fit the effective thermal conductivity obtained from a detailed DNS of the composite geometry in the ballistic limit. Volume-averaged bulk relaxation times are calibrated using DNS in the Fourier limit, while accounting for both the matrix and particle geometry and thermal properties.

The result is a phonon BTE written in terms of the volume-averaged phonon energy density, and involving volumetric scattering terms resulting from both bulk scattering and scattering at the particle interfaces in the REV. The model is general and can addresses anisotropic scattering from matrix interfaces accounting for interface selectivity from acoustic and density-of-states mismatch between composite materials in the geometric as well as the Rayleigh and Mie limits. We will employ analytical expressions for scattering phase functions in the Mie limit for transverse phonons [66, 72]. We consider gray phonon dispersion for this study. We solve the resulting governing equations using the numerical procedure mentioned in earlier sections. The method is used to solve for the intrinsic volume-averaged phonon energy density. Using the above

energy density field, we compute the effective thermal conductivity for the two-material nanocomposite domain. This gray model is tested for the full-range of phonon transport by varying Knudsen number. The study is adapted to determine the effective properties for a range of composite particulate volume-fractions in the domain.

1.4 DISSERTATION ORGANIZATION

The dissertation is organized as follows:

Chapter 2: In chapter 2 we present the detailed derivation of the volume-averaged model. We will develop additional analytical relations for effective thermal conductivity in the limiting cases under the gray approximation of phonon dispersion. We will discuss in detail the different model parameters including the calibration procedure for the interface scattering relaxation, τ_B and the volume-averaged bulk relaxation time, $\bar{\tau}$. We will present our general ray tracing technique used to determine the scattering phase function in the geometric limit.

Chapter 3: We will present formulations relevant to the non-gray or **K**-resolved volume-averaged BTE model for nanoporous composites. We will discuss the expansion of the scattering phase function for non-gray simulations and the calibration of the volume-averaged relaxation times, $\overline{\tau_k}$, as well as the interface-based relaxation time like parameters, $\tau_{B,k}$ using a Newton Rhapson iterative procedure.

Chapter 4: We will apply the volume-averaged model developed above on a two-material nanocomposite domain. We will discuss the assumptions and semi-analytical approach to compute the scattering phase function in the Mie scattering limit. We will

discuss the calibration procedure for the volume-averaged relaxation time and the interface-scattering relaxation time in the Mie limit for a nanocomposite structure.

Chapter 5: In this chapter we will discretize the equations developed in previous chapters and present the numerical technique used to solve the volume-averaged BTE. We will discuss the different boundary conditions applied in solving the models. For the volume-averaged BTE model to be effective the domain length must be large enough. For reduction in computation time, we will instead simulate a periodic unit cell for the composite. This is done by implementing a periodic jump boundary condition for a unit cell, such that the effective properties thus obtained can be compared to the direct numerical simulation.

Chapter 6: We present results and discussions in this chapter. The volume-averaged model will be benchmarked against a direct numerical simulation (DNS) for nanoporous structures. The DNS on the nanporous structure will be solved for both gray and non-gray limits of the phonon dispersion. For the nanoporous gray model we will compare the model with the benchmark DNS solution. For the nanoporous non-gray model, we compare the model solution with that of the DNS. The volume-averaged models on nanoporous and nanocomposite structures will be validated using experimental data available for real geometries and materials [71] where possible. For experimental validation we compare the DNS directly to nanoporous silicon measurements. Recent experimental work on nanoporous silica by Hopkins *et al.* [73] has data on 500-nm-thick films with a square array of pores with diameters and pitches between 300 and 800 nm. Hopkins *et al.* use the time domain thermo reflectance (TDTR) technique for their

measurement. These geometries are easily obtainable and can be solved using the volume-averaged formulation.

For nanocomposites we present results for the gray approximation of phonon dispersion in the Mie scattering limit. We will calibrate the nanocomposite gray model at the bulk and ballistic limits using the DNS on the composite geometry. We consider realistic properties and geometries for these studies.

Validation with the benchmark solution will allow the theory to be used for the prediction of the effective properties in nanoporous and nanocomposite structures without the need to fully resolve the geometry. This will ease computational expense and will be an invaluable technique for the analysis and design of future nanocomposites.

Chapter 7: We will conclude the dissertation by summarizing the dissertation contributions and limitations. We will discuss the relevance of the dissertation research to nanoscale thermal transport. Finally we will layout the future directions for this research.

Chapter 2: Theory of Volume-Averaging for Phonon Boltzmann Transport Equation (BTE) in Nanoporous Composites

In this chapter we will consider the phonon Boltzmann Transport Equation (BTE) and develop a volume-averaged theory of the BTE for a nanoporous composite. We will derive the Fourier law for the volume-averaged BTE model corresponding to the bulk and ballistic limits of the model in a gray approximation. We also develop a formulation for the interface and boundary conditions. A methodology for determining the model parameters in the volume-averaged BTE, including the volume-averaged bulk relaxation time $\overline{\tau}$ and the interface scattering relaxation time τ_B is presented. The model uses a scattering phase function, $\Phi_{KK'}$, that we compute using a ray tracing algorithm in the geometric scattering limit. We discuss in detail the algorithm and validate it against the published literature. The fundamentals of the volume-averaged BTE model and the procedural framework developed in this chapter will be extended to non-gray transport and to nanocomposites in later chapters in this dissertation.

2.1 PHONON BOLTZMANN TRANSPORT EQUATION

The semi-classical BTE may be used to describe heat transfer in semi-conductors and dielectrics. In the absence of phase coherence, phonon transport in steady state may be described using the phonon Boltzmann transport equation (BTE) in the energy moment, as shown below [74]:

$$\nabla_x \cdot \left(\mathbf{v} e_p^{"}(\mathbf{x},\mathbf{K})\right) = \left(\frac{\partial e_p^{"}(\mathbf{x},\mathbf{K})}{\partial t}\right)_{scattering} \qquad (1)$$

$$e_p^{"}(\mathbf{x},\mathbf{K}) = \hbar\omega_p(\mathbf{K}) f_p^{"}(\mathbf{x},\mathbf{K}) \qquad (2)$$

Where **v** is the phonon group velocity vector, and e" is the non-equilibrium phonon energy density, which is dependent on the polarization p, the spatial location, **x**, and the wave vector, **K**. The magnitude of the phonon group velocity is denoted by v_g. The convective term on the LHS describes phonon free flight and the scattering term on the RHS accounts for energy exchange due to inter-phonon and phonon-carrier collisions. The scattering term couples the energy densities of all the phonons. It is purely re-distributive, and energy lost by one phonon group is gained by others through scattering interactions [75]. The scattering term is very complex in its entirety, and requires the imposition of energy and crystal momentum conservation rules. To overcome the challenges in solving the full BTE, the scattering term has been approximated using the single-mode relaxation time approximation (SMRT) [46]. We also employ this approximation in the present work. SMRT approximates the scattering term [43] as follows:

$$\left(\frac{\partial e_p^{"}(\mathbf{x},\mathbf{K})}{\partial t}\right)_{scattering} = \frac{e_0 - e"}{\tau};\ e_0 = \frac{\hbar\omega}{exp\left(\frac{\hbar\omega}{k_B T}\right)-1} \qquad (3)$$

where τ is an effective relaxation time, ħ is the reduced Planck's constant, k_B is Boltzmann's constant, ω is the phonon frequency, T is the equilibrium temperature, and e_0 is the Bose-Einstein distribution function multiplied by the phonon energy.

The SMRT approximation is based on the idea that the scattering process perturbs the phonon mode under consideration, while the modes that it is interacting with remain unperturbed; the interaction serves to drive the mode towards equilibrium. Using the

SMRT approximation, Holland derived the bulk thermal conductivity of a crystal [76]. Additionally, using specific functional forms of relaxation time, one can model phonon-phonon, phonon-carrier, phonon-boundary, and phonon-impurity scattering using Matthiessen's rule [76], with constants in the scattering models being calibrated to bulk thermal conductivity data. It is also possible to derive mode-wise relaxation times in a more fundamental manner using Fermi's Golden Rule [74]. A number of papers have also published phonon lifetimes computed using classical molecular dynamics [77].

2.2 THEORY OF VOLUME AVERAGED PHONON BTE MODEL

In this section we present the development of the volume averaged form of the gray phonon BTE model for a nanoporous composite. For simplicity, we first develop the theory for a nanoporous medium where the inclusion is essentially replaced with a vacuum, i.e., we consider transport through a matrix material with pores in it. Figure 2(a) shows a nanoporous domain and Figure 2(b) is a corresponding representative volume (REV).

The REV is the volume over which the BTE is averaged in order to derive the volume averaged equations. A sufficiently large REV consisting of several pores is chosen such that averaging over it is equivalent to averaging over any other REV in the domain.

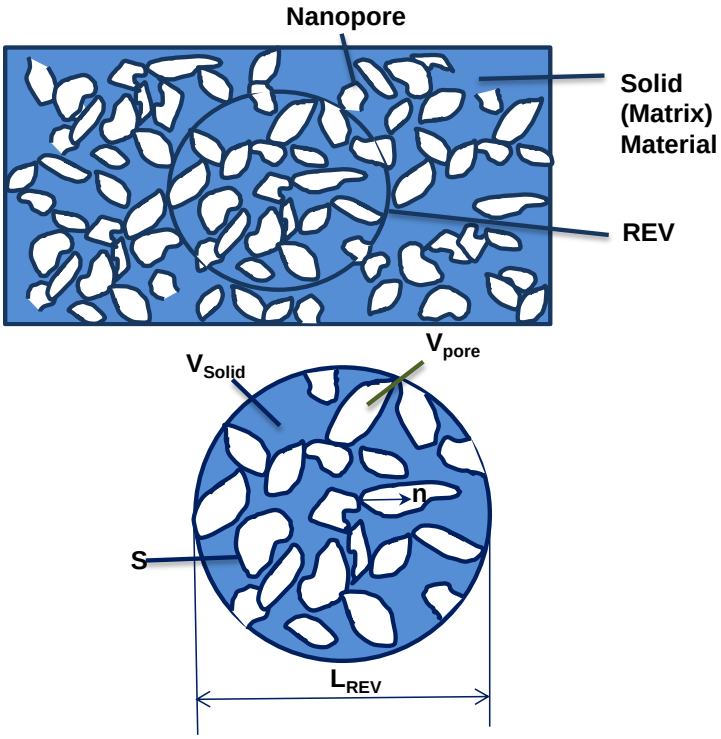

Figure 2: (a) Nanoporous medium (b) Representative Elemental Volume (REV)

Let us define a few operators for clarity:

$$V = V_{Solid} + V_{pore}$$

$$\langle x \rangle = \frac{1}{V_{Solid}} \int_{V_{Solid}} x dV$$

$$\bar{x} = \frac{1}{V} \int_{V} x dV = \frac{1}{V} \int_{V_{Solid}} x dV + \underbrace{\frac{1}{V} \int_{V_{pore}} x dV}_{=0}$$

$$\overline{x} = \alpha \langle x \rangle; \qquad \alpha = \frac{V_{Solid}}{V} \tag{4}$$

Here, $'V'$ is the volume of the REV, $'V_{Solid}'$ is the volume of the solid part of the matrix and $'V_{pore}'$is the volume of the pores in the composite matrix. The "–" variables represent

volume averaged quantities and "< >" variables represent the intrinsic volume average of the quantity in the solid. For clarity we will use bolds for vectors.

Integrating the gray steady state BTE over the REV, we obtain:

$$\frac{1}{V}\int_V \left[\nabla \cdot \mathbf{v}e" = \frac{e_0 - e"}{\tau}\right] dV \qquad (5)$$

We approximate the right hand side as:

$$\overline{\left(\frac{e_0 - e"}{\tau}\right)} \cong \frac{\overline{e_0} - \overline{e"}}{\overline{\tau}} \qquad (6)$$

The volume average of the divergence operator [78, 79] is applied on equation Eq. (5):

$$\nabla \cdot \overline{\mathbf{v}e"} + \frac{1}{V}\int_S e"\mathbf{v}.\mathbf{n}\, ds = \frac{\overline{e_0} - \overline{e"}}{\overline{\tau}} \qquad (7)$$

We now separate the surface integral in Eq. (7) into two parts, corresponding to the surface for which phonon transport is pointing from the solid to the interface $(\mathbf{v}.\mathbf{n} > 0)$and that for which phonon transport points from the interface to the solid$(\mathbf{v}.\mathbf{n} < 0)$.

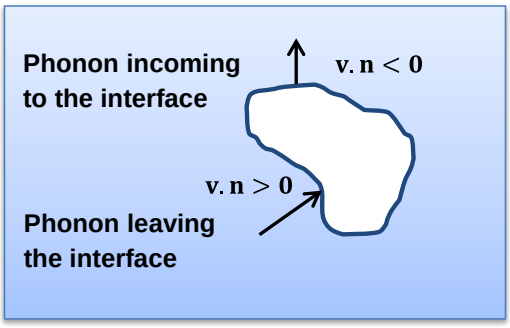

Figure 3: Interface, S, of a pore

$$\nabla \cdot \overline{\mathbf{v}e"} + \frac{1}{V}\int_{S,\mathbf{v}.\mathbf{n}>0} e"\mathbf{v}.\mathbf{n}\, ds + \frac{1}{V}\int_{S,\mathbf{v}.\mathbf{n}<0} e"\mathbf{v}.\mathbf{n}\, ds = \frac{\overline{e_0} - \overline{e"}}{\overline{\tau}} \qquad (8)$$

We now consider the first term on the LHS of Eq. (8):

$$\overline{\mathbf{v}e"} = \frac{1}{V}\int_V \mathbf{v}e"dV = \frac{1}{V}\int_{V_{Solid}} \mathbf{v}e"dV + \frac{1}{V}\int_{V_{pore}} \mathbf{v}e"dV$$

$$\Rightarrow \overline{\mathbf{v}e"} = \frac{1}{V}\int_{V_{Solid}} \mathbf{v}e"dV = \frac{V_{Solid}}{V}\mathbf{v}\langle e"\rangle = \alpha\mathbf{v}\langle e"\rangle \quad (9)$$

where $\overline{e"} = \alpha\langle e"\rangle$

Writing Eq. (8) in terms of the intrinsic average, and making the approximation $e" \cong \langle e"\rangle$ in the RHS intergrals, we have:

$$\alpha\nabla\cdot\mathbf{v}\langle e"\rangle = \alpha\frac{\langle e_0\rangle - \langle e"\rangle}{\overline{\tau}} - \frac{1}{V}\int_{S,\mathbf{v}.\mathbf{n}>0}\langle e"\rangle\mathbf{v}.\mathbf{n}\,ds - \frac{1}{V}\int_{S,\mathbf{v}.\mathbf{n}<0}\langle e"\rangle\mathbf{v}.\mathbf{n}\,ds \quad (10)$$

The process of volume-averaging produces the surface integral terms in Eq. (10) which must be closed through modeling. For the surface integral involving phonons incoming from the solid interior to the surface, $(\mathbf{v}.\mathbf{n} > 0)$, we assume:

$$\frac{1}{V}\int_{S,\mathbf{v}.\mathbf{n}>0}\langle e"\rangle\mathbf{v}.\mathbf{n}\,ds = \frac{\langle e_k"\rangle}{\tau_B} \quad (11)$$

The second surface integral term, for $(\mathbf{v}.\mathbf{n} < 0)$, represents the in-scattering of phonon energy to phonons of wave vector $\mathbf{K}$ from phonons of other wave vectors $\mathbf{K}'$. This is modeled as:

$$\frac{1}{V}\int_{S,\mathbf{v}.\mathbf{n}<0}\langle e"\rangle\mathbf{v}.\mathbf{n}\,ds = -\frac{1}{\tau_B}\frac{1}{V_{BZ}}\int_{\mathbf{K}'}\Phi_{kk'}\,\langle e_{k'}"\rangle d^3\mathbf{K}' \quad (12)$$

where the subscript $"k"$ pertains to a given $\mathbf{K}$-space point in the Brillouin zone and the summation over $\mathbf{K}$ or $\mathbf{K}'$ is equivalent to summation over the entire Brillouin zone volume V_{BZ}. For clarity, from hereafter, we will use the subscript $`k'$ for the phonon BTE corresponding to a given $\mathbf{K}$-space point in the Brillouin zone. Therefore, we may write the volume-averaged BTE as:

$$\alpha\nabla\cdot\mathbf{v}\langle e_k"\rangle = \alpha\frac{\langle e_0\rangle - \langle e_k"\rangle}{\overline{\tau}} - \frac{\langle e_k"\rangle}{\tau_B} + \frac{1}{V_{BZ}}\frac{1}{\tau_B}\int_{\mathbf{K}'}\Phi_{kk'}\,\langle e_{k'}"\rangle d^3\mathbf{K}' \quad (13)$$

We now have a volume-averaged equation (13) in terms of the intrinsic energy density of the REV. There are two types of scattering terms in equation (13). The first term on the RHS, involving $\overline{\tau}$, results from phonon scattering in the bulk matrix. The second and third terms on the RHS, involving τ_B, represent interface scattering in the domain due to the pores. Of these, the second term represents out-scattering at the interface, i.e., it accounts for energy leaving the solid for wave vectors whose group velocities point out of the solid domain. The third term on the RHS represents in-scattering at the interface, i.e. it represents energy transfer from other wave vectors to the one under consideration due to scattering at the interface. The term α is the solid volume fraction of the composite matrix, as defined earlier. The variable τ_B is a relaxation time-like parameter. This parameter represents the time scale on which phonons scatter on the interface. τ_B is a function of both the geometry of the representative volume and the phonon wave vector space. To model the composite accurately, we calibrate it from direct numerical simulations of the REV in the ballistic limit. The scattering phase function, $\Phi_{kk'}$, governs the fraction of energy from wave vector $\mathbf{K}'$ that is scattered into wave vector $\mathbf{K}$. We note that $\langle e_k" \rangle$ and $\langle e_{k'}" \rangle$ are distinct from each other. The former is the intrinsic energy density corresponding to a given **K**-space point in the Brillouin zone, and the latter term appears within the integral which is to be summed over the entire Brillouin zone. We now describe how the different **K** points are coupled using the conservation of energy principle, thereby introducing the concept of the volume-averaged lattice temperature.

2.2.1 Volume-Averaged Lattice Temperature

We now define the volume-averaged lattice temperature. Since scattering is purely a re-distributive process we can write:

$$\int_{BZ} \frac{e_0 - e_k{}''}{\tau} \, \mathrm{d}^3\mathbf{K} = 0 \qquad (14)$$

Here, "BZ" denotes integration over the Brillouin zone. Integrating over the physical volume, we get:

$$\frac{1}{V} \iint_{V\,BZ} \frac{e_0 - e_k{}''}{\tau} \, d^3\mathbf{K} dV = 0$$

$$\Longrightarrow \int_{BZ} \frac{1}{V} \int_V \frac{e_0 - e_k{}''}{\tau} dV d^3\mathbf{K} = 0$$

$$\Longrightarrow \int_{BZ} \frac{1}{V} \int_V \frac{e_0}{\tau} dV d^3\mathbf{K} = \int_{BZ} \frac{1}{V} \int_V \frac{e_k{}''}{\tau} dV d^3\mathbf{K}$$

$$\Longrightarrow \int_{BZ} \frac{\overline{e_0}}{\overline{\tau}} d^3\mathbf{K} = \int_{BZ} \frac{\overline{e_k{}''}}{\overline{\tau}} d^3\mathbf{K} \qquad (15)$$

If $\Delta T/T \ll 1$ or $T > T_{Debye}$, we can assume that the specific heat is constant with temperature. Thus, we can write the energy density in terms of the specific heat capacity, $C_{V,\Delta K,}$ as follows:

$$\overline{e_0} = C_{V,\Delta K}\left(\overline{T} - T_{ref}\right)$$

$$\therefore \sum_{BZ} C_{V,\Delta K}\left(\overline{T} - T_{ref}\right)\Delta^3\mathbf{K} = \sum_{BZ} \overline{e_k{}''}\,\Delta^3\mathbf{K} \qquad (16)$$

Furthermore, $\overline{e_0} = \alpha\langle e_0 \rangle$

Here, $\overline{T}$ is the volume-averaged lattice temperature, and T_{ref} is the reference temperature datum based on which the energy density is defined.

2.2.2 Fourier's Law for Volume-Averaged BTE

In the diffuse limit Kn ($= v_g \tau_{eff}/L$) <<1, we can retrieve the Fourier's law of conduction from the phonon BTE. We begin with the volume-averaged BTE:

$$\nabla \cdot \mathbf{v}\langle e_k" \rangle = \frac{\langle e_0 \rangle - \langle e_k" \rangle}{\overline{\tau}} - \frac{\langle e_k" \rangle}{\alpha \tau_B} + \frac{1}{\alpha \tau_B}\left(\frac{1}{V_{BZ}} \int_{\mathbf{K}'} \Phi_{kk'} \langle e_{k'}" \rangle d^3\mathbf{K}'\right) \quad (17)$$

We can re-write Eq. (17) as:

$$\nabla \cdot \mathbf{v}\langle e_k" \rangle = \frac{\langle e_0 \rangle - \langle e_k" \rangle}{\overline{\tau}} + \frac{\tilde{e}_{0,int} - \langle e_k" \rangle}{\alpha \tau_B}$$

$$\text{Where, } \tilde{e}_{0,int} = \frac{1}{V_{BZ}} \int_{\mathbf{K}'} \Phi_{kk'} \langle e_{k'}" \rangle d^3\mathbf{K}' \quad (18)$$

Under the assumption $\langle e_0 \rangle \approx \tilde{e}_{0,int}$ for isotropic scattering and gray phonon dispersion:

$$\nabla \cdot \mathbf{v}\langle e_k" \rangle = (\langle e_0 \rangle - \langle e_k" \rangle)\left[\frac{1}{\overline{\tau}} + \frac{1}{\alpha \tau_B}\right] \quad (19)$$

For small departures from equilibrium, a thermodynamic temperature may be defined, and the phonon energy density may be approximated by its equilibrium value. Thus,

$$\nabla \langle e_k" \rangle = \nabla \overline{T} \frac{\partial \langle e_k" \rangle}{\partial \overline{T}} \approx \nabla \overline{T} \frac{\partial \langle e_0 \rangle}{\partial \overline{T}} \quad (20)$$

In the diffusion limit, also known as the acoustically thick limit, the volume-averaged phonon energy density can be written as:

$$\overline{e_0} = \alpha \langle e_0 \rangle = \frac{C_{V,\Delta K}}{4\pi}\left(\overline{T} - T_{ref}\right) \quad (21)$$

Differentiating with respect to $\overline{T}$, we get:

$$\frac{\partial \langle e_0 \rangle}{\partial \overline{T}} = \frac{C_{V,\Delta K}}{4\pi\alpha} \quad (22)$$

From equations (20) and (21), we get:

$$\nabla \langle e_k" \rangle = \frac{C_{V,\Delta K}}{4\pi\alpha} \nabla \overline{T} \quad (23)$$

We assume τ_B and $\overline{\tau}$ to be independent of wave vector **K**. Multiplying equation (18) by (**v**) and integrating over 4π , we get:

$$\frac{4\pi}{3}\frac{C_{V,\Delta K}}{4\pi\alpha}\mathrm{v}^2\nabla\overline{T} = -\int_{4\pi}\langle e_k"\rangle\left[\frac{1}{\overline{\tau}}+\frac{1}{\alpha\tau_B}\right]\mathbf{v}d\Omega = -\frac{q_\omega}{\alpha\tau_{eff}}$$

$$\text{Where, } \frac{1}{\tau_{eff}} = \left[\frac{1}{\overline{\tau}}+\frac{1}{\alpha\tau_B}\right] \qquad (24)$$

The effective thermal conductivity is based on the entire area, i.e., it is averaged over the solid and the pores. The mean heat flux must therefore be multiplied with the volume fraction:

$$q_\omega = -\frac{1}{3}\alpha C_{V,\Delta K}v^2\tau_{eff}\nabla\overline{T} \qquad (25)$$

Integrating over the Brillouin zone and all polarizations, p, we obtain the total heat flux:

$$q = \sum_p \int_{BZ} q_\omega d\omega = -K\nabla\overline{T} \qquad (26)$$

$$\text{Where, } K = \sum_p \int_{BZ}\frac{1}{3}\alpha C_{V,\Delta K}v^2\tau_{eff}d\omega$$

In the limit when τ is very large (there is no bulk scattering) and all scattering is due to the presence of pores, we obtain:

$$\tau_{eff} = \alpha\tau_B \qquad (27)$$

Using equation (24), therefore, in the limit when all scattering is due to inclusions, we

$$\text{obtain: } q_\omega = -\frac{1}{3}C_{V,\Delta K}v_g^2\alpha^2\tau_B\nabla\overline{T}$$

$$\Longrightarrow q = \sum_p \int_{BZ} q_\omega d\omega = -K_{eff}\nabla\overline{T} \qquad (28)$$

By comparison with the Fourier's law, and assuming that the group velocity, specific heat and boundary scattering time scale are independent of frequency, therefore, we have:

$$K_{eff} = \frac{1}{3} C_v v_g^2 \alpha^2 \tau_B \qquad (29)$$

This shows that, in the limit when scattering is dominated by boundary scattering on the inclusions, the effective thermal conductivity, K_{eff} predicted by the volume-averaged model depends quadratically on the volume-fraction.

2.3 Model Methodology for Gray Phonon Dispersions

In this section we will discuss the calibration procedure for determining the volume-averaged relaxation time, $\bar{\tau}$ and the interface-based relaxation time, τ_B. We also discuss the computation of the scattering phase function, $\Phi_{\mathbf{KK'}}$.

2.3.1 Fourier's Law for Volume-Averaged BTE

In the presence of pores, heat must flow around the physical obstruction. The longer heat flow path results in a fall in the effective thermal conductivity of the medium compared to the intrinsic thermal conductivity of the bulk material. This deviation can be quantified in terms of thermal tortuosity [79, 80]. In a volume-averaged BTE model, we consider homogenized domains without any structural information. Hence it is of great importance to include the deviation from bulk properties due to tortuosity of the domain through the volume-averaged relaxation time $\bar{\tau}$.

In the Fourier limit when $\bar{\tau} \ll \tau_B$ and $v\bar{\tau}/L \ll 1$, using equations (24)-(28), the volume-averaged BTE yields an effective thermal conductivity of:

$$K_{eff} = \frac{1}{3} C_v v_g^2 \alpha \bar{\tau} \qquad (30)$$

We will further employ the Bruggeman theory for composites in determining a functional relationship between the effective and bulk thermal conductivity of a nanocomposite. Bruggeman theory for composites is widely used in the battery community for both thermal and electrochemical simulations [81, 82]. In the Fourier limit, Bruggeman theory [83] for effective thermal conductivity for a composite system with a range of sizes of thermally non-interfering spherical inclusions can be expressed as:

$$K_{eff} = K_{bulk}(\alpha)^{d} \qquad (31)$$

Where, the bulk thermal conductivity K_{bulk} is given by $C_v v^2 \tau/3$, α is the solid volume fraction of the composite and d is the Bruggeman exponent and is equal to 1.5 for spherical shapes under the aforementioned assumptions. Without a range of sizes for the spheres, we expect departure from the Bruggeman exponent value of 1.5. To account for this departure, we solve for heat conduction in the composite domain at the Fourier limit for K_{eff}. A Fourier conduction simulation of a periodic unit cell with inclusions is conducted with a solid (intrinsic) thermal conductivity of $\frac{1}{3} C_v v_g^2 \tau$ to obtain an effective thermal conductivity. With known bulk and effective thermal conductivity, we determine the exponent, d, using equation (31).

Using equations (30) and (31), we get:

$$\bar{\tau} = \tau(\alpha)^{d-1} \qquad (32)$$

Where, $\bar{\tau}$ is the volume-averaged relaxation time and τ is the bulk relaxation time parameter. Thus, the value of $\bar{\tau}$ is found by calibrating it to the effective thermal conductivity found from direct numerical simulation of Fourier conduction in a periodic

unit cell domain. The value of $\bar{\tau}$ thus computed is an input to the volume-averaged BTE model.

2.3.2 Determination of Interface Scattering Relaxation Time τ_B

In the diffuse limit $\bar{\tau} \to \infty$ and $\frac{v_g \tau_B}{L} \ll 1$, i.e., in the limit when transport is dominated by boundary scattering on the inclusions, the volume-averaged BTE yields the effective thermal conductivity given by Eq. (29). We determine τ_B from equation (29). This may be used directly in the volume-averaged BTE model for isotropic scattering. For anisotropic scattering, however, this value is only an approximation. It is obtained by calibration against the effective thermal conductivity obtained by a direct numerical simulation in a fully-resolved periodic unit cell in the limit $\bar{\tau} \to \infty$ such that:

$$K_{eff,Volume-Averaged\ BTE} = K_{Ballistic,\ DNS} \quad (33)$$

The value of τ_B thus calibrated is used as an input to the volume-averaged BTE model.

2.3.3 Scattering Phase Function $\phi_{kk'}$

The scattering phase function, $\Phi_{kk'}$, in the volume-averaged model is determined using a ray tracing technique, similar to that used in radiative transport [64]. This treatment is valid in the geometric optics limit, when the wavelength of the dominant phonon groups is smaller than the length scale of the inclusions. Alternative treatments accounting for wave effects may also be used to deduce $\Phi_{kk'}$ when this condition is not satisfied [63]. We verify the ray tracing with an analytical formulation for large diffusely-reflecting spheres in the geometric optics limit [63]. The procedure is briefly explained here.

Computation of $\phi_{kk'}$: Ray Tracing Methodology and Validation

Consider the computation of $\Phi_{kk'}$ for the case of a large diffusely-reflecting sphere. We consider incoming phonons with intensity $I_k \left(= v_g \langle e_k^{"} \rangle\right)$ incident on the sphere from a direction, $\mathbf{K}'$ and reflected into direction, **K** (Figure 4).

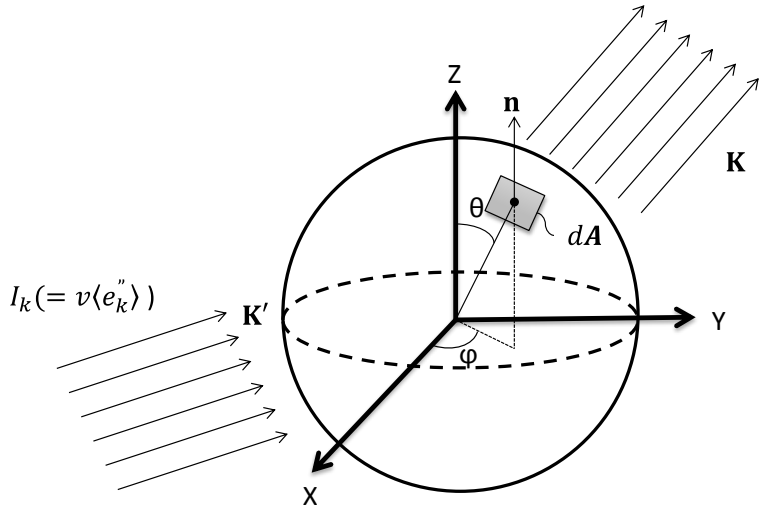

Figure 4: Scattering of incident rays by a large diffusely reflecting sphere

Here $\Phi_{kk'}$ is proportional to the scattered intensity to the total scattered flux. We consider reflection from a differential area $d\boldsymbol{A}$ on the sphere with outward normal **n**. The incident rate of phonon energy received by the differential surface is given by:

$$I_k(-\mathbf{n}\bullet\mathbf{K}')d\boldsymbol{A} = I_k \cos(\theta_i) d\boldsymbol{A} \qquad (34)$$

The rate of phonon energy leaving the surface in the direction **K** is given by:

$$I_k(-\mathbf{n}\bullet\mathbf{K}')(\mathbf{n}\bullet\mathbf{K})d\boldsymbol{A} = I_k \cos(\theta_i)\cos(\theta_o) d\boldsymbol{A} \qquad (35)$$

Here θ_i is the angle between the incident ray and the normal, and θ_o is the angle between the reflected ray and the normal. The value of $\Phi_{kk'}$ is given by:

$$\Phi_{kk\prime} = \frac{F_{kk\prime}}{\sum_k F_{kk\prime}} \qquad (36)$$

where,

$F_{kk\prime}$= Sum of rate of phonon energy in rays reflected in the **K** direction that are contributions of incoming rays from direction **K'**. Note that the rate for each ray is computed by Eq. (35) and is determined by the normal at its points of impact.

$\sum_k F_{kk\prime}$=Total rate of phonon energy in the reflected rays in all directions that are produced by incident rays in **K'**.

To compute the above formula numerically, we define a spherical surface surrounding the inclusion (sphere or cylinder) from which the rays originate. Using a random number generator, we pick a location uniformly at random on the external surface as a point of origin for the incoming ray (Figure 5).

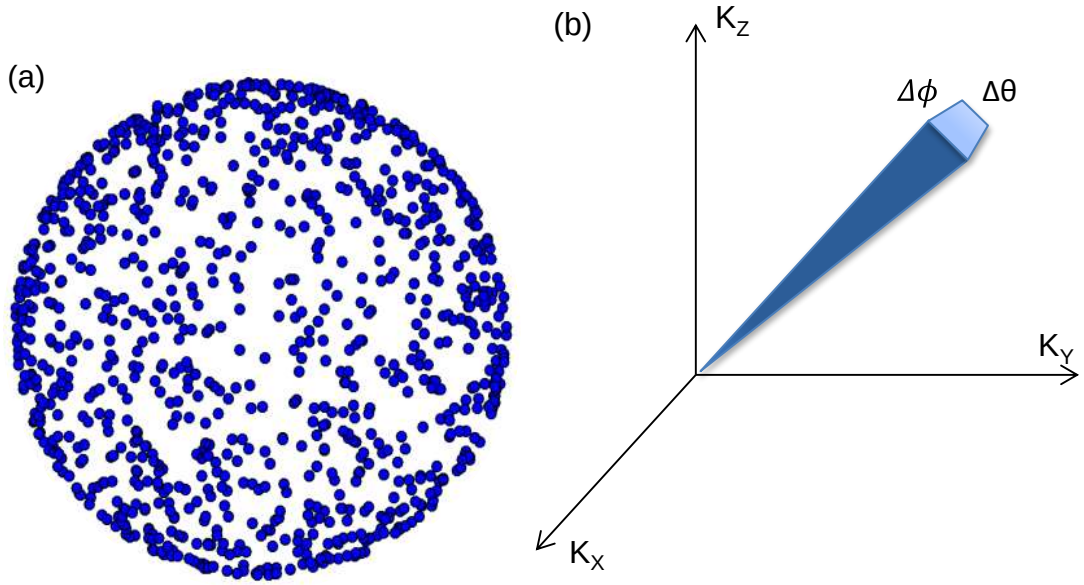

Figure 5: (a) Points of origin of fired rays on the external sphere. (b) Spherical coordinate system for rays.

The rays are defined using a spherical coordinate system as shown, where $0 < \theta < \pi$ and $0 < \phi < 2\pi$. The ray directions belong to the discretization domain N_θ x $N_\emptyset$ which is the same as the phonon discretization of the spherical Brillouin zone (BZ).

We calculate the point of intersection of the incoming ray with the inclusion surface. For every intersecting incoming ray, the reflected ray is chosen randomly in a direction on the hyperspace separated by the tangent plane on the sphere (Figure 6). We generate multiple rays with different directions from each location of the external surface and repeat the process for all locations over the external sphere. We allocate the phonon energy rate for all incoming and outgoing ray pairs to their respective discretized **K**-space bins using Eq. (35).

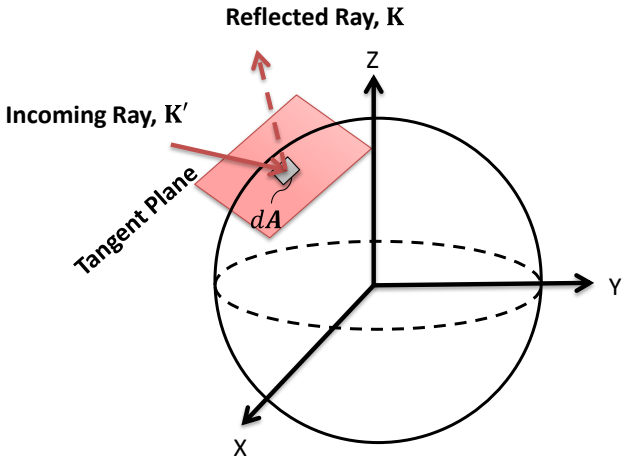

Figure 6: Reflection on the surface of a spherical inclusion

Finally we compute the scattering phase function $\Phi_{kk'}$ as the ratio of the scattered intensity to the total scattering heat flux using Eq. (36).

In Figure 7, the value of $\Phi_{kk'}$ obtained through ray tracing is plotted along with the average of the analytical value over the solid angle of each discretization. The x-axis is Θ/π, where Θ is the angle between incident and reflected ray directions. This result is for a K-space discretization of (N_θ x N_ϕ =8x16). A total number N_θ x $N_\emptyset x 10^6$ rays were used for this computation. The scattering phase function obtained through ray tracing compares well with respect to the analytical solution.

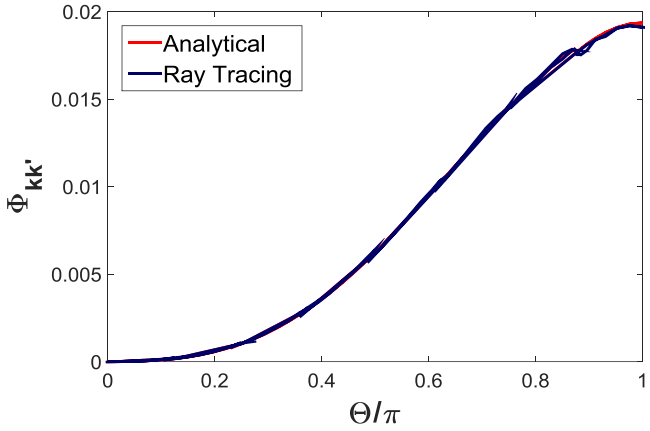

Figure 7: Comparison of ray traced and analytical scattering phase function for a large diffusely reflecting sphere. [63]

The normalized error with respect to the analytical solution is shown in Figure 8. We normalize using the maximum analytical $\Phi_{kk'}$ value.

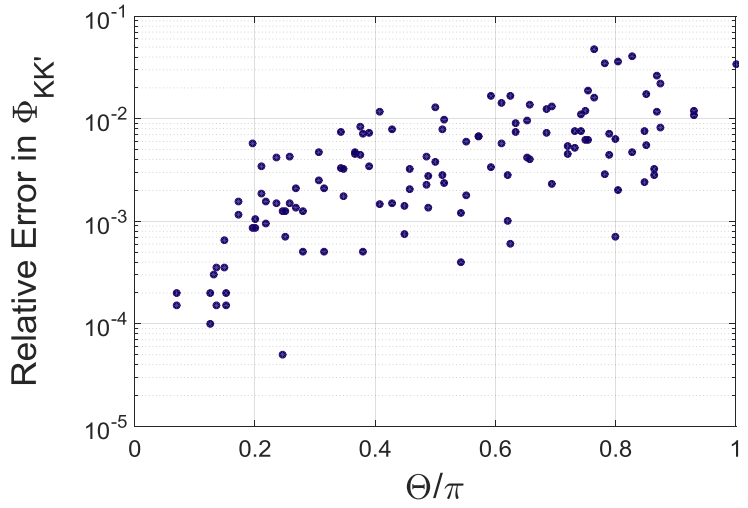

Figure 8: Relative error in $\boldsymbol{\Phi_{KK'}}$ for spherical inclusions

The scattering phase function for a cylindrical inclusion is determined using the same algorithm. Due to lack of analytical expressions for short cylinders in the geometric limit, we show $\Phi_{kk'}$ from the ray tracing method alone (Figure 9). The multiple lines is due to the same angle being formed by multiple discretized data points.

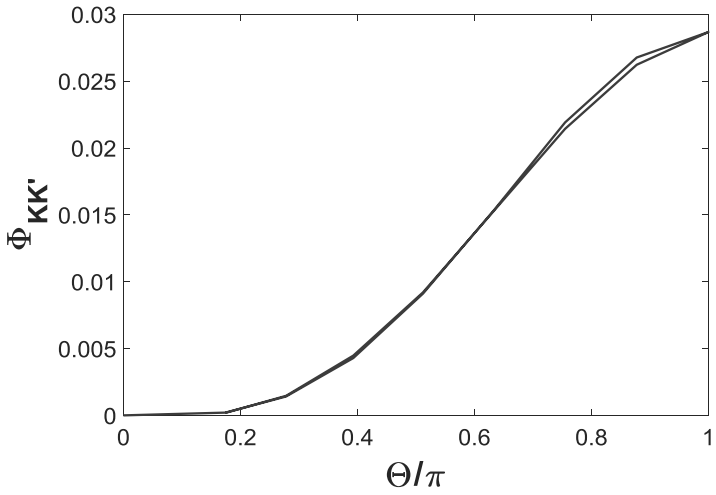

Figure 9: Scattering phase function for a short diffusely reflecting cylinder ($\theta = \frac{\pi}{2}, 0 < \emptyset < 2\pi$; aspect ratio $= 0.7$)

2.4 BOUNDARY CONDITIONS

For the problems considered in the present work, the volume-averaged phonon BTE is solved with the following boundary conditions: specified-temperature, wherein the population of phonons is governed by the Bose-Einstein distribution at the specified temperature, a reflecting or symmetry condition whereby phonons are reflected specularly or diffusely [54], and a periodic boundary condition, whereby the solution is performed on a periodic module across which a specified jump in lattice temperature is assumed to occur. This boundary condition is intended to model transport through a composite consisting of regularly repeating units. These are described below.

2.4.1 Specified Temperature

Specified-temperature boundaries are treated as diffusely emitting and completely absorbing. For a phonon whose group velocity vector points from the boundary into the domain, the boundary value is taken to be the equilibrium energy density at the boundary temperature. For a phonon whose group velocity vector points from the interior of the domain to the boundary, the phonon is assumed to be traveling ballistically out of the domain at the domain boundary such that:

$$\langle e_k" \rangle_{v.n<0}(\mathbf{x}_b) = \langle e_0 \rangle(\overline{T}_{wall}(\mathbf{x}_b))$$

$$\langle e_k" \rangle_{\mathbf{v.n<0}}(\mathbf{x}_b) = \langle e_k" \rangle_{\mathbf{v.n<0}}(\mathbf{x}_b^-) \qquad (37)$$

Here, $\mathbf{x}_b$ is the spatial location of the boundary, $\mathbf{n}$ is the outward pointing normal of the boundary, and $\mathbf{x}_b^-$ is a location in the domain interior just upwind of the boundary.

2.4.2 Reflecting Boundary

Reflecting boundaries may be fully specular, fully diffuse, or partially specular/diffuse. For specular reflection, the energy of a phonon incoming to the wall is reflected into a phonon with the same tangential wave vector component with opposite normal wave vector component. For diffuse reflection, the energy of all incoming phonons to the wall is reflected equally to all out-going phonons. The reflecting boundary condition may be written as:

$$\langle e_k" \rangle_{v.n<0}(\mathbf{x}_b) = p\langle e_k" \rangle(\mathbf{x}_b, \mathbf{K}_{spec}) + (1-p)\langle e_0 \rangle(\bar{T}_{diffuse})$$

$$\mathbf{K}_{spec} = \mathbf{K} - 2(\mathbf{K}.\mathbf{n})\mathbf{n}$$

$$\langle e_0 \rangle(\bar{T}_{diffuse}) = \frac{\hbar\omega}{exp\left(\frac{\hbar\omega}{k_B \bar{T}_{diffuse}}\right)-1} \qquad (38)$$

where p is the specularity of the wall, a number between zero and one. $\mathbf{K}_{spec}$ is the specular direction corresponding to the **K** vector of interest. $\langle e_0 \rangle(\bar{T}_{diffuse})$ is the equilibrium distribution function at the equilibrium temperature corresponding to the incoming energy. The temperature, $\bar{T}_{diffuse}$, is found through a non-linear solution of the following conservation equation:

$$\int_{\mathbf{v}.\mathbf{n}<0} \langle e_0 \rangle(\bar{T}_{diffuse})\mathbf{v}.\mathbf{n}\, d^3\mathbf{K} = \int_{\mathbf{v}.\mathbf{n}>0} \langle e_k" \rangle \mathbf{v}.\mathbf{n}\, d^3\mathbf{K} \qquad (39)$$

2.4.3 Periodic Jump Boundary

A periodic jump boundary condition is used to simulate the heat transfer in periodic structures in the bulk limit [10] as shown in Figure 10. In this limit, the temperature of each periodic module of length L_P must fall by a constant amount in the direction of heat flow, "**t**".

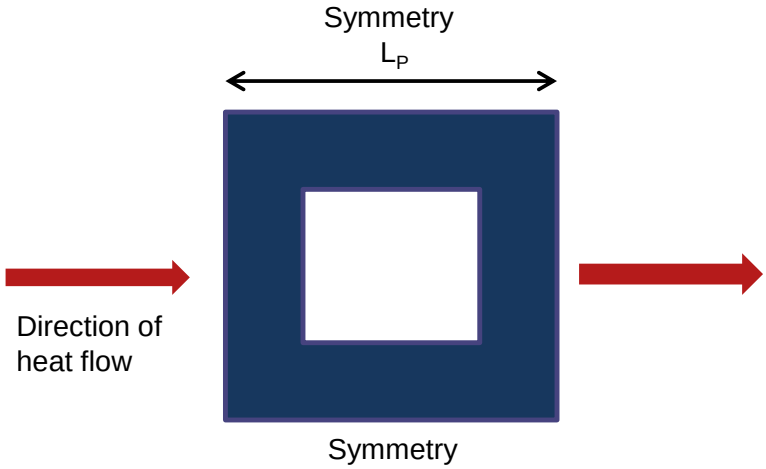

Figure 10: Periodic Unit Cell

Correspondingly, the energy densities at the unit cell boundaries perpendicular to the heat flow direction must be related by:

$$\text{For } \mathbf{n}.\mathbf{t} > 0: \qquad \langle e_k"(0,y)\rangle = \langle e_k"(\mathrm{L_P},y)\rangle + \frac{1}{4\pi} C_{v,\Delta K} \Delta T_{drop}$$

$$\text{For } \mathbf{n}.\mathbf{t} < 0: \qquad \langle e_k"(\mathrm{L_P},y)\rangle = \langle e_k"(0,y)\rangle - \frac{1}{4\pi} C_{v,\Delta K} \Delta T_{drop} \qquad (40)$$

Where, ΔT_{drop} signifies temperature drop in the unit cell in the heat flow direction"**t**". The problem is linear because $C_{v,\Delta K}$ is independent of lattice temperature.

2.5 CLOSURE

In this chapter we developed the volume-averaged model for BTE for a nanoporous composite. We discussed the procedure to determine the different model parameters and the boundary conditions under a gray approximation of the phonon dispersion. In the next chapter, we will discuss the volume-averaged BTE model for a nanoporous composite using a non-gray approximation.

Chapter 3: Non-Gray Volume-Averaged Theory for Phonon Boltzmann Transport Equation (BTE) in Nanoporous Composites

In this chapter we expand the volume-averaged BTE developed in chapter 2 to include effects of the full **K**-space resolved phonon dispersion and the wave-vector and polarization dependence of phonon mean free paths. We refer to this as the **K**-resolved or non-gray theory. For non-gray transport, the Brillouin zone is discretized into a number of **K** points. For each discrete **K**-point of the Brillouin zone, a phonon BTE needs to be solved. This results in as many BTEs as there are are discrete **K** points in the Brillouin zone. Thus, there are an equivalent number of interface scattering relaxation times $\tau_{B,k}$ to be determined, along with a number of volume-averaged bulk relaxation time $\overline{\tau}_k$. This is in contrast to the gray model, where only a single volume-averaged bulk relaxation time and a single interface scattering relaxation times. This difference is due to the non-gray approximation that each phonon mode has different properties based on the material's phonon dispersion curves. We include the effects of non-gray dispersion through appropriately calibrating the volume-averaged bulk relaxation times $\overline{\tau}_k$ to the Fourier limit solution and the interface scattering relaxation times, $\tau_{B,k}$ to the ballistic limit heat transfer rate using a Newton Rhapson iterative procedure. Finally, we describe the procedure to adapt the scattering phase function evaluated using the ray tracing algorithm to account for the different phonon polarizations. Finally, we present an algorithm to set up a non-gray volume-averaged BTE problem using the methodology developed in this chapter.

3.1 K-Resolved Volume-Averaged Phonon Boltzmann Transport Equation

We build upon the derivation of the volume-averaged BTE for nanoporous domains under a gray approximation. We begin by considering Eq. (10) in chapter 2. For a non-gray phonon dispersion, the surface integral involving phonons incoming to the solid matrix ($\mathbf{v}.\mathbf{n} > 0$) is modeled as:

$$\frac{1}{V}\int_{S,\mathbf{v}.\mathbf{n}>0}\langle e"\rangle \mathbf{v}.\mathbf{n}\, ds = \frac{\langle e_k"\rangle}{\tau_{B,k}} \qquad (41)$$

The second surface integral term in Eq. (10) for ($\mathbf{v}.\mathbf{n} < 0$) is modeled as:

$$\frac{1}{V}\int_{S,\mathbf{v}.\mathbf{n}<0}\langle e"\rangle \mathbf{v}.\mathbf{n}\, ds = -\frac{1}{\tau_{B,k}}\frac{1}{V_{BZ}}\int_{\mathbf{K}'}\Phi_{kk'}\,\langle e_{k'}{}"\rangle d^3\mathbf{K}' \qquad (42)$$

The relaxation time is no longer a single value for all **K** points in this **K**-resolved (non-gray) approximation; therefore, each "k" point pertaining to a given **K**-space point in the Brillouin zone has a different relaxation time to account for the phonon polarization. Therefore, we may write the volume-averaged BTE as:

$$\alpha\nabla\cdot\mathbf{v}\langle e_k"\rangle = \alpha\frac{\langle e_0\rangle-\langle e_k"\rangle}{\overline{\tau_k}} - \frac{\langle e_k"\rangle}{\tau_{B,k}} + \frac{1}{V_{BZ}}\frac{1}{\tau_{B,k}}\int_{\mathbf{K}'}\Phi_{kk'}\,\langle e_{k'}{}"\rangle d^3\mathbf{K}' \qquad (43)$$

We note that the difference in the non-gray volume-averaged BTE from the gray model is the number of BTEs to be solved. Each BTE has a unique relaxation time and therefore, the total number of equations and model parameters to be determined is equal to the discretization of the Brillouin zone.

3.2 Model Methodology for K-Resolved Phonon Transport

For non-gray phonon dispersions, we approximate the Brillouin zone as a sphere. The sphere is discretized into $N_\theta x N_\phi$ discrete solid angles, and the radius of the Brillouin

zone $K_{max}|$ is discretized into N_k divisions. Furthermore, there are N_{pol} phonon polarizaitons. Thus there are $N_\theta x N_\phi x N_k$discrete points in the Brillouin zone, resulting in as many phonon BTEs to be solved. Thus a non-gray problem engenders $(N_k x N_{pol})$ times more computational expense than a gray approximation for the same physical geometry. The volume-averaged BTE model reduces the physical mesh requirement since inclusions do not need to be resolved, thereby reducing the overall numerical expense. Indeed, the volume-averaged equations are one-dimensional in physical space for all the problems presented in this thesis, whereas the DNS solutions are three-dimensional. For the volume-averaged model to be solved on the representative elemental volume, we need to evaluate the model parameters $\bar{\tau}_k$ and $\tau_{B,k}$ which are functions of the **K**-space. The scattering phase function $\Phi_{\mathbf{KK}'}$ requires evaluation for the non-gray phonon dispersion as well. We will describe each of these processes below.

3.2.1 Determination of Volume-Averaged Relaxation Time $\bar{\tau}_k$

We will account for thermal tortuosity in the nanoporous domain due to the presence of pores using a method similar to that for the gray model. In the non-gray volume-averaged BTE model, we need to evaluate the volume-averaged bulk relaxation time $\bar{\tau}_k$ at each **K**-point. We include this departure from bulk properties using the exponent d [Eq. (31)] similar to that in chapter 2. First we solve a Fourier conduction problem on a periodic unit cell with fully-resolved inclusions. Using a known bulk intrinsic thermal conductivity of the material and having found the effective thermal

conductivity from the simulation, we determine the exponent, d, using equation (31). From equation (32), we determine $\bar{\tau}_k$ at each **K**-point using:

$$\bar{\tau}_{\mathrm{k}} = \tau_k(\alpha)^{\mathrm{d}-1} \qquad (44)$$

where, $\bar{\tau}_k$ is the volume-averaged bulk relaxation time and τ_{k} is the bulk relaxation time parameter at point **K** in the discretized wave vector space. The details of determining bulk relaxation times are discussed in chapter 6.

The effective thermal conductivity obtained from the direct numerical simulation of Fourier conduction in a periodic unit cell domain is, therefore, used to calibrate values of $\bar{\tau}_k$s. The set of $\bar{\tau}_k s$ thus computed is used as an input to the non-gray volume-averaged BTE model.

3.2.2 Determination of Interface Scattering Relaxation Time $\tau_{\mathrm{B,k}}$

Under the elastic scattering assumption, energy scattered at the interface is assumed to be redistributed without a change in wave vector and polarization. Thus, for a given phonon polarization (N_{pol}) and wave vector discretization(N_k), conservation principles dictate that phonon energy may be re-distributed between the different angular discretizations (N_θ, N_ϕ). Therefore, under this approximation, only $N(= N_{pol}\, x\, N_k)$ numbers of interface scattering relaxation times are required. Furthermore, it is possible to simplify the problem further and ascribe a single boundary scattering time scale, τ_B , for all the **K** points and polarizations if desired. We investigate both options in this thesis.

To determine the interface scattering relaxation times, we calibrate them to the thermal conductivity at the ballistic limit. As discussed in chapter 2, the calibration requires:

$$K_{eff,Volume-Averaged\ BTE} = K_{Ballistic,\ \ DNS} \quad (45)$$

In order to resolve all the N values of $\tau_{B,k}$, the individual contributions to the total heat rate of each discretized **K** -point for each polarization also be matched.

Therefore,

$$\sum_{BZ} q_{k,Volume-Averaged\ BTE} = \sum_{BZ} q_{k,DNS} \quad (46)$$

$$q_{k,Volume-Averaged\ BTE} = q_{k,DNS} \quad (47)$$

The system of Eqs. (47) are coupled in **K** space through the out-scattering term. Therefore, an optimization scheme is required to meet the constraints of Eq. (46) and (47). We choose to apply a Newton-Raphson iterative scheme to determine the N number of unknown $\tau_{B,k}$ values, given the N values of the K-resolved DNS heat transfer rates $q_{k,DNS}$.

A good starting guess for the $\tau_{B,k}$ values may be obtained from Eq. (26) in Chapter 2. In the isotropic limit, the effective thermal conductivity may be written as:

$$K_{eff} = \sum_{BZ} \left(\frac{de_0}{dT}\right)_k v_k . v_k \alpha^2 \tau_{B,k} \Delta^3 K \quad (48a)$$

Assuming each of the N individual BTEs to be independent, $\tau_{B,k}$ may be estimated from:

$$q_{k,DNS} = \left(\frac{de_0}{dT}\right)_k v_k . v_k \alpha^2 \tau_{B,k} \Delta^3 K \quad (48b)$$

Since the scattering phase function is not generally isotropic, Eq. (48b) is only approximate, and must be improved through Newton Raphson iteration.

Newton-Raphson Iterative Procedure

The Newton-Raphson method is a popular root-finding method which may be applied to multivariate problems. For a single-variable problem for function $f(x)$, the method estimates a root, x_1 such that:

$$x_1 = x_0 - \frac{f(x_0)}{f'(x_0)} \qquad (49)$$

where x_0 is an initial guess and $f'(x_0)$ is the function's derivative. The tangent of the function $f(x_0)$ intersects the x-axis at $(x_1, 0)$. The method is iterated until an accurate solution is achieved, such that,

$$x_{n+1} = x_n - \frac{f(x_n)}{f'(x_n)} \qquad (50)$$

For a multi-variable problem, a Jacobian consisting of the partial derivatives of the function with respect to the unknown variable is determined from previous guesses. We make an initial guess for a set of $\tau_{B,k}$'s and solve for the heat rate q_k's. Using this data, we generate a function $q(\tau_{B,k})$. The system is thus solved for $\tau_{B,k}$ using:

$$\tau_{B,k,new} = \tau_{B,k,old} - J\left(\tau_{B,k,old}\right)^{-1}\left(q_{desired} - q(\tau_{B,k,old})\right) \qquad (51)$$

where J is the Jacobian of function $q(\tau_{B,k})$. The Jacobian is computed as follows:

$$J(\tau_{B,1}, \tau_{B,2}, .., \tau_{B,N}) = \begin{bmatrix} \partial q_1/\partial\tau_{B,1} & \partial q_1/\partial\tau_{B,2} & . & . & \partial q_1/\partial\tau_{B,N-1} & \partial q_1/\partial\tau_{B,N} \\ \partial q_2/\partial\tau_{B,1} & \partial q_2/\partial\tau_{B,2} & & & . & . \\ . & & \partial q_1/\partial\tau_{B,1} & & . & . \\ . & . & & . & . & . \\ . & . & & & . & . \\ . & . & & & . & . \\ \partial q_{N-1}/\partial\tau_{B,1} & . & & & . & . \\ \partial q_N/\partial\tau_{B,1} & . & . & . . . & \partial q_{N-1}/\partial\tau_{B,N-1} & \partial q_N/\partial\tau_{B,N} \end{bmatrix}_{NxN} \qquad (52)$$

where N is $\left(N_k x N_{pol}\right)$. The Jacobian in Eq. (52) is approximated by its diagonal for simplicity. This does not the final solution for $\tau_{B,k}$, only the path to solution. If the off-diagonal terms are large, slow convergence, or even divergence may occur. For the problems computed in this thesis, we found the diagonal approximation to be adequate. The derivatives $\partial q_N / \partial \tau_{B,N}$ in Eq. (52) were found using a finite difference approximation. We iterate until Eqs. (46) and (47) are satisfied within 2% of the direct numerical solution.

In Figure 11 we demonstrate a Newton-Raphson procedure to predict a set of $\tau_{B,k}$ that satisfies Eqs. (45) – (47) for a periodic unit with a cylindrical inclusion. We assume a spherical Brillouin zone with angular discretization of $(N_\theta x N_\phi)$=2x8, a radial discretization of $N_k = 8$ and $N_{pol} = 4$ as the total number of phonon polarizations. Therefore, there are $\left(N_k x N_{pol}\right) = 32$ unique values of $\tau_{B,k}$. We pick a constant $\tau_{B,k}$ for all the **K** –points as an initial guess such that Eq. (45) is satisfied. The solution converges within four iterations.

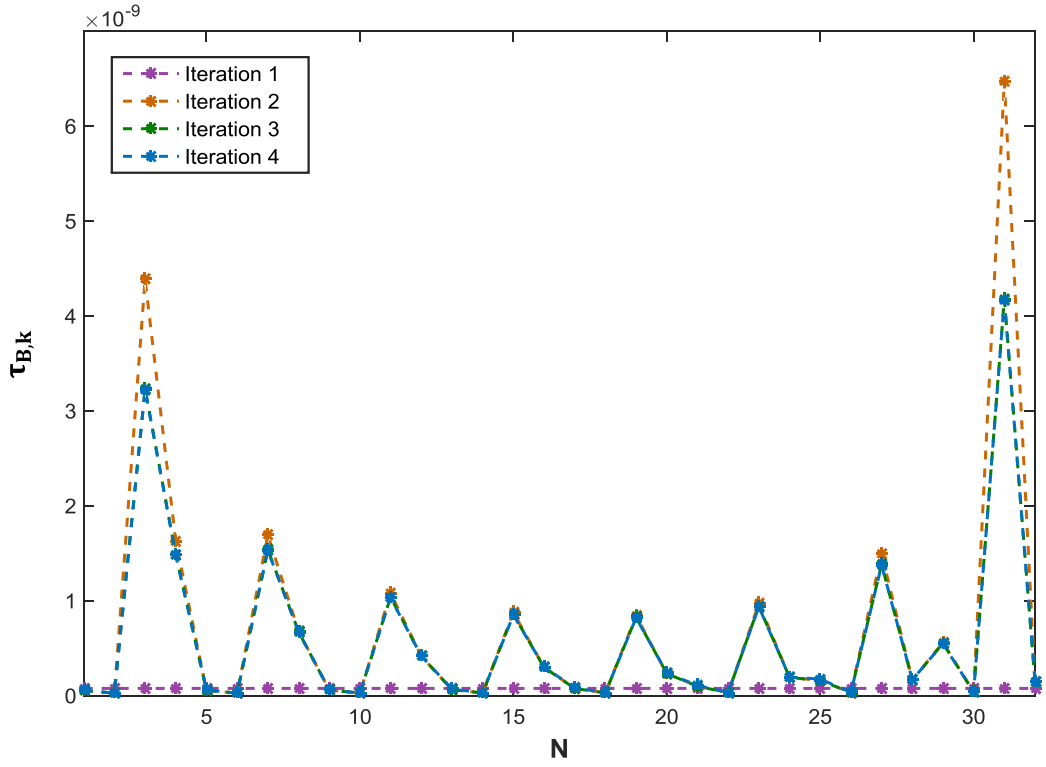

Figure 1: Newton-Raphson iteration for $\tau_{B,k}$

Figures (12) - (15) show the convergence of the predicted heat rate contribution for each polarization with each Newton-Raphson iteration of $\tau_{B,k}$. A faster convergence is observed for the longitudinal phonon modes [Figures (13) and (15]) compared to the transverse modes (Figures (12) and (14)].

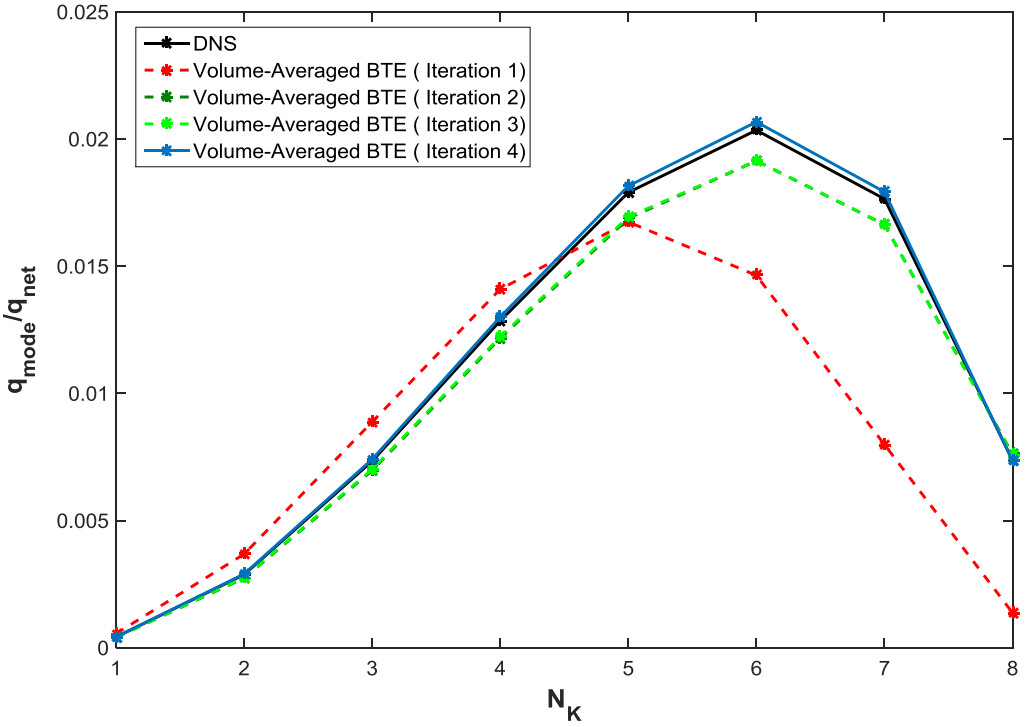

Figure 2: Convergence using Newton-Raphson iterative scheme for transverse acoustic (TA) branch of phonon dispersion.

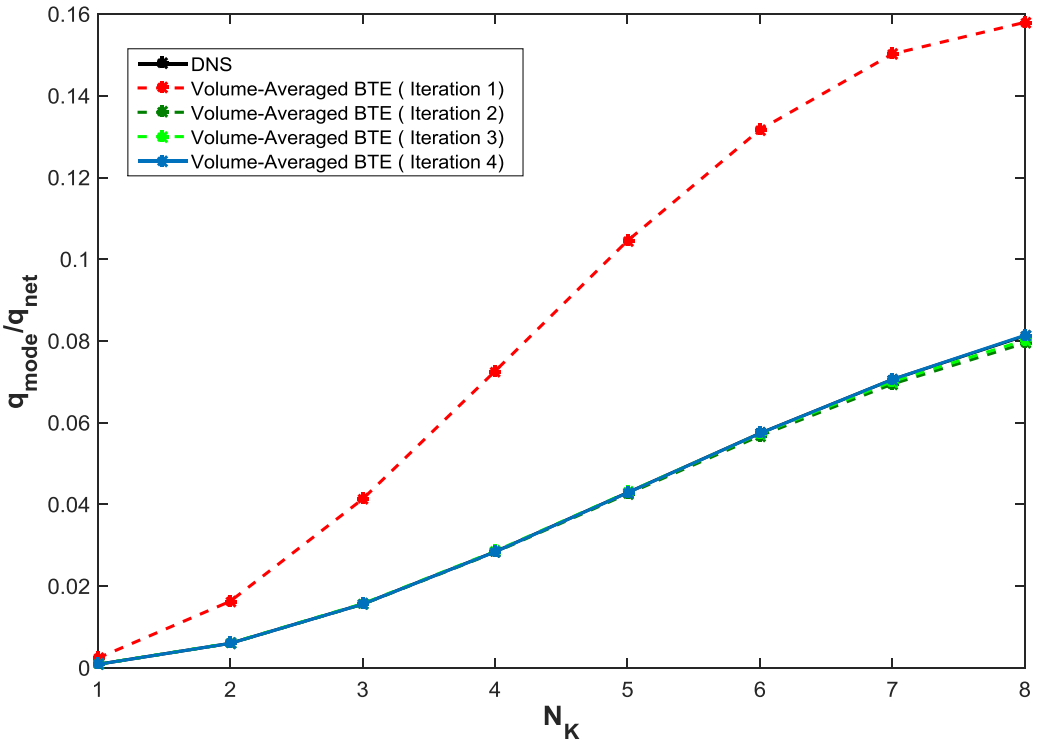

Figure 3: Convergence using Newton-Raphson iterative scheme for longitudinal acoustic (LA) branch of phonon dispersion.

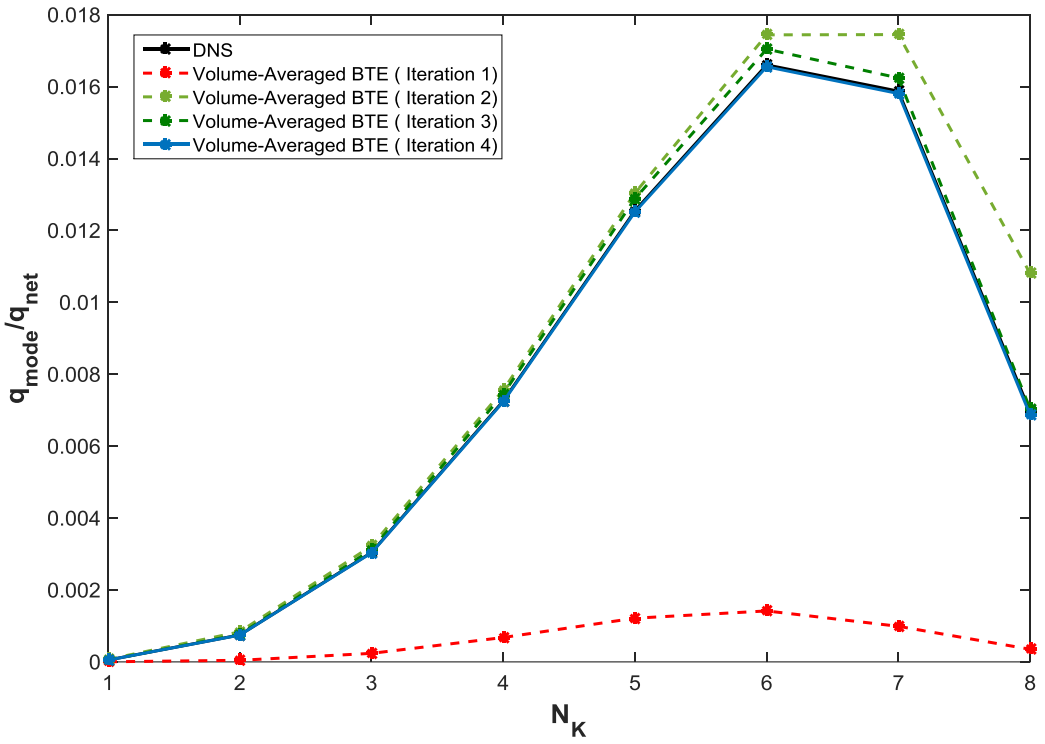

Figure 4: Convergence using Newton-Raphson iterative scheme for transverse optical (TO) branch of phonon dispersion.

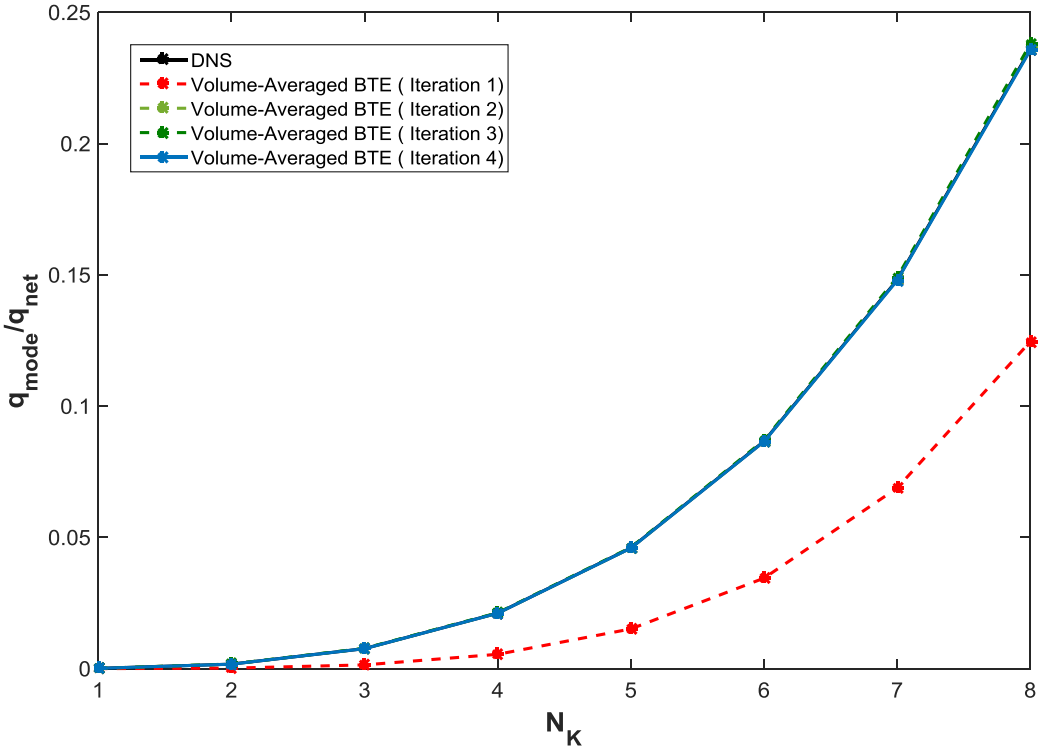

Figure 5: Convergence using Newton-Raphson iterative scheme for longitudinal optical (LO) branch of phonon dispersion.

3.2.3 Computation of Scattering Phase Function $\phi_{KK'}$

The scattering phase function is computed using the general ray tracing algorithm discussed in chapter 2. Under an elastic scattering assumption, phonon-phonon scattering is assumed not redistribute energy between phonons of different wave vectors and polarizations; all energy re-distribution is between phonons of the the same K value and polarization. Thus, in a spherical coordinates discretization of the Brillouin zone, energy is redistributed between different angular discretization (N_θ, N_ϕ) for a given radial discretization(N_k) and for a given polarization N_{pol}. Therefore the scattering phase function matrix needs to be expanded to account for this.

For a gray approximation, there is only one phonon mode or polarization and no radial discretization of the Brillouin zone. As a result the $\Phi_{\mathbf{KK'}}$ matrix is of size $(N_\theta x N_\phi) x (N_\theta x N_\phi)$. For a non-gray approximation, the $\Phi_{\mathbf{KK'}}$ matrix is a block diagonal matrix of size $(N_\theta x N_\phi x N_k x N_{pol}) x (N_\theta x N_\phi x N_k x N_{pol})$. The block diagonal nature of the matrix is due to the lack of interaction between the different polarizations and radial discretizations. Since phonons of different angular discretization for a given (N_k, N_{pol}) interact in the same way as for a gray approximation, we can expand the scattering phase function matrix to repeat for different polarizations and radial discretizations.

For illustration, in a gray problem with an angular discretization of $(N_\theta x N_\phi) = (2x2)$, the scattering phase function $\Phi_{\mathbf{KK'}}$ matrix will have $(N_\theta x N_\phi) x (N_\theta x N_\phi)$ number of matrix elements. Under the elastic scattering assumption, phonons in wave vector $\mathbf{K'}$are reflected into the **K** direction without a change in phonon frequency and polarization.

The scattering phase function matrix for a gray approximation will therefore be:

$$[\Phi_{\mathbf{KK'}}] = \begin{bmatrix} \Phi_{11} & \Phi_{12} & \Phi_{13} & \Phi_{14} \\ \Phi_{21} & \Phi_{22} & \Phi_{23} & \Phi_{24} \\ \Phi_{31} & \Phi_{32} & \Phi_{33} & \Phi_{34} \\ \Phi_{41} & \Phi_{42} & \Phi_{43} & \Phi_{44} \end{bmatrix} \quad (53)$$

In the non-gray limit with four phonon polarization mode, $N_{pol} = 4$ and a radial discretization of $N_k = 2$, for the same angular discretization as the gray example, the matrix $\Phi_{\mathbf{KK'}}$ will be of size $(N_\theta x N_\phi x N_k x N_{pol})\ x\ (N_\theta x N_\phi x N_k x N_{pol}) (= 32x32)$.

However, from the assumption of elastic scattering, phonons in $\mathbf{K}'$ belonging to a given (N_{pol}, N_k) will not be reflected in to a **K** direction belonging to a different (N_{pol}, N_k). Therefore, we have a sparse block matrix for $\Phi_{\mathbf{KK}'}$ of the order NxN where $N = (N_\theta x N_\phi x N_k x N_{pol})$.

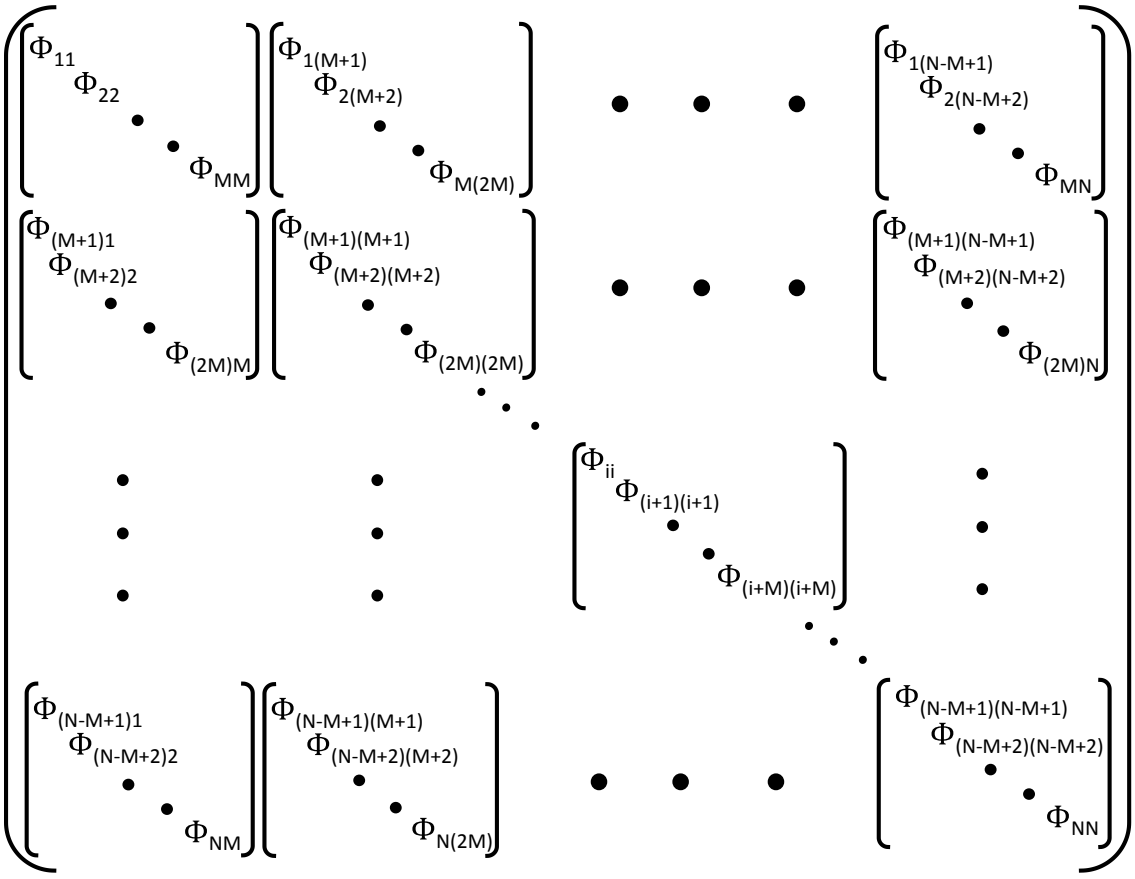

(54)

Here the index $M = (N_k x N_{pol})$.

In the next section, we briefly outline the steps in solving a non-gray volume-averaged BTE model on a nanoporous domain.

3.3 FLOWCHART FOR A NON-GRAY SOLUTION

The flow chart for the solution of non-gray phonon transport in a nanoporous domain may be summarized by the steps below.

STEP 1: We solve the BTE in a nanoporous periodic unit in the Fourier and ballistic limits

STEP 2: Determine the scattering phase function, $\Phi_{KK'}$using the ray-tracing algorithm accounting for different polarizations and discretization.

STEP 3: Using Eq. (32) and the Fourier limit solution we determine the volume-averaged bulk relaxation times ($\overline{\tau_k}$) for non-gray phonon dispersion.

STEP 4: We calibrate $\tau_{B,k}$using the Newton-Rhapson iterative procedure to match the ballistic limit solution

STEP 5: Solve the volume-averaged BTE under a non-gray approximation by using realistic material properties and the relaxation times computed in steps 3 and 4.

3.4 CLOSURE

In this chapter we discussed the volume-averaged model for BTE for a nanoporous composite using a non-gray approximation. We discussed the procedures to determine the different model parameters and presented a flowchart for solving a volume-averaged BTE for non-gray transport. In the next chapter, we will discuss the volume-averaged BTE model for a two-material nanocomposite, and include a scattering phase function for phonon-phonon scattering in the Mie limit.

Chapter 4: Volume-Averaged Theory for BTE in Nanocomposite Domains

In developing the next generation of thermoelectric materials for energy storage and conversion, two distinct approaches have been undertaken traditionally [84]. One involves developing thermoelectric materials with advanced bulk properties [85]. The second approach uses low-dimensional materials [68]. Recent advancements involve merging the two efforts by utilizing thermoelectric materials with advanced bulk properties as a host in a matrix of engineered nanoscale inclusions [86]. Therefore, nanocomposite structuring has become an important technique for optimizing efficiency in thermoelectrics [84].

Characterization of transport properties in engineered nanocomposite thermoelectric materials is challenging especially in relation to thermal transport [87]. In designing advanced nanocomposites with varying particle geometries, the ability to predict thermal properties computationally is, therefore, of great value. The nanocomposites are particularly designed to reduce the thermal conductivity by enhancing interface scattering and suppressing thermal transport through a mismatch in phonon spectra. This is possible through appropriate distribution of composite particles of varying geometries and different phonon dispersions in host and particles in the composite matrix. Figure 16 shows the different phonon dispersion curves for Silicon and Germanium and a comparison of the phonon mean free paths. Certain high-frequency phonons in Si are absent in Ge along and phonon group velocities in Si, particularly in the LA mode, are higher.

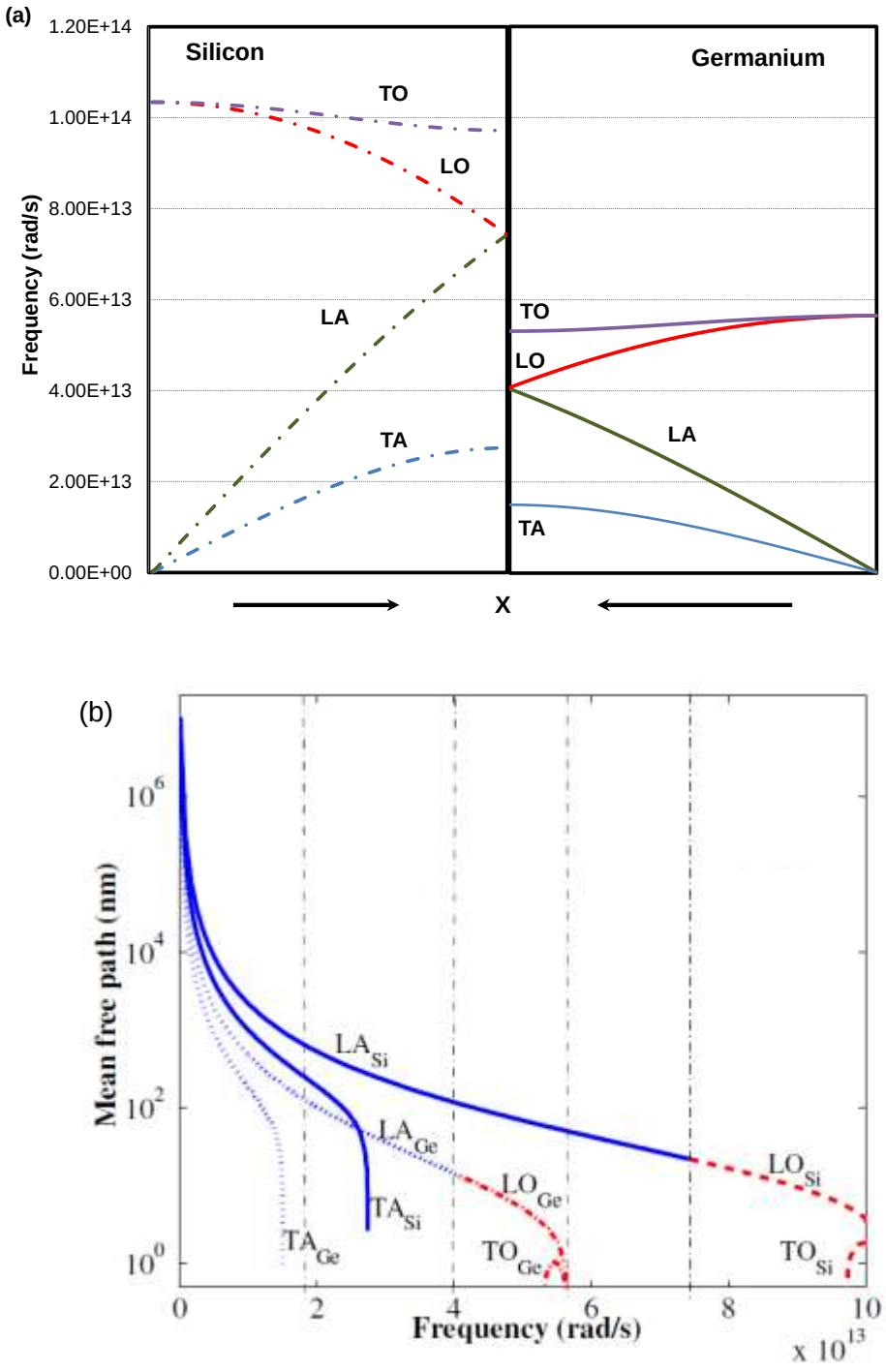

Figure 6: (a) Phonon dispersion in Si and Ge along [100]. (b) Mean free path of phonons in Si and Ge [10]

4.1 VOLUME-AVERAGED PHONON BOLTZMANN TRANSPORT EQUATION IN TWO-MATERIAL COMPOSITE

In this section we will extend our nanoporous formulation to consider two-material composites. The nanocomposite under consideration has particles of a second material embedded in a host material, as shown in Figure 17.

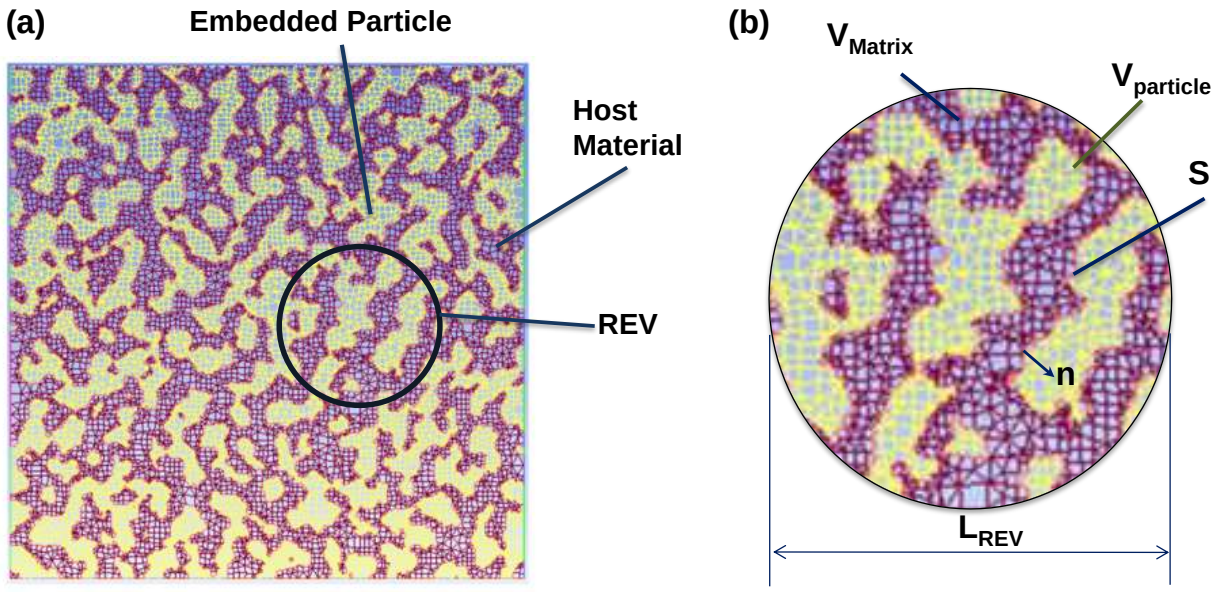

Figure 7: (a) Particulate nanocomposite medium generated from a CT scan **[54]**. (b) Representative Elemental Volume (REV)

We consider a nanocomposite domain with particles of a second material embedded in the host matrix. In the development of this model, we will consider the phonon BTE of the host material and will model the particle in the composite as a scattering site, i.e., using the interface scattering relaxation time and the scattering phase function. Similar to the nanoporous volume-averaged BTE model development, we integrate the phonon BTE of the host material on the representative elemental volume (REV). Instead of the pore,

we will now consider the volume of the particle. We re-define a few operators for our present model:

$$V = V_{Matrix} + V_{particle}$$

$$\langle x \rangle = \frac{1}{V_{Matrix}} \int_{V_{Matrix}} x dV$$

$$\bar{x} = \frac{1}{V} \int_V \ x dV = \frac{1}{V} \int_{V_{Matrix}} x dV + \frac{1}{V} \int_{V_{particle}} x dV \qquad (55)$$

For this model, we consider very small particles, such that $\frac{1}{V} \int_{V_{particle}} x dV = 0$. Therefore,

$$\overline{x} = \alpha_m \langle x \rangle; \qquad \alpha_m = \frac{V_{Matrix}}{V} \qquad (56)$$

Here, $'V'$ is the volume of the REV, $'V_{Matrix}'$ is the volume of the host material and $'V_{particle}'$is the volume of the particles in the composite. The "–" variables represent volume averaged quantities and "< >" variables represent the intrinsic volume average of the quantity in the matrix.

By integrating the gray steady state BTE for the matrix material over the REV similar to the process developed in chapter 2 [Eqs. (5) - (9)], the resulting volume-averaged BTE for a two-material composite can be written as:

$$\alpha_m \nabla \cdot \mathbf{v} \langle e_k" \rangle = \alpha_m \frac{\langle e_0 \rangle - \langle e_k" \rangle}{\overline{\tau}} - \frac{\langle e_k" \rangle}{\tau_B} + \frac{1}{V_{BZ}} \frac{1}{\tau_B} \int_{\mathbf{K}'} \Phi_{kk'} \langle e_{k'}" \rangle d^3\mathbf{K}' \qquad (57)$$

where the subscript "k" pertains to a given **K**-space point in the Brillouin zone of the host material and the summation over **K** or $\mathbf{K}'$ is equivalent to summation over the entire

Brillouin zone volume V_{BZ} of the host. Equation (57) is the volume-averaged model for the composite in terms of the intrinsic energy density of the material in the REV.

As seen previously for the nanoporous volume-averaged BTE model, two different types of scattering terms appear in Eq. (57). The first term on the RHS, consisting of $\overline{\tau}$, results from phonon scattering in the bulk of the composite REV. The remaining two terms in the RHS consisting of the interface scattering relaxation time, τ_B, represent interface scattering in the domain due to the particles in the composite. Out-scattering at the interface, i.e., energy leaving the specific **K** phonon group, is represented by the second term on the RHS. The third term represents the in-scattering at the particle interface by considering energy transfer from other wave vectors to the current **K** point. The term α_m is the volume fraction of the host material in the composite REV.

The coupling between the different **K**-space points in the Brillouin zone is governed using the concept of energy conservation as previously stated in chapter 2. The volume-averaged lattice temperature $\overline{T}$ is determined using Eq. (16) as derived earlier. Next we discuss the evaluation of the different model parameters.

4.2 Model Methodology for Gray Phonon Dispersions

In this section we present the calibration procedure for determining the volume-averaged relaxation time, $\overline{\tau}$, and the interface scattering relaxation time, τ_B. We also discuss the choice and computation of the scattering phase function, $\Phi_{\mathbf{KK'}}$ for the two-composite domain. The model is general and can address anisotropic scattering from the particle interfaces. In the particle limit, the scattering phase function obtained through

geometric scattering would suffice. We will, however, consider, sparsely distributed particle-composite systems and very small particle sizes, where wave effects need to be considered. We will evaluate our scattering phase function using existing Mie scattering theory. We are using a gray approximation and will consider properties for a single phonon mode. Scattering phase functions in the Mie limit have been derived for transverse phonons in the literature [66, 72].

4.2.1 Determination of Volume-Averaged Relaxation Time $\bar{\tau}$

The thermal pathway is modified in the presence of particles of a second material in the composite matrix. The volume-averaged bulk relaxation time, $\bar{\tau}$, will therefore need to be calibrated using DNS in the Fourier limit, while accounting for the detailed composite geometry and the thermal properties of both the materials in the REV.

Using the method previously discussed, we will compute exponent d [Eq. (31)] for the composite problem. We first solve the Fourier conduction problem on a periodic unit cell of REV containing the host material and the particle. With known bulk intrinsic thermal conductivity of the both materials, the effective thermal conductivity of the composite unit cell may be computed from the Fourier solution. We then evaluate the exponent, d, using Eq. (31). From Eq. (32), we determine $\bar{\tau}$. We are using a gray approximation and therefore, only a single value of $\bar{\tau}$ is required for the model. We will use this as an input to the composite volume-averaged BTE.

4.2.2 Determination of Interface Scattering Relaxation Time, τ_B

We will determine the interface scattering relaxation time, τ_B, using the previously developed method for the nanoporous volume-averaged BTE model. The interface scattering relaxation time, τ_B represents the time scale on which phonons scatter on the particle interface. We calibrate τ_B from direct numerical simulations of the REV in the ballistic limit, when $\bar{\tau} \to \infty$.

In the ballistic limit, there is no bulk scattering in either the host or the particle. If the particle is sufficiently small compared to the domain size, we can perform the calibration of τ_B on an equivalent nanoporous domain, where instead of composite particles, we consider pores. We estimate the τ_B using Eq. (29), and calibrate against the effective thermal conductivity obtained by a direct numerical simulation in a periodic unit cell with pore in the limit $\bar{\tau} \to \infty$ such that Eq. (33) is satisfied. This calibrated value of τ_B is an input to the volume-averaged BTE model.

Next we discuss the scattering phase function for the composite problem.

4.2.3 Scattering Phase Function, $\boldsymbol{\Phi_{KK'}}$

In the development of our nanoporous models, we evaluated the scattering phase function, $\boldsymbol{\Phi_{KK'}}$, in the geometric scattering limit using a ray tracing technique [64]. This method is valid when we consider pore sizes much larger than the wavelengths of the dominant phonon groups. The consideration of the particle size, a, compared with the phonon wavelength, λ is important in determining the interaction between the phonon and the composite particle. For $a \ll \lambda$, we are in the Rayleigh limit and geometric scattering will not be valid. For $a \gg \lambda$, the scattering is in the geometric optics limit and

a ray tracing approach as adopted earlier is relevant. However, for modern nanocomposites with bulk and nanoparticles being used simultaneously for new designs, the particle sizes can be of the range of the phonon wavelength in the domain, requiring an investigation using the Mie scattering theory [66]. It is important to note that in the scenario where embedded particles are of comparable dimensions to the phonon wavelength of the host material, the particle treatment and hence phonon BTE is still valid for the host material as long as the phonon mean free path (Λ) is much larger compared to the spacing between particles. Here, we employ the assumption that the particle acts as a point scatterer. The scattering of phonons in the host material due to the particle is represented through a scattering term with a scattering phase function derived from Mie theory. A similar treatment may be used for Rayleigh scattering as well.

To summarize, the following condition must be satisfied for the volume-averaged BTE model to be applicable while using a Mie scattering based phase function, $\Phi_{\mathbf{KK'}}$:

$$a \ll \Lambda \text{ and } L>>a \qquad (58)$$

where L is a measure of the distance between particles. Moreover, for particle sizes much smaller than the mean free path and comparable to the phonon wavelength, Mie scattering theory will be necessary as geometric scattering is no longer valid.

$$a \sim \lambda \qquad (59)$$

For a composite REV where the particles satisfy the above conditions, we can determine the scattering phase function in the model in the Mie-scattering limit. For most composites of interest, phonon mean free paths are in the range of tens to a few hundred nanometers, while wavelengths may be of the order of a few nanometers [88]. This

implies the particle size should be of the order of a few nanometers and interparticle distance must be at least of the order of tens of nanometers. Thus, this treatment would generally be valid at low particle volume fraction.

We will use the analytical expression for the Mie scattering phase function for transverse phonons available in the literature to compute the scattering phase function matrix $\Phi_{\mathbf{KK'}}$ [66]. The formulation assumes specular scattering of phonons by spherical particles.

Mie scattering of phonons is analogous to that of photons. For photons, it is an exact solution of the Maxwell's equations subjected to boundary conditions at the scatterer interface, while for phonons it is an exact solution of the elastic wave equations with the specified boundary conditions at the interface. Since it is an exact solution to the wave equation, in the wave-limit, the Mie scattering will, therefore, be valid for all sizes of particles.

Analytical Mie-Scattering Phase Function

Phonon scattering in the Mie limit has been studied and a theory analogous to radiation Mie scattering has been developed by Prasher [66]. We apply the scattering phase function developed for horizontal transverse phonons. The theory used assumes no mode conversion. No mode conversion means at the interface only two different types of waves are generated [Figure 18]. Mode conversion will be necessary for longitudinal and vertically polarized transverse phonons as there will be four different waves generated at the interface [66].

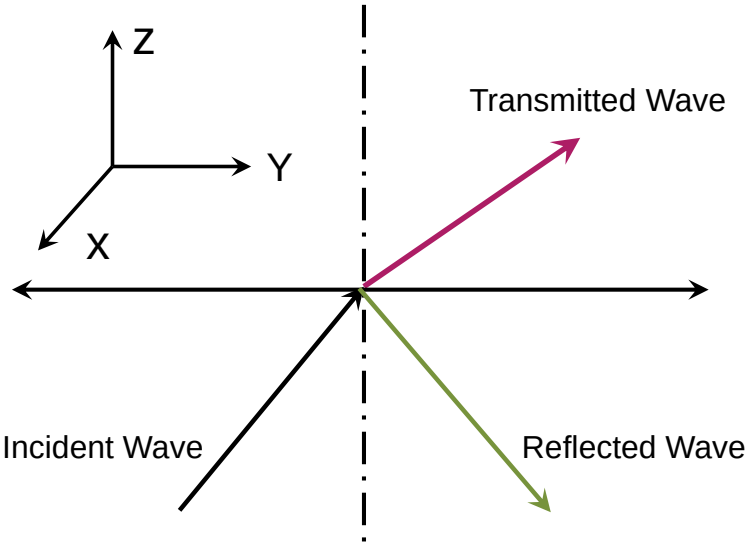

Figure 8: Scattering by a transverse wave

In radiation, electromagnetic waves are transverse waves. Therefore, the equations of the Mie theory for phonon scattering are identical to scattering of transverse waves in radiation, except that there is no coupling between horizontal and vertical polarized transverse waves in phonons. The development assumes independent scattering and neglects multiple scattering effects for specular reflection at a spherical scatterer interface.

The scattering phase function is given by:

$$\Phi(\theta,\phi) = 4\pi \frac{F(\theta,\phi)}{\int_0^{\pi}\int_0^{2\pi} F(\theta,\phi) sin\theta d\theta d\phi} = \frac{4\pi F(\theta,\phi)}{\sum_{n=1}^{\infty}(2n+1)a_n\overline{a_n}} \qquad (60)$$

where $F(\theta,\phi)$ is the dimensionless scattering function and is a function of (θ,ϕ) in the spherical coordinate system, Figure 19.

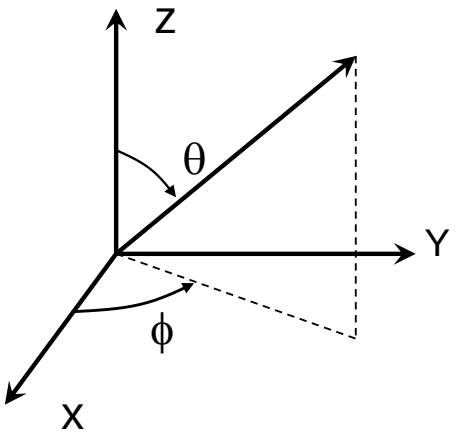

Figure 9: Spherical coordinate system convention usedin $\Phi_{\mathbf{KK'}}$

$$F(\theta,\phi) = 2\sum_{n-1}^{\infty}\sum_{m-1}^{\infty}\frac{2n+1}{n(n+1)}\frac{2m+1}{m(m+1)}a_n\overline{a_m}[\tau_n\tau_m\sin^2\phi + \pi_n\pi_m\cos^2\phi]$$

(61)

The coefficient $a_n$can be evaluated by the expression below:

$$a_n = -\frac{\mu_2 j_n(x_1)[x_2 j_n'(x_2) - j_n(x_2)] - \mu_1 j_n(x_2)[x_1 j_n'(x_1) - j_n(x_1)]}{\mu_2 h_n(x_1)[x_2 j_n'(x_2) - j_n(x_2)] - \mu_1 j_n(x_2)[x_1 h_n'(x_1) - h_n(x_1)]} \qquad (62)$$

The overline $'-'$ represents complex conjugate. The functions π_n and τ_n are evaluated as follows:

$$\pi_n(\cos\theta) = \frac{1}{\sin\theta}p_n^1(\cos\theta)$$

$$\tau_n(\cos\theta) = \frac{d}{\mathrm{d}\,\theta}p_n^1(\cos\theta) \qquad (63)$$

Where $p_n^1$is the associated Legendre function of order 1. The function $j_n$is expressed as:

$$h_n^2(x) = j_n(x) - i\eta_n(x) \qquad (64)$$

Where, h_n^2 is the spherical Hankel function of the second kind and of order n, and η_n is the spherical Bessels function of the second kind and of order n. The size parameter x is expressed in terms of the radius of the spherical scatterer and the wave number of the transverse wave in the media under consideration. Here '1' represents the host material and the '2' represents the spherical particle:

$$x_1 = k_1 a; x_2 = k_2 a \qquad (65)$$

The wave number is computed from the frequency of the transverse phonon under consideration and the velocity of the transverse wave:

$$k_1 = \frac{\omega_1}{V_{T_1}};\ V_{T_1} = \sqrt{\frac{\mu_1}{\rho_1}};\ \lambda_1 = \frac{2\pi V_{T_1}}{\omega} \qquad (66)$$

The transverse phonon speed in host material is given by V_{T_1}, λ_1 is the wavelength of the phonon under consideration, $\rho_1$is the density of the host material and μ_1 is the shear Lamé constant. The same definitions apply for the particle properties. We assume an isotropic medium in determining the Lamé constants from the stiffness matrix of the materials under consideration.

To validate our calculations, we compare the scattering efficiency obtained from the study with that of a rigid scatterer from Mie theory in photons. The scattering efficiency is expressed in terms of the previously defined parameters:

$$C = \frac{4}{x_1^2}\sum_{n-1}^{\infty}(2n+1)a_n\overline{a_n} \qquad (67)$$

In Figure 20, we show the scattering efficiency of rigid scatterers by assuming a very dense particle, with a low phonon speed in the medium. We vary the scatterer radius; for very large values of x_1, the scattering efficiency approaches a value of 2, which is

consistent with the Mie theory. Large values of $x_1$implies geometric scattering. We consider 40 terms in the series to ensure convergence in the calculation of the scattering efficiency and the phase function. The Mie theory for radiation and the transverse phonons compare very well.

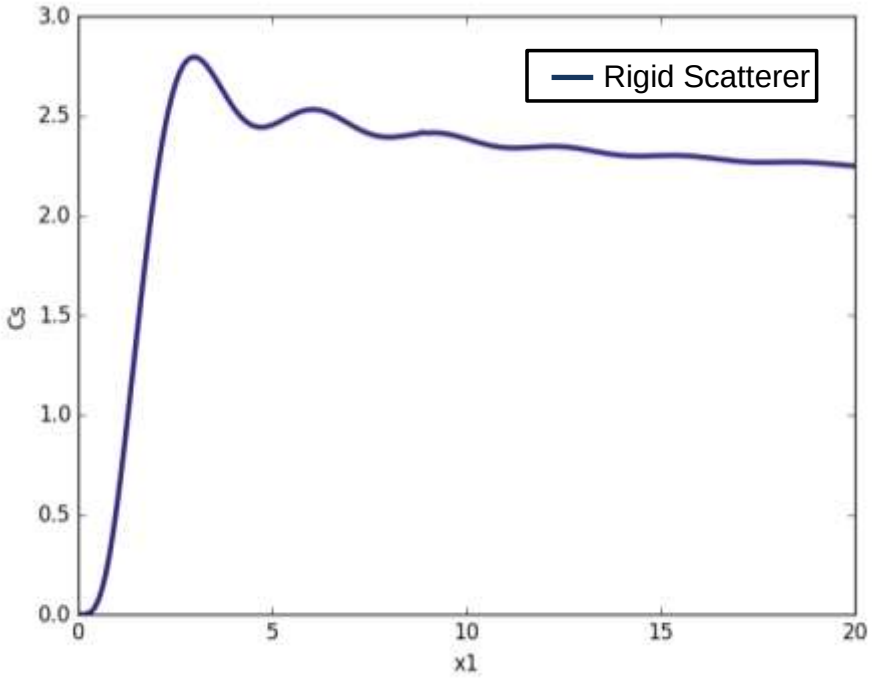

Figure 20: Scattering efficiency of a rigid scatterer

Next we compute the scattering phase function for a realistic silicon-germanium composite structure.

Mie Scattering in Silicon Host with Germanium Particle

We determine the scattering phase function for transverse phonons for scattering in a silicon medium by a spherical germanium scatterer [Figure 21]. Using the following properties for Si and Ge for a shear wave propagating in the [1 1 0] direction [89]:

$$\mu_{Ge} = \frac{6.71x10^{10}N}{m^2};\ \rho_{Ge} = 5322kg/m^3$$

$$\mu_{Si} = 7.956x10^{10}N/m^2;\ \rho_{Si} = 2332kg/m^3 \quad (68)$$

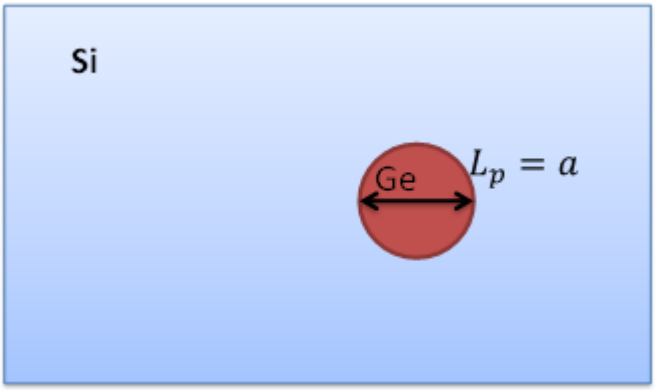

Figure 10: Nanocomposite domain with a silicon host matrix containing a germanium particle.

We consider a gray approximation of the volume-averaged model. Therefore we choose the phonon group velocity of the transverse wave as the speed of sound wave in silicon ($v_g = 5843\ m/s$). In Figure 22, we plot the scattering efficiency [69] in the above system as we vary the germanium particle size, keeping other properties constant.

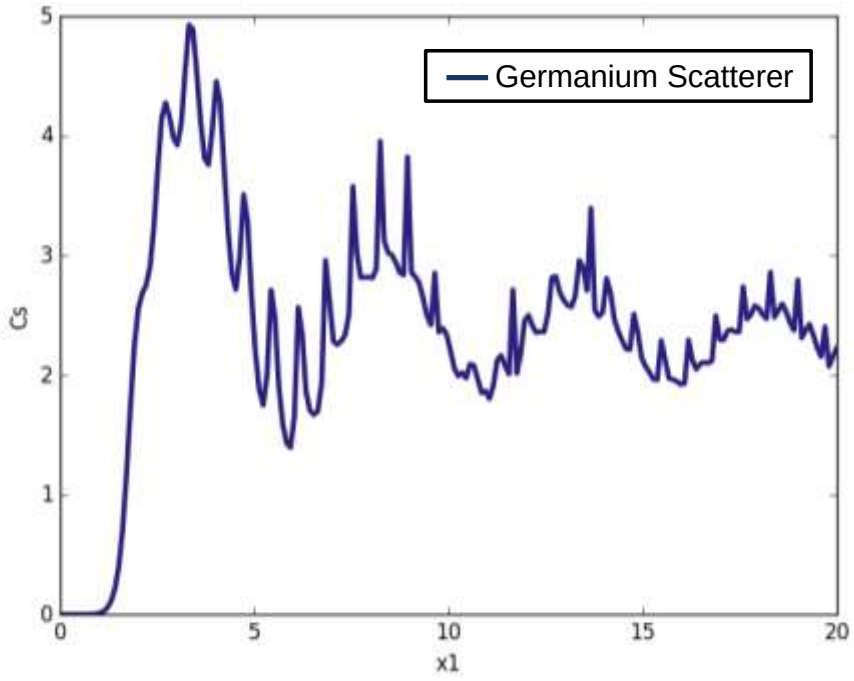

Figure 11: Scattering efficiency for varying sizes of germanium scatterers in silicon [66] [69].

4.2.4 Rotation of the Scattering Phase Function and Computing the $\Phi_{KK'}$ Matrix

The Mie scattering phase function ($\Phi(\theta, \phi)$) reported in the literature is generally defined for an incoming wave travelling along the Z-axis. For our case, where the input and output waves can have different directions, the right θ and ϕ must to be computed to determine the value of the phase function. These are computed by rotating the incoming wave appropriately. Say, the input plane wave is at an angle θ with respect to the Z-axis. Therefore, we rotate the incoming wave to align with the Z-axis [Figure 23].

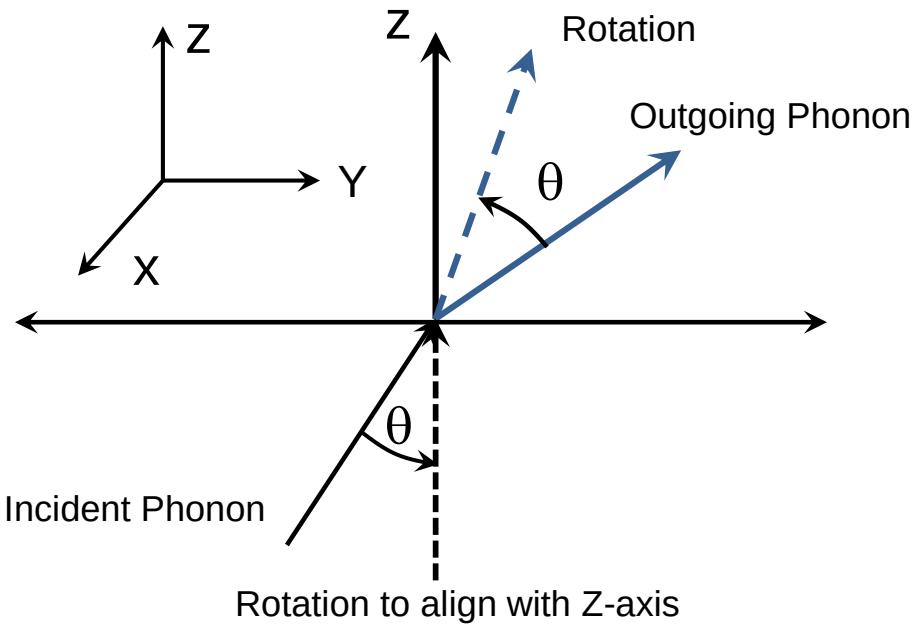

Figure 12: Rotation of the incident wave directions to align with the Z-axis.

Now the output wave vectors from this incident wave will also be rotated by θ in the same direction by using the same rotation matrix. It is known that the rotation matrix for rotating the unit vector $\boldsymbol{a}$ to unit vector $\boldsymbol{b}$ is given by $\boldsymbol{R}$ [90]:

$$R = I + [v]_x + [v]_x^2 \frac{1-c}{s^2}; \qquad (69)$$

where $$\boldsymbol{v} = \boldsymbol{a} \times \boldsymbol{b};\ s = \|v\|;\ c = \boldsymbol{a} \cdot \boldsymbol{b}$$

Here $\boldsymbol{v}_x$ is the skew symmetric cross product of matrix $\boldsymbol{v}$.

$$\boldsymbol{v}_x \stackrel{\text{def}}{=} \begin{bmatrix} 0 & -v_3 & v_2 \\ v_3 & 0 & -v_1 \\ -v_2 & v_1 & 0 \end{bmatrix} \qquad (70)$$

Note that here ***a*** is the unit vector in the direction of the incoming wave while ***b*** is the unit vector in the direction of the Z-axis. After the rotation operation (multiplying ***R*** with the outgoing wave vector), we determine the angle (θ, ϕ), and $\Phi(\theta, \phi)$ corresponding to the output direction. This allows us to determine $\Phi_{KK'}$ matrix for any given input and output direction.

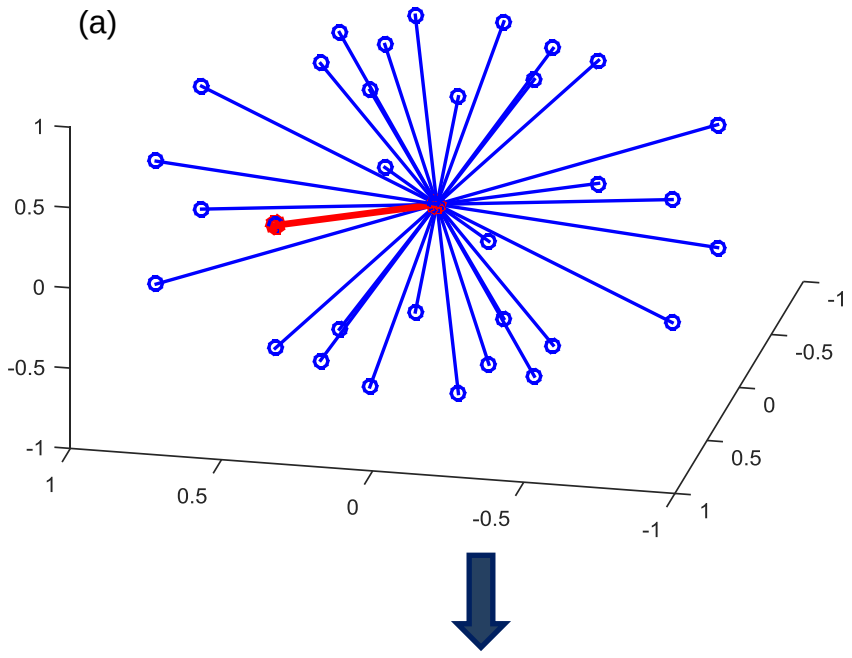

Figure 13: Continued next page

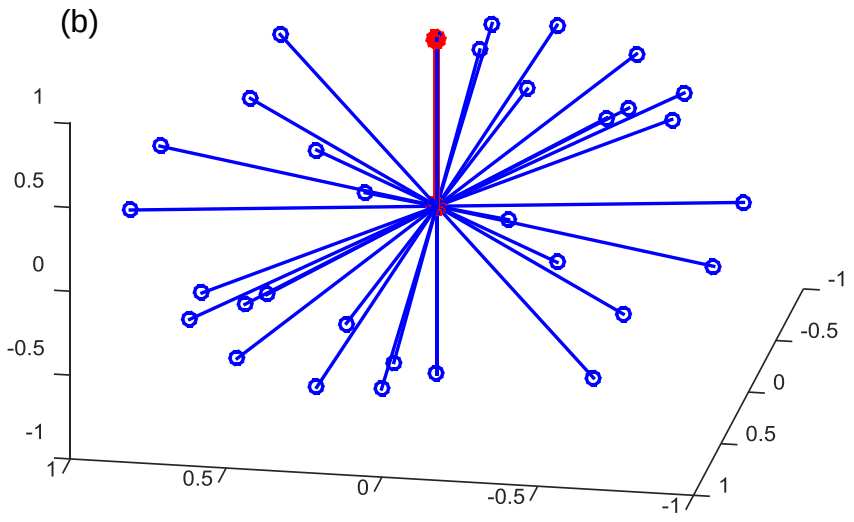

Figure 14: Visualization of rotation for a given input direction (in red) and all outgoing directions. (a) Shows the wave vectors before rotation, and (b) shows the wave vectors after rotation

Next we outline the steps involved in calculating the matrix.

4.2.5 Mie Algorithm

Step 1: Discretize θ and ϕ by picking $N_\theta \; and \; N_\phi$ where $0 \leq \theta \leq \pi; 0 \leq \phi \leq 2\pi$

Step 2: To take values at the centroid of the control angle off-set starting angles by $\frac{\theta}{2}$ and

$\frac{\phi}{2}$

Step 3: Define incoming direction as $(sin\theta sin\phi\, \hat{\imath} + sin\theta cos\phi\, \hat{\jmath} + cos\theta\, \hat{k})$

Step 4: Define Z-axis [0 0 1]

Step 5: Loop over all incoming directions and calculate the rotation matrix

Step 6: Calculate θ_{diff} and ϕ_{diff}, the angle between input and Z-axis based on rotation and apply that to the output directions while being mindful of the quadrant in which each outgoing direction belongs

Step 7: Compute $\Phi_{kk'}$ using θ_{diff} and ϕ_{diff} values for the outgoing directions.

We align our computation of the scattering phase function with the angular discretization of the phonon wave vector space in the silicon in the volume-averaged BTE model. We use an angular discretization of $(N_\theta, N_\phi) = (8x16)$ where $0 < \theta < \pi$ and $0 < \phi < 2\pi$. In Figure 25, we present the scattering phase function values for all outputs for three different incident directions of the phonon wave for $N_\phi = 1$. The black dotted line represents the case of incidence in the direction of the positive Z-axis.

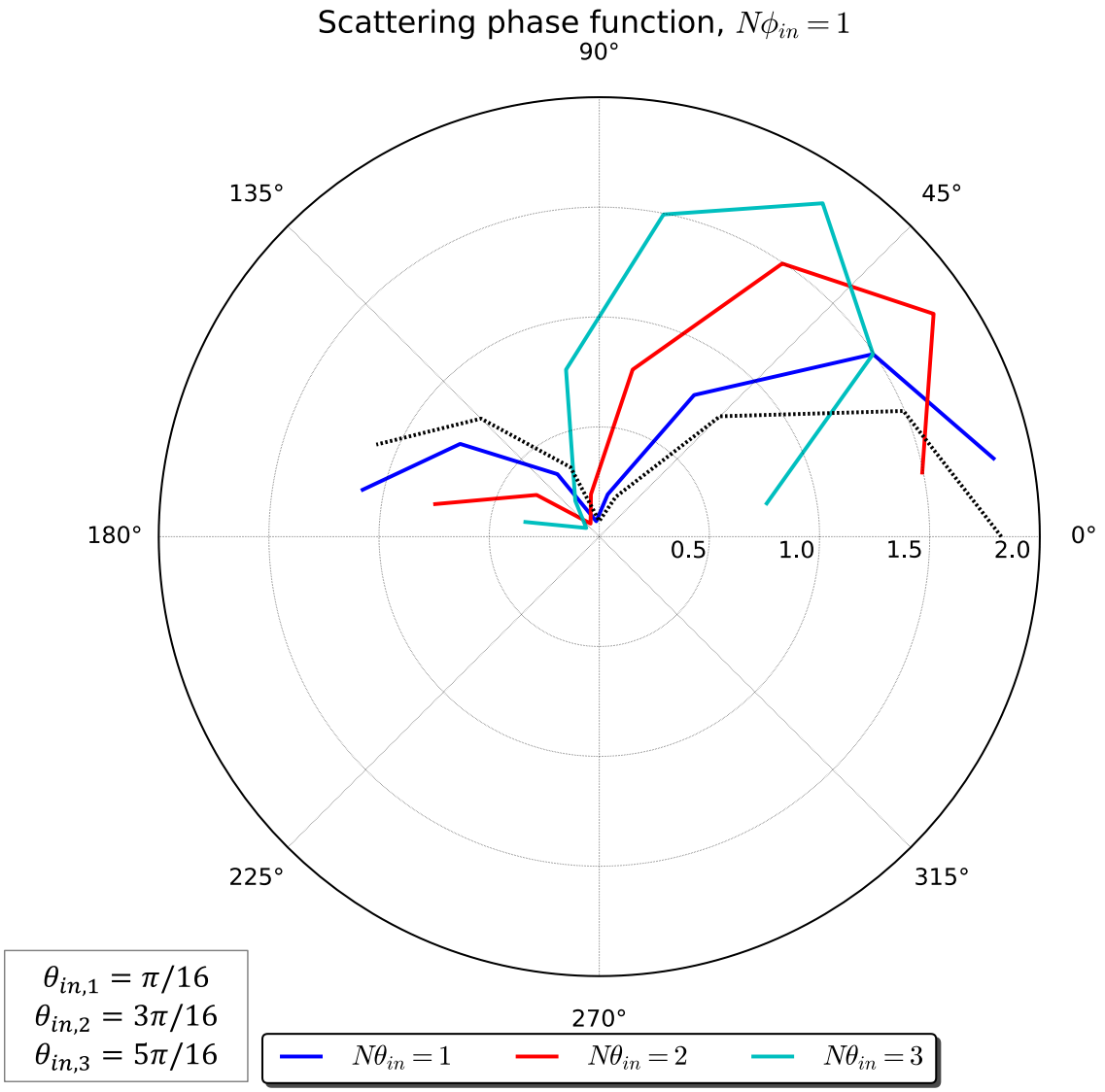

Figure 15: Scattering phase function as a function of output angle θ for three different incidence angles and for $N_\phi = 1$

The scattering phase function matrix thus obtained is an input to the volume-averaged BTE for the composite. The model parameters are determined based on the geometry and properties of the composite materials and are used as an input to equation (57). The

model will be discretized using the finite volume method and solved using the coupled ordinates method (COMET), as described in the next chapter.

4.3 CLOSURE

In this chapter we discussed the volume-averaged model for BTE for a two-material nanocomposite using a gray approximation. We discussed the procedure to determine the different model parameters and. In the next chapter, we will present the numerical procedure to solve the different models developed in the dissertation so far.

Chapter 5: Numerical Procedure

In this chapter we will discuss the discretization of the different volume-averaged Boltzmann Transport Equation (BTE) models developed thus far as well as the numerical method for their solution. We will discretize the equations using a finite volume method (FVM) [43, 91, 92]. The resulting system of discrete equations will be solved using the Coupled Ordinates Method (COMET) [54]. We will discuss in detail the discretization procedure for the volume-averaged BTE model for the nanoporous domain using a gray approximation. We will then present the discretized equations for the nanoporous non-gray model and for the two-material composite volume-averaged BTE model.

5.1 DISCRETIZATION

The volume-averaged BTE models are discretized using a standard finite volume procedure. The physical domain and the wave-vector space are each discretized into control volumes. Figures (26) and (27) show a schematic of the control volume in the physical and wave vector spaces. The physical space is discretized into arbitrary unstructured convex polyhedral. The Brillouin zone is assumed spherical and is discretized using a spherical coordinate representation.

5.1.1 Volume-Averaged BTE Model for a Gray Phonon BTE in a Nanoporous Domain

In this section we focus on the gray model in a nanoporous domain. To discretize, we will first integrate equation (13) over both the physical and wave-vector control volumes and then apply the divergence theorem. Applying the divergence theorem and discretizing we get the following:

$$\int_{\Delta^3\mathbf{K}}\int_{\Delta V}\left[\alpha\nabla\cdot\mathbf{v}\langle e_k{''}\rangle = \alpha\frac{\langle e_0\rangle-\langle e_k{''}\rangle}{\bar{\tau}} - \frac{\langle e_k{''}\rangle}{\tau_B} + \frac{1}{V_{BZ}}\frac{1}{\tau_B}\int_{\mathbf{K}'}\Phi_{kk'}\,\langle e_{k'}{''}\rangle d^3\mathbf{K}'\right]dV\,d^3\mathbf{K} \quad (71)$$

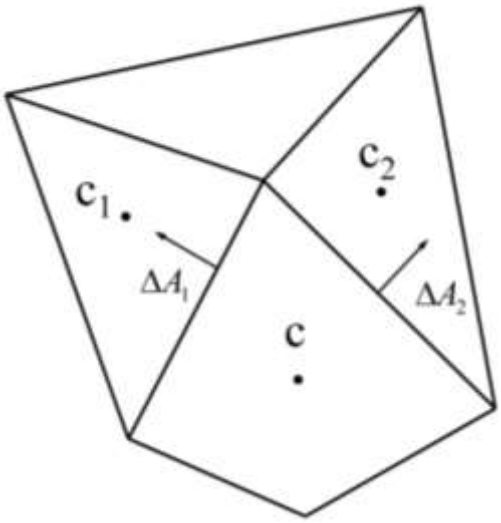

Figure 16: Schematic of a control volume in physical space [70]

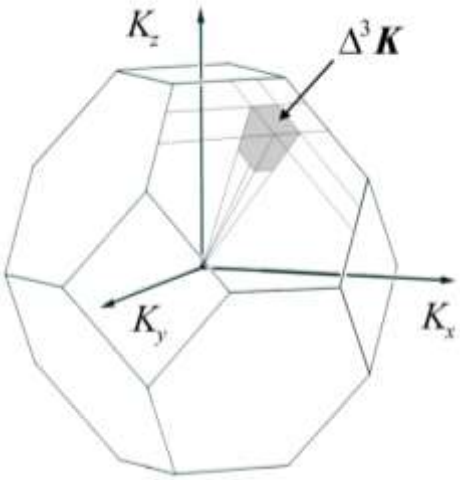

Figure 17: Schematic of a control volume in wave vector space for a face centered cubic lattice [74].

We get the following equation:

$$\sum_f \alpha\langle e_{k,f}"\rangle \mathbf{v}\cdot\Delta\mathbf{A}_f = \alpha\frac{\langle e_{0,c}\rangle-\langle e_{k,c}"\rangle}{\overline{\tau}}\Delta V - \frac{\langle e_{k,c}"\rangle}{\tau_B}\Delta V + \left(\frac{1}{V_{BZ}}\frac{1}{\tau_B}\sum_{\mathbf{K}'}\Phi_{kk'}\langle e_{k',c}"\rangle\Delta^3\mathbf{K}'\right)\Delta V \quad (72)$$

$$\sum_{\mathbf{v}\cdot\Delta\mathbf{A}_f>0}\alpha\langle e_{k,c}"\rangle\mathbf{v}\cdot\Delta\mathbf{A}_f + \sum_{\mathbf{v}\cdot\Delta\mathbf{A}_f<0}\alpha\langle e_{k,nb}"\rangle\mathbf{v}\cdot\Delta\mathbf{A}_f = \alpha\frac{\langle e_{0,c}\rangle-\langle e_{k,c}"\rangle}{\overline{\tau}}\Delta V - \frac{\langle e_{k,c}"\rangle}{\tau_B}\Delta V + \left(\frac{1}{V_{BZ}}\frac{1}{\tau_B}\sum_{\mathbf{K}'}\Phi_{kk'}\langle e_{k',c}"\rangle\Delta^3\mathbf{K}'\right)\Delta V \quad (73)$$

Values associated with the cell centroid have the subscript "c", ΔV is the volume of the control volume and $\Delta\mathbf{A}_f$ is the outward-pointing area vector of the face f. Equation (72) is summed over all faces f of the control volume. $\Delta^3\mathbf{K}$ is the extent of the control volume in wave-vector space. We make a second-order spatial approximations in equation (73) in integrating in **K** space [44]. The face values in equation (72) are computed using a first order upwinding scheme giving us the discrete equation (73). Cells neighboring the face cells f of interest are referred with the subscript "nb".

Equation (73) represents the discrete form of the BTE at a given discrete point **K** in wave-vector space. The terms on the LHS represent the "advection" or streaming of phonons of wave vector **K** in the direction of the group velocity vector **v**, and only involve spatial coupling between **K**-type phonons at location "c", and **K**-type phonons at the neighbor locations "nb". The terms on the RHS represent scattering events, either due to bulk scattering or due to scattering on inclusions and interfaces contained in the control volume. Here phonons of type **K** scatter on phonons with other wave vectors through the terms $\langle e_{0,c}\rangle$ and the third term on the RHS. For low Knudsen number, the scattering terms dominate, whereas for high Knudsen numbers, the advection terms dominate. For

semiconductors like silicon, the large range of phonon mean free paths (MFPs) implies that most problems of practical interest involve a range of Knudsen numbers.

Once we have obtained a discrete set of algebraic equations, such as equation (73), we must devise a solution procedure to solve them. Typical published methods [43-45] employ a sequential solution algorithm whereby the BTE corresponding to each discrete point in **K** space is solved over all physical space, holding the energy density values at other **K** points temporarily known. The solution procedure cycles over all **K** points in this manner, and updates the coupling term, $\langle e_{0,c} \rangle$, once every outer iteration. This type of procedure couples spatial points tightly, but **K** points loosely. Consequently, low Knudsen number problems are slow to converge with sequential procedures. In this dissertation, we employ an efficient solution procedure called the Coupled Ordinates Method (COMET) to ensure efficient coupling, both in the physical space and in **K** space [54].

5.2 COMET ALGORITHM

The COMET algorithm is described in detail in [54]. We recapitulate the main points here for completeness. COMET seeks to achieve strong coupling in both the physical and **K** spaces through a point-coupled multigrid strategy. At each physical control volume or cell, the discrete BTEs at all the **K** points are solved simultaneously, assuming physical neighbor values known. This point-coupled solution is used as the relaxation sweep in a full-approximation storage full multigrid (FAS-FMG) procedure [93]. The point-coupled procedure ensures strong coupling in **K** space, whereas the multigrid procedure promotes strong coupling in physical space. Previous work [70] has

shown that speed-ups over sequential solution algorithms of 10-200 times may be obtained.

5.2.1 Point Coupled Solution

A direct point-coupled solution for all of the phonon energies and the lattice temperature is performed at each physical cell, c [94]. All the equations are written in delta form. Thus, we solve for the correction to the current solution approximation. We cast equation (73) ($= Q$) in the delta form:

$$Q = 0$$

$$\Longrightarrow Q - Q_{prev} = -Q_{prev} \qquad (74)$$

$$\sum_{\mathbf{v}\cdot\Delta\mathbf{A}_f>0} \alpha\Delta\langle e_{k,c}{}''\rangle\mathbf{v}\cdot\Delta\mathbf{A}_f - \alpha\frac{\Delta\langle e_{0,c}\rangle - \Delta\langle e_{k,c}{}''\rangle}{\overline{\tau}}\Delta V + \frac{\Delta\langle e_{k,c}{}''\rangle}{\tau_B}\Delta V$$

$$-\left[\sum_{\mathbf{K}'}\Phi_{kk'}\,\langle e_{k',c}{}''\rangle\Delta^3\mathbf{K}' - \left(\sum_{\mathbf{K}'}\Phi_{kk'}\,\langle e_{k',c}{}''\rangle\Delta^3\mathbf{K}'\right)^{prev}\right]\frac{\Delta V}{V_{BZ}\tau_B}$$

$$= -\Big[\textstyle\sum_{\mathbf{v}\cdot\Delta\mathbf{A}_f>0}\alpha\langle e_{k,c}{}''\rangle\mathbf{v}\cdot\Delta\mathbf{A}_f + \sum_{\mathbf{v}\cdot\Delta\mathbf{A}_f<0}\alpha\langle e_{k,nb}{}''\rangle\mathbf{v}\cdot\Delta\mathbf{A}_f - \alpha\frac{\langle e_{0,c}\rangle-\langle e_{k,c}{}''\rangle}{\overline{\tau}}\Delta V +$$

$$\frac{\langle e_{k,c}{}''\rangle}{\tau_B}\Delta V - \left(\frac{1}{V_{BZ}}\frac{1}{\tau_B}\textstyle\sum_{\mathbf{K}'}\Phi_{kk'}\,\langle e_{k',c}{}''\rangle\Delta^3\mathbf{K}'\right)\Delta V\Big]^{prev} = -R \qquad (75)$$

The Δe's are corrections to the previous iteration, referred to as "$prev$" in equation (75). The solution variables are on the left hand side and the right hand is the residual, R, of the current solution approximation. The influence of the neighbor values is treated explicitly. Equation (75) uses correction to the equilibrium energy density, $\Delta\langle e_{0,c}\rangle$. We will now apply a Taylor series expansion in temperature for the prevailing temperature such that:

$$\Delta\langle e_0\rangle \approx \left[\frac{\partial\langle e_0\rangle}{\partial\overline{T}}\right]^{prev}\Delta\overline{T} \qquad (76)$$

At a particular physical cell, all phonon modes share the same equilibrium average lattice temperature. Therefore, the correction to the current temperature does not vary in wave vector space. Hence we can write:

$$\sum_{\mathbf{v}\cdot\Delta\mathbf{A}_f>0} \alpha\Delta\langle e_{k,c}"\rangle \mathbf{v}\cdot\Delta\mathbf{A}_f + \Delta\langle e_{k,c}"\rangle \left[\frac{\alpha}{\overline{\tau}} + \frac{1}{\tau_B}\right]\Delta V - \frac{\alpha\Delta V}{\overline{\tau}}\left[\frac{\partial\langle e_{0,c}\rangle}{\partial\overline{T}}\right]^{prev}\Delta\overline{T_c} -$$

$$\left[\sum_{\mathbf{K}'}\Phi_{kk'}\langle e_{k',c}"\rangle\Delta^3\mathbf{K}' - \left(\sum_{\mathbf{K}'}\Phi_{kk'}\langle e_{k',c}"\rangle\Delta^3\mathbf{K}'\right)^{prev}\right]\frac{\Delta V}{V_{BZ}\tau_B} = -R \qquad (77)$$

Scattering is a re-distributive process, and therefore, the net scattering term integrated over the Brillouin zone must be zero, following energy conservation in each cell. Therefore, from equation (15), we can write:

$$\sum_{BZ}\frac{\langle e_{0,c}\rangle}{\overline{\tau}}\Delta^3\mathbf{K} - \sum_{BZ}\frac{\langle e_{k,c}"\rangle}{\overline{\tau}}\Delta^3\mathbf{K} \qquad (78)$$

Here "*BZ*" refers to a summation over the entire Brillouin zone and over all polarizations. The above energy equation can be written in the correction form as follows:

$$\sum_{BZ}\left(\frac{\Delta\langle e_{0,c}\rangle - \Delta\langle e_{k,c}"\rangle}{\overline{\tau}}\right)\Delta^3\mathbf{K} = -\sum_{BZ}\left(\frac{\Delta\langle e_{0,c}\rangle - \Delta\langle e_{k,c}"\rangle}{\overline{\tau}}\right)^{prev}\Delta^3\mathbf{K} = -R_L \qquad (79)$$

(41)

As with equation (75), the right hand is the residual, R_L of the current solution approximation and solution variables are on the left hand side. Using equations (76) and (79), we can state the energy conservation statement in terms of the average lattice temperature:

$$\Delta\overline{T_c}\sum_{BZ}\left[\left(\frac{\partial\langle e_{0,c}\rangle}{\partial\overline{T}}\right)^{prev}\frac{\Delta^3\mathbf{K}}{\bar{\tau}}\right] - \sum_{BZ}\Delta\langle e_{k,c}"\rangle\frac{\Delta^3\mathbf{K}}{\bar{\tau}} = -R_L \quad (80)$$

Using the above forms, we can now relate the volume averaged lattice temperature $\overline{T}$ and the phonon energy density *e''*. The point-coupled linear system can then be written as:

$$\begin{bmatrix} \left(\alpha \sum_{\mathbf{v}\cdot\Delta\mathbf{A}_f>0} \mathbf{v}\cdot\Delta\mathbf{A}_f + \Delta V\left(\frac{\alpha}{\bar{\tau}}+\frac{1}{\tau_B}\right)\right)_1 & & & \left(-\frac{\partial\langle e_0\rangle}{\partial\bar{T}}\Delta V\left(\frac{\alpha}{\bar{\tau}}+\frac{1}{\tau_B}\right)\right)_1 \\ & \left(\alpha \sum_{\mathbf{v}\cdot\Delta\mathbf{A}_f>0} \mathbf{v}\cdot\Delta\mathbf{A}_f + \Delta V\left(\bar{\tau}+\frac{1}{\tau_B}\right)\right)_2 & & \left(-\frac{\partial\langle e_0\rangle}{\partial\bar{T}}\Delta V\left(\frac{\alpha}{\bar{\tau}}+\frac{1}{\tau_B}\right)\right)_2 \\ & & \ddots & \vdots \\ & & \left(\alpha \sum_{\mathbf{v}\cdot\Delta\mathbf{A}_f>0} \mathbf{v}\cdot\Delta\mathbf{A}_f + \Delta V\left(\frac{\alpha}{\bar{\tau}}+\frac{1}{\tau_B}\right)\right)_n & \left(-\frac{\partial\langle e_0\rangle}{\partial\bar{T}}\Delta V\left(\frac{\alpha}{\bar{\tau}}+\frac{1}{\tau_B}\right)\right)_n \\ \left(-\frac{\Delta^3\mathbf{K}}{\bar{\tau}}\right)_1 & \left(-\frac{\Delta^3\mathbf{K}}{\bar{\tau}}\right)_2 & \cdots \left(-\frac{\Delta^3\mathbf{K}}{\bar{\tau}}\right)_n & \sum_{BZ}\left[\left(\frac{\partial\langle e_0\rangle}{\partial\bar{T}}\right)\bar{\tau}\right] \end{bmatrix} \begin{bmatrix} \Delta\langle e_1^{"}\rangle \\ \Delta\langle e_2^{"}\rangle \\ \cdot \\ \cdot \\ \cdot \\ \cdot \\ \Delta\langle e_n^{"}\rangle \\ \Delta\bar{T} \end{bmatrix} = \begin{bmatrix} R_1 \\ R_2 \\ \cdot \\ \cdot \\ \cdot \\ \cdot \\ R_n \\ R_L \end{bmatrix}$$

(81)

We now have $(n+1)$ total number of equations to be solved at each cell, where n is the number of **K** points times the number of polarizations. The Jacobian matrix shown above has an "arrowhead" structure which is exploited in the point-coupled solution procedure so that the linear system may be solved in O(n) operations. This carefully engineered Jacobian is the key to obtaining efficient solutions through the COMET algorithm.

The last row represents the energy conservation equation in the bulk while coupling the lattice temperature to all the phonons. The last column couples the phonons to the lattice temperature. The Jacobian in equation (81) is non-linear due to the non-linear dependence of the Bose-Einstein distribution on the lattice temperature in the last column. Multiple direct solutions of the system have to be performed while updating the last column. When constant specific heats are assumed, the problem becomes linear, and the multiple outer iterations are no longer required.

In the next section we will present the discretized form of the volume-averaged BTE models for the nanoporous domain with a non-gray approximation and the nanocomposite model with a gray approximation for completeness.

5.3 VOLUME-AVERAGED BTE MODEL FOR A NON-GRAY PHONON BTE IN A NANOPOROUS DOMAIN

We present the discretized system of equations for the non-gray model in a nanoporous domain. In a process as described earlier in this chapter, we integrate equation (43) over both the physical and wave-vector control volumes and apply the divergence theorem.

$$\int_{\Delta^3\mathbf{K}}\int_{\Delta V}\left[\alpha\nabla\cdot\mathbf{v}\langle e_k"\rangle = \alpha\frac{\langle e_0\rangle-\langle e_k"\rangle}{\overline{\tau_k}} - \frac{\langle e_k"\rangle}{\tau_{B,k}} + \frac{1}{V_{BZ}}\frac{1}{\tau_{B,k}}\int_{\mathbf{K}'}\Phi_{kk'}\,\langle e_{k'}"\rangle d^3\mathbf{K}'\right]dVd^3\mathbf{K} \quad (82)$$

The resulting equations are shown below.

$$\sum_f \alpha\langle e_{k,f}"\rangle\mathbf{v}\cdot\Delta\mathbf{A}_f = \alpha\frac{\langle e_{0,c}\rangle-\langle e_{k,c}"\rangle}{\overline{\tau_k}}\Delta V - \frac{\langle e_{k,c}"\rangle}{\tau_{B,k}}\Delta V + \left(\frac{1}{V_{BZ}}\frac{1}{\tau_{B,k}}\sum_{\mathbf{K}'}\Phi_{kk'}\,\langle e_{k',c}"\rangle\Delta^3\mathbf{K}'\right)\Delta V$$

(83)

$$\sum_{\mathbf{v}\cdot\Delta\mathbf{A}_f>0}\alpha\langle e_{k,c}"\rangle\mathbf{v}\cdot\Delta\mathbf{A}_f + \sum_{\mathbf{v}\cdot\Delta\mathbf{A}_f<0}\alpha\langle e_{k,nb}"\rangle\mathbf{v}\cdot\Delta\mathbf{A}_f = \alpha\frac{\langle e_{0,c}\rangle-\langle e_{k,c}"\rangle}{\overline{\tau_k}}\Delta V - \frac{\langle e_{k,c}"\rangle}{\tau_{B,k}}\Delta V +$$

$$\left(\frac{1}{V_{BZ}}\frac{1}{\tau_{B,k}}\sum_{\mathbf{K}'}\Phi_{kk'}\,\langle e_{k',c}"\rangle\Delta^3\mathbf{K}'\right)\Delta V \quad (84)$$

Casting the above equations in the delta form, the residual can be written as:

$$\sum_{\mathbf{v}\cdot\Delta\mathbf{A}_f>0}\alpha\Delta\langle e_{k,c}"\rangle\mathbf{v}\cdot\Delta\mathbf{A}_f + \Delta\langle e_{k,c}"\rangle\left[\frac{\alpha}{\overline{\tau_k}}+\frac{1}{\tau_{B,k}}\right]\Delta V - \frac{\alpha\Delta V}{\overline{\tau_k}}\left[\frac{\partial\langle e_{0,c}\rangle}{\partial\overline{T}}\right]^{prev}\Delta\overline{T_c} -$$

$$\left[\sum_{\mathbf{K}'}\Phi_{kk'}\,\langle e_{k',c}"\rangle\Delta^3\mathbf{K}' - \left(\sum_{\mathbf{K}'}\Phi_{kk'}\,\langle e_{k',c}"\rangle\Delta^3\mathbf{K}'\right)^{prev}\right]\frac{\Delta V}{V_{BZ}\tau_{B,k}} = -R \quad (85)$$

We note that the difference in the previously described discretization equations and the present is that along with $\langle e_{k,c}"\rangle$, the interface and volume-averaged bulk scattering relaxation times, $\tau_{B,k}$ and $\overline{\tau_k}$, now vary in **K**-space. Special care has to be taken in evaluating the in-scattering term in this **K** –resolved volume-averaged BTE as $\Phi_{kk'}$ is a function of the angular discretization of the wave vector space **K** and is different for

different polarizations. The volume-averaged lattice temperature equation is the same as before [Eq. (78) – Eqs. (80)]. The relaxation time parameters are determined using the methods described in chapter 3 and are input to the problem. The resulting system of equations has the arrowhead matrix structure shown in Equation (81).

5.4 VOLUME-AVERAGED BTE MODEL FOR A GRAY PHONON BTE IN A NANOCOMPOSITE DOMAIN

We now present the discretization for the gray model in a two-material nanocomposite domain. As a reminder, this is obtained by volume-averaging the BTE of the host-material in a nanocomposite representative elemental volume. As described earlier in this chapter, we integrate equation (57) over both the physical and wave-vector control volumes and apply the divergence theorem.

$$\int_{\Delta^3\mathbf{K}}\int_{\Delta V}\left[\alpha_m\nabla\cdot\mathbf{v}\langle e_k"\rangle = \alpha_m\frac{\langle e_0\rangle-\langle e_k"\rangle}{\overline{\tau}} - \frac{\langle e_k"\rangle}{\tau_B} + \frac{1}{V_{BZ}}\frac{1}{\tau_B}\int_{\mathbf{K}'}\Phi_{kk'}\,\langle e_{k'}"\rangle d^3\mathbf{K}'\right]dV\,d^3\mathbf{K} \quad (86)$$

The resulting equations are shown below.

$$\sum_f \alpha_m\langle e_{k,f}"\rangle\mathbf{v}\cdot\Delta\mathbf{A}_f =$$

$$\alpha_m\frac{\langle e_{0,c}\rangle-\langle e_{k,c}"\rangle}{\overline{\tau}}\Delta V - \frac{\langle e_{k,c}"\rangle}{\tau_B}\Delta V + \left(\frac{1}{V_{BZ}}\frac{1}{\tau_B}\sum_{\mathbf{K}'}\Phi_{kk'}\,\langle e_{k',c}"\rangle\Delta^3\mathbf{K}'\right)\Delta V \quad (87)$$

$$\sum_{\mathbf{v}\cdot\Delta\mathbf{A}_f>0}\alpha_m\langle e_{k,c}"\rangle\mathbf{v}\cdot\Delta\mathbf{A}_f + \sum_{\mathbf{v}\cdot\Delta\mathbf{A}_f<0}\alpha_m\langle e_{k,nb}"\rangle\mathbf{v}\cdot\Delta\mathbf{A}_f = \alpha_m\frac{\langle e_{0,c}\rangle-\langle e_{k,c}"\rangle}{\overline{\tau}}\Delta V -$$

$$\frac{\langle e_{k,c}"\rangle}{\tau_B}\Delta V + \left(\frac{1}{V_{BZ}}\frac{1}{\tau_B}\sum_{\mathbf{K}'}\Phi_{kk'}\,\langle e_{k',c}"\rangle\Delta^3\mathbf{K}'\right)\Delta V \quad (88)$$

Casting the above equations in the delta form, the residual can be written as:

$$\sum_{\mathbf{v}\cdot\Delta\mathbf{A}_f>0}\alpha_m\Delta\langle e_{k,c}"\rangle\mathbf{v}\cdot\Delta\mathbf{A}_f + \Delta\langle e_{k,c}"\rangle\left[\frac{\alpha_m}{\overline{\tau}}+\frac{1}{\tau_B}\right]\Delta V - \frac{\alpha_m\Delta V}{\overline{\tau}}\left[\frac{\partial\langle e_{0,c}\rangle}{\partial\overline{T}}\right]^{prev}\Delta\overline{T_c} -$$

$$\left[\sum_{\mathbf{K}'}\Phi_{kk'}\,\langle e_{k',c}"\rangle\Delta^3\mathbf{K}' - \left(\sum_{\mathbf{K}'}\Phi_{kk'}\,\langle e_{k',c}"\rangle\Delta^3\mathbf{K}'\right)^{prev}\right]\frac{\Delta V}{V_{BZ}\tau_B} = -R \quad (89)$$

The difference between these discretized equations and the gray model for the nanoporous domain in section 5.1.2 is only in the coefficient, α_m, which is the volume fraction of the host material in the nanocomposite. We determine the volume-averaged lattice temperature equation as earlier, using Eq. (78) – Eq. (80). The current set of discretized equations is exactly the same as the arrowhead matrix shown in Equation (81).

Now we discuss the solution procedure for the above discretized models.

5.5 SOLUTION PROCEDURE

As discussed above, the point-coupled procedure is used as a relaxation sweep in a multigrid procedure. A full approximation storage (FAS) [93] geometric multigrid method is used, with a point-coupled Gauss-Seidel scheme as the relaxation sweep. A standard V-cycle with one pre-sweep and two post-sweeps is used [93] for the work presented here, though any of the numerous published multigrid cycling schemes may be used as well.

5.5.1 Single Relaxation Sweep

Figure 28 is a flow chart of one relaxation sweep for the COMET solution procedure. One sweep involves an outer loop over all points in physical space, each point requiring a direct solve of equation (81).

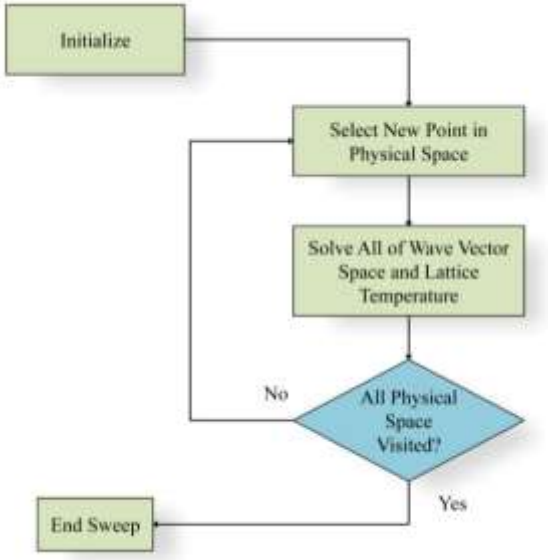

Figure 18: Flow chart for one relaxation sweep for COMET [54]

The relaxation sweep shown in the figure is embedded in the multigrid scheme, with similar relaxation sweeps at each multigrid level [Fig. 29].

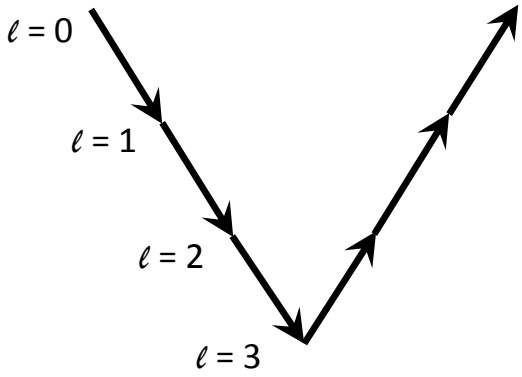

Figure 19: Cycling strategy in a multigrid scheme with V-cycle

The numerical scheme described here is also used for direct numerical simulations of the periodic unit cell of the composite, albeit using intrinsic and not

volume-averaged quantities. In the next chapter, we present results using this procedure for both sets of equations.

5.6 CLOSURE

In this chapter we discussed the discretization procedure and presented the discretized equations for the models developed thus far in this dissertation. We presented the final form of the equation structure and described the underlying numerical algorithm for the solution procedure. In the next chapter we will discuss the problems solved using these models and present results.

Chapter 6: Results and Discussion

In this chapter we present effective thermal conductivity results obtained by using the three volume-averaged BTE models developed in previous chapters. We will structure the chapter as follows: first we present model verification and validation. Next we consider the volume-averaged BTE model for a nanoporous composite in the gray limit. Then we consider the nanoporous model under the non-gray approximation. Finally we consider the volume-averaged model for a two-material composite using a gray approximation.

For all three models, we utilize the direct numerical simulation (DNS) of the phonon Boltzmann Transport Equation (BTE) in the diffuse and ballistic limits for determining model parameters. For the first two models, we compare the accuracy of these volume-averaged models with the detailed analysis obtained through the DNS on the original composite domain. The DNS results are considered a benchmark solution for these cases. For the final model, a direct comparison with the DNS is not applicable since the choice of scattering phase function considers wave effects, whereas, the DNS considers only scattering in the geometric limit.

6.1 Model Verification and Validation

In this section we discuss model verification and validation. We first establish mesh independence in both the physical and wave vector spaces. The volume-averaged BTE model is compared to the Heaslet and Warming [95] [63] analytical solution for radiative transport equation in an isotropically scattering medium in the gray limit. The DNS under

the non-gray approximation is validated against experimental data [71]. This validation justifies the use of DNS "data" as a benchmark against which to validate the volume-averaged BTE model.

Physical Mesh Independence

We present a physical mesh convergence study for the volume-averaged BTE model for the domain shown in Figure 30. The domain has the left and right boundaries held at given temperatures, as shown; the top and bottom boundaries are assumed specularly reflecting. CUBIT [96] is used to generate the mesh. Similar convergence studies in the physical space are performed for all simulations presented.

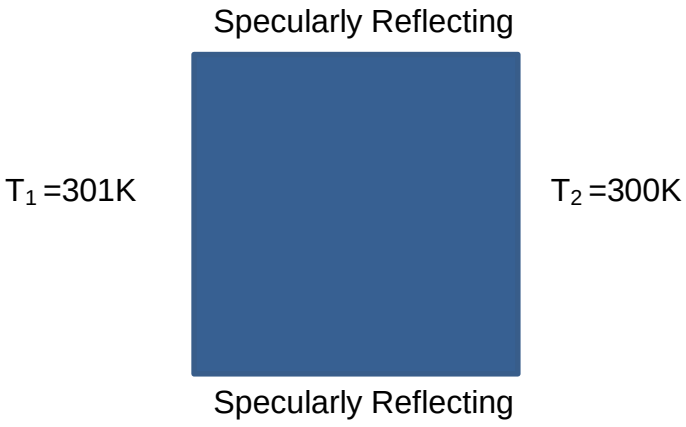

Figure 30: Domain for volume-averaged model simulation for mesh convergence study

The results presented in Figure 31 are for the gray limit. The study is performed in the ballistic limit by maintaining high bulk Knudsen number by setting $\bar{\tau} \to \infty$. The simulation is performed for a **K**-space resolution of $(N_\theta x\, N_\phi) = (2x8)$ in the octant. The temperature at the right and left wall are 301K and 300K respectively. K_{bulk} is computed from $Cv_gL/3$. The effective thermal conductivity is non-dimensionalized using K_{bulk}.

The baseline mesh has 12 cells in the direction of heat flow. We see that mesh independence to 0.2% (with respect to the finest mesh) is obtained at 96 cells in the direction of the heat flow.

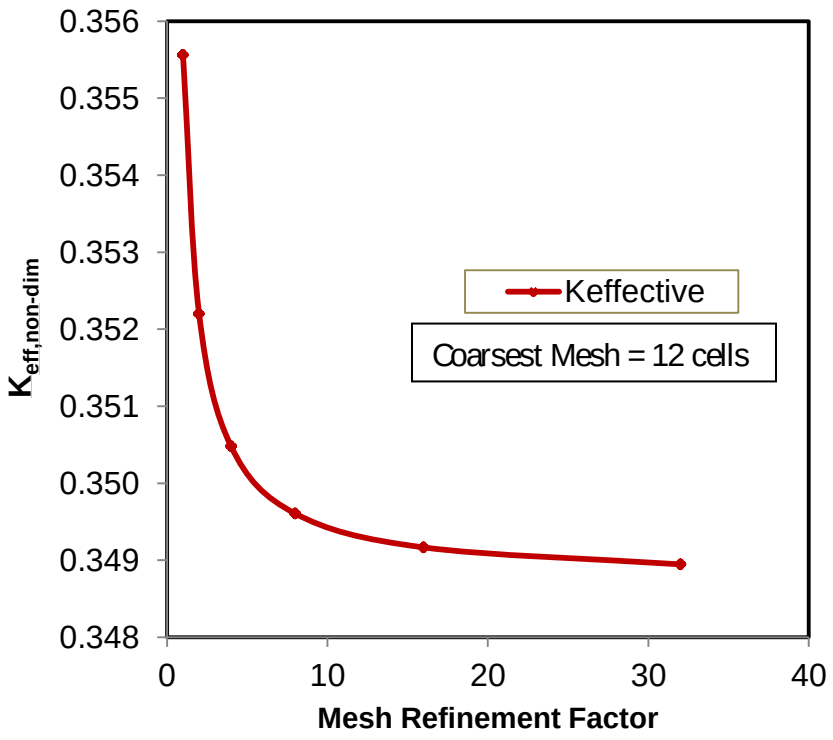

Figure 31: Mesh convergence for nanoporous gray volume-averaged BTE model

K-Space Mesh Independence

In addition to physical space, we ensure convergence is obtained in the wave vector space. We present the convergence test for a square domain with a square pore for a direct numerical simulation of the phonon BTE. A periodic square domain of side $L = 1.0\ \mu m$ is considered, with a single square pore of side $L/2$, giving a solid volume

fraction of $\alpha = 0.75$ (Figure 10). A temperature difference of 1K is applied across the periodic boundaries at the left and right wall. A specular reflecting boundary condition is applied at top and bottom wall. A converged physical mesh is used and has 110592 cells. The study is performed in the ballistic limit. The bulk Knudsen number is held high by keeping the volume-averaged bulk relaxation time $\bar{\tau} \to \infty$. The presented effective thermal conductivity is non-dimensionalized using $Cv_g L/3$.

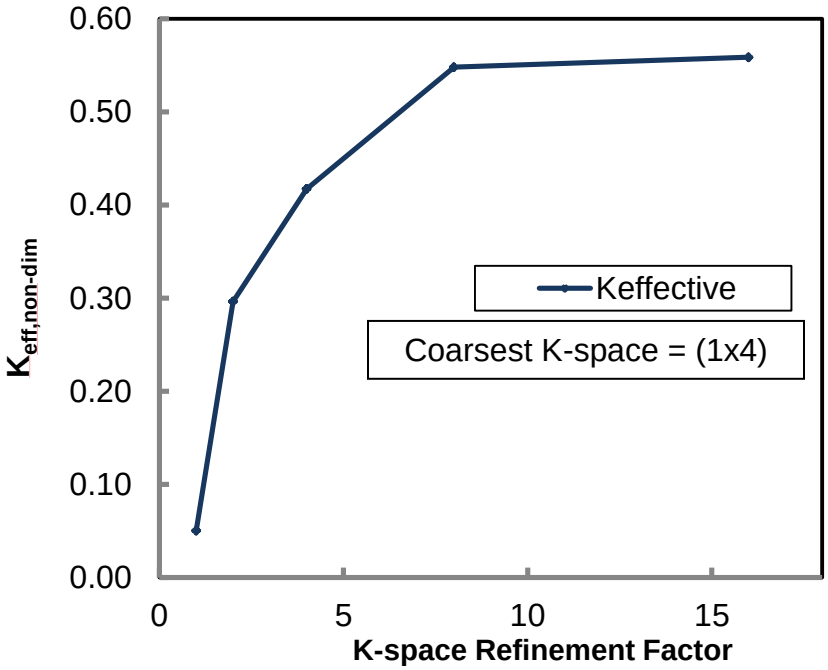

Figure 32: Effective thermal conductivity as a function of **K**-space refinement

As shown in Figure 32, for a physical mesh converged domain we find that wave vector space convergence is attained at a K-space discretization of 8x32 in the octant.

Volume-Averaged BTE Model Verification

For model verification, we compare the model solution in the Fourier limit to the analytical solution of Heaslet and Warming [63] [95] for radiative transport equation in a gray isotropically scattering medium with Dirichlet boundaries as shown in Figure 33. We further verify that the volume-averaged model with isotropic scattering predicts the correct effective thermal conductivity in the limit of low Knudsen number, i.e. it reproduces the Fourier limit to within 1%.

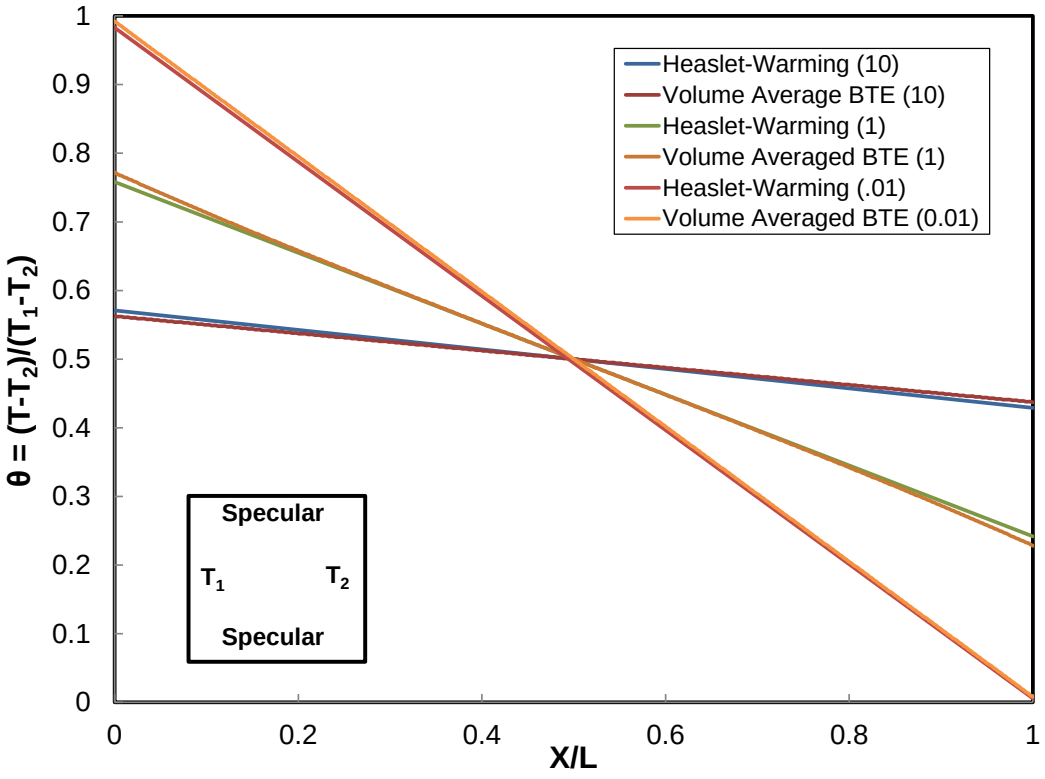

Figure 33: Validation of volume-averaged BTE model with Heaslet and Warming analytical solution [63] of the radiative transport equation for a gray isotropically scattering medium

Validation of Direct Numerical Solution of BTE

We validate the direct numerical solution of the BTE with experimental results [71] for in-plane thermal conductivity of nanoporous silicon films with cylindrical pores. The characteristic dimensions of the periodic nanoporous blocks are thickness, pore separation a and pore diameter d as shown in Figure 34.

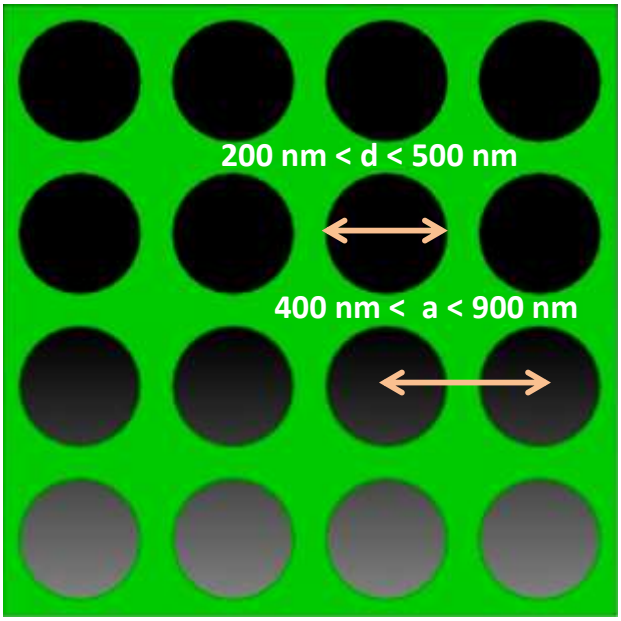

Figure 34: Top view of a nanoporous material with an array of through cylindrical pores

The direct numerical solution with a non-gray approximation and periodic boundaries is performed. The boundary conditions are applied as shown in Figure 35.

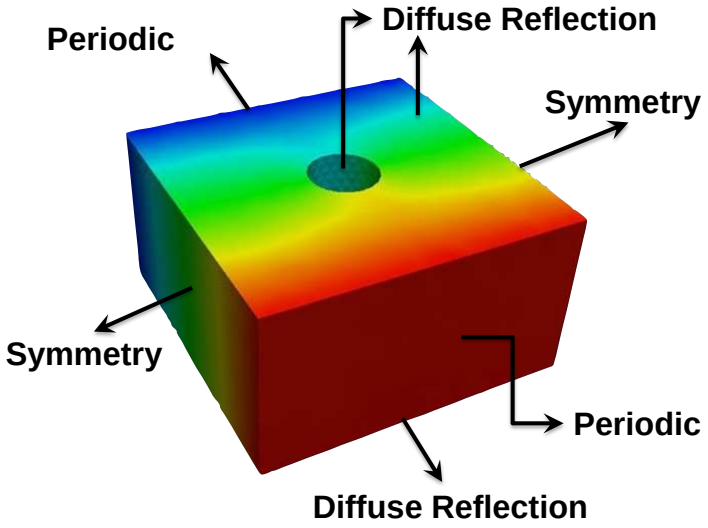

Figure 35: Boundary conditions on periodic domain for DNS

Figure 36 compares the direct numerical solution of the BTE with experimental thermal conductivity measurements by El Kady *et al.* [71] and free path sampling technique by McGaughey *et al.* [97] for varying porosities. The effective thermal conductivity is non-dimensionalized using the experimental bulk thermal conductivity value of 144 W/m-K for silicon.

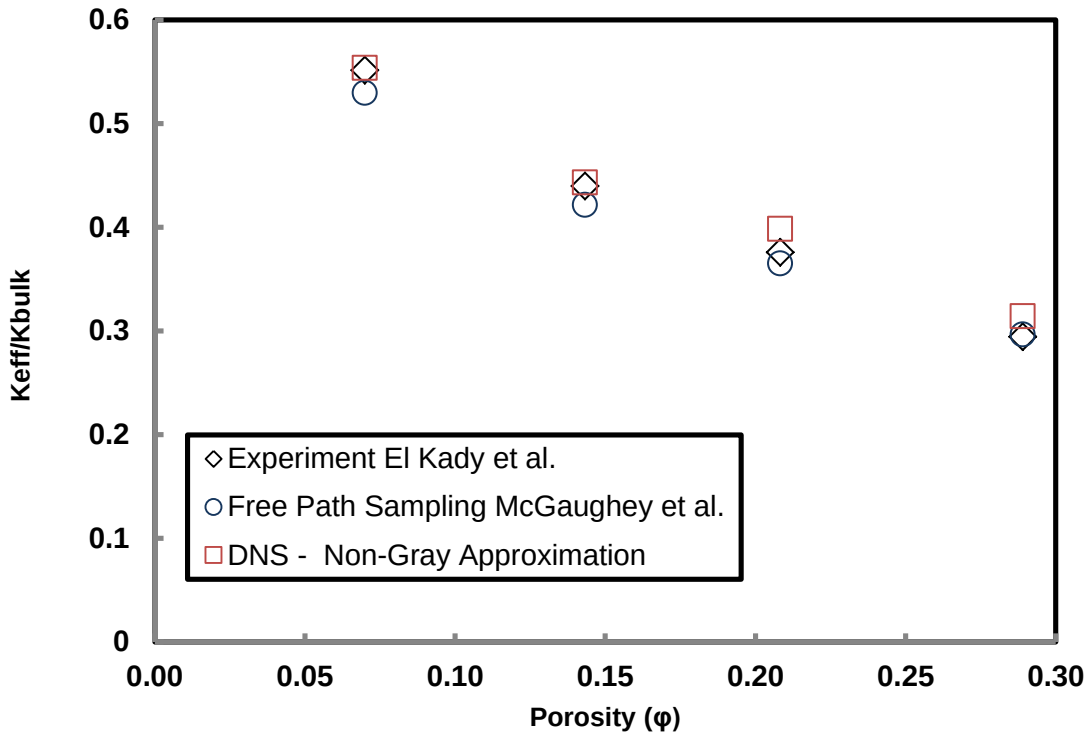

Figure 36: Validation of direct numerical solution of phonon BTE

The maximum difference of the DNS with the experimental results is 6.7% and average difference is 3.4%. The maximum difference with the free sampling model [97] is 9.2% and the average difference is 6.2%. Since the DNS reproduces experimental data well, it is used as a benchmark for validating the different volume-averaged BTE models in this dissertation.

6.2 Gray Volume-Averaged BTE Model for Nanoporous Composite

In this section we present the predictions of the effective thermal conductivity for nanoporous materials using the volume-averaged theory. The results are validated using the direct numerical solution of the composite.

COMPUTATIONAL DOMAIN

We consider periodic nanoporous blocks with thickness, pore separation and pore diameters such as shown in Figure 34. The problem domains and hence the representative elemental volume (REV) geometries are based on available experimental studies[71, 73]. We will present results obtained from the volume averaged BTE model for nanoporous blocks with: (i) spherical inclusions, and (ii) cylindrical inclusions.

In order for us to be able to benchmark our volume-averaged theory we need direct numerical simulations (DNS) of the nanoporous material. Such a simulation provides the baseline against which approximations such as volume averaging can be evaluated. Furthermore, DNS results provide "data" which can be used to calibrate unknowns in the volume averaged theory.

NANOPOROUS DOMAIN WITH SPHERICAL INCLUSIONS

For our study of spherical inclusions, we first consider a periodic block of 700 nm x 700 nm x 500 nm with inclusion diameter of 360 nm. The mesh is generated using the CUBIT software [96] and consists of hexahedral cells, although the numerical method admits arbitrary convex polyhedral cells. A spherical Brillouin zone is assumed and the wave vector space is discretized as ($N_\theta x N_\phi$) in the angular direction, where $0 < \theta < \pi$ and $0 < \phi < 2\pi$. In addition to physical space, we ensure convergence is obtained in the wave vector space.

DIRECT NUMERICAL SOLUTION

We first solve for the domain using DNS of the phonon transport BTE. We apply periodic boundary conditions on left and right walls, symmetry conditions on front and

back walls and diffusely reflecting conditions on top, bottom and the inclusion interface. Figure 35 depicts the boundary conditions on a domain with cylindrical pores for visualization purposes. The converged physical mesh has 1,323,824 cells. A spherical isotropic Brillouin zone is considered. For a physical mesh-converged domain we find that wave vector space convergence is attained at a **K**-space discretization of 8x16 in the octant. For all gray nanoporous DNS simulations we use this converged physical and **K**-space discretization. We compute the effective thermal conductivity of the nanoporous unit from the solution to the BTE.

For verification we compare the DNS solution for the periodic unit with the Fourier solution in the thick limit, i.e. $Kn \to 0$. The DNS predicts the effective thermal conductivity within 3.3% of the Fourier solution. Using the Fourier solution we determine the volume-averaged bulk relaxation time, $\overline{\tau}$ using Eq. (32) in Chapter 2. We then solve the DNS in the ballistic limit and calibrate the value of model parameter, τ_B, using Eq. (33) in Chapter 2. These two parameters will be used as an input to the volume-averaged BTE model.

VOLUME-AVERAGED BTE MODEL IMPLEMENTATION

We present simulation results for the volume-average model. We solve Eq. (13) on a 2D rectangular domain of dimensions 700 nm x 500 nm, which is a 2-D equivalent of the homogenized periodic REV. The geometry is prepared in CUBIT [96] using quadrilateral cells. The converged mesh used in the following studies has 1000 cells in the direction of heat flow and 50 cells in the direction perpendicular to the heat flow. The converged **K**-space is 8x16 in the octant. We use these meshes for all the following

simulations. We apply periodic boundary conditions on the left and right walls and diffuse reflecting conditions on the top and bottom walls as shown in Figure 37. The parameter α is based on the periodic unit used in the DNS simulation, and is equal to 0.89. The parameters $\bar{\tau}$ and τ_B determined from DNS in the previous section are used as input to the model.

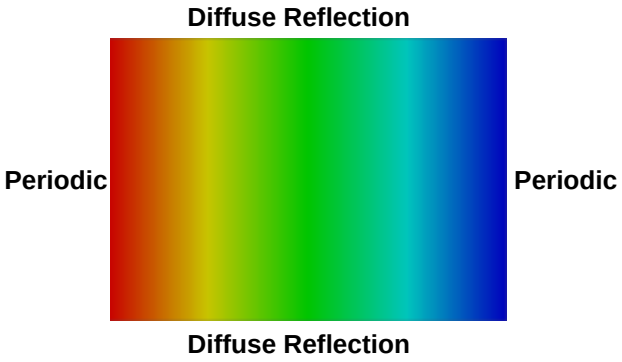

Figure 37: Boundary conditions on simulation domain for volume-average BTE model

The scattering phase function, $\Phi_{KK'}$ for the spherical inclusion is calculated using the ray tracing method as discussed in chapter 2 and is an input to the model. The numerical solution is obtained using COMET algorithm [70].

Next, we perform simulations for the full range of Knudsen numbers based on $\bar{\tau}$ and pore separation a, $Kn_{\bar{\tau}}\left(=\frac{v_g\bar{\tau}}{a}\right)$, while keeping $\tau_B$constant. The value of the Knudsen number based on τ_B, $Kn_{\tau_B}\left(=\frac{v_g\tau_B}{a}\right)$ in these simulations is 1.14. In Figure 38 we present a comparison of the predicted effective thermal conductivity obtained from DNS with the volume-average BTE model for spherical inclusions. The results presented are non-

dimensional and the non-dimensionalizing parameter for thermal conductivity is $K_{Non-dim} = C_v V_g^2 \tau_B / 3$.

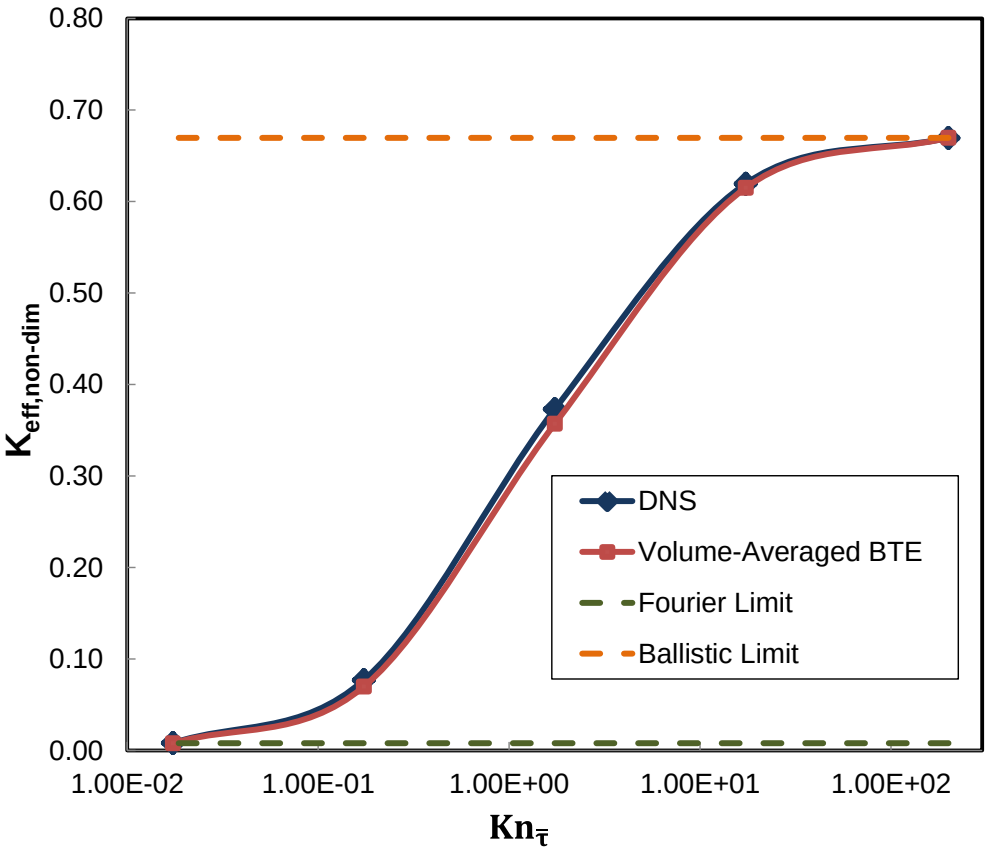

Figure 38: Comparison of volume-averaged BTE model with DNS for varying Knudsen number for a periodic domain with spherical inclusions and solid volume fraction $\alpha = 0.89$ and $\mathrm{Kn}_{\tau_B} = 1.14$

As expected, in the acoustically thick limit, i.e., the low Knudsen number limit, when bulk scattering dominates, we see excellent agreement between the DNS and the model. This is expected because $\bar{\tau}$ was calibrated to the Fourier thermal conductivity, and the DNS in the limit of low Kn recovers the Fourier solution. Similarly, at the other extreme, i.e., at the ballistic limit (large Kn) we obtain excellent agreement with DNS.

This too is expected since τ_B was calibrated to the ballistic DNS solution. In the mid-range of Knudsen numbers, when both bulk and interface scattering have influence, we see good agreement. The average relative error over the full range of Knudsen number is 3.28% and the maximum relative error is 9.26%. This indicates that the volume averaged model performs quite well with respect to the DNS solution across the range of Knudsen numbers, at least as far as effective thermal conductivity is concerned.

We now turn to the question of how well the model predicts the details of the mode-wise heat transfer. In Figure 39, since the model is gray, we consider transport in the different angular directions and compare the predictions of the heat rate at the left wall from the DNS and the volume-averaged BTE model. The x-axis represents the various discrete points in K-space. In our case, we have $\left(N_\theta x N_\phi\right) = (2x8) = 16$ points. The individual heat rate contributions are non-dimensionalized using the net heat rate obtained from the DNS at the left wall.

We see from Figure 39 that the mode-wise predictions from the volume-averaged model match those from DNS quite well. The maximum error in the mode-wise rate presented is 1.12%. The volume–averaged model takes approximately 0.5 CPU hours to converge to a solution. The corresponding DNS solution takes 8 CPU hours. Thus, reasonably accurate solutions may be obtained from the volume-averaged model at far less computational cost than the DNS solution.

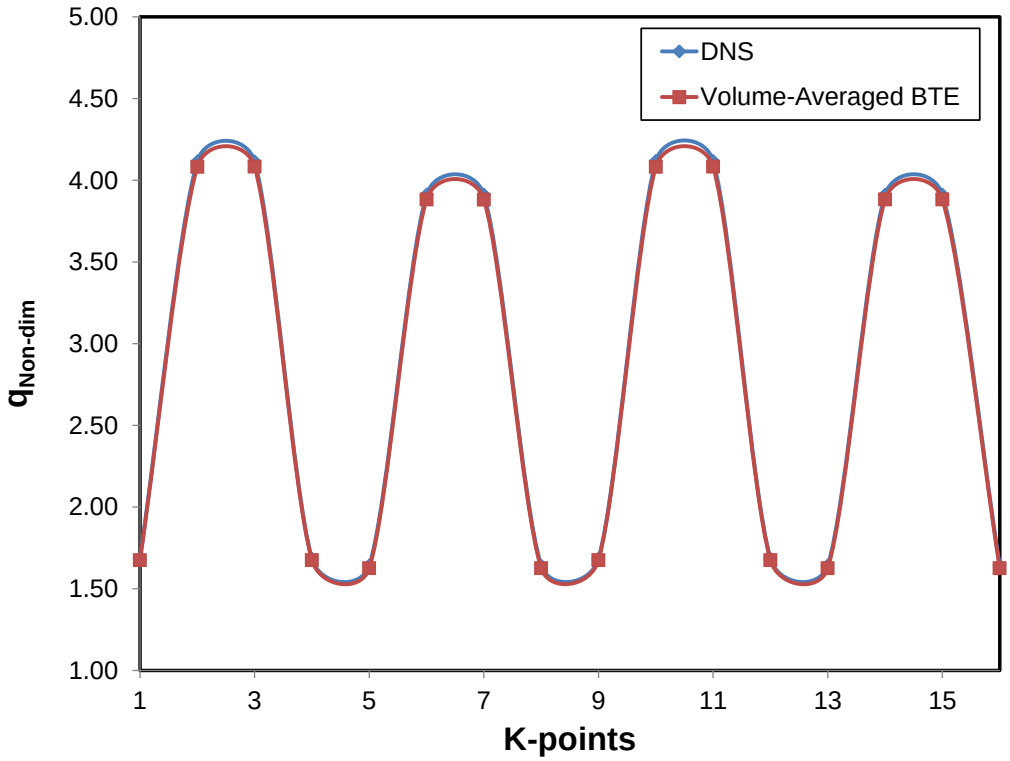

Figure 39: Comparison of volume-averaged BTE model with DNS at different **K**-space points.

NANOPOROUS DOMAIN WITH CYLINDRICAL INCLUSIONS

We now demonstrate the model for periodic domains with cylindrical pores based on the geometry from experimental studies by El Kady *et al.* [71]. The domain under consideration is an REV of a periodic nanoporous thin film with through cylindrical holes. The characteristic lengths of the domain are the interpore distance, pore diameter and the thickness of the film. We first chose a periodic unit of domain size 700 nm x 700 nm x 500 nm with a through cylindrical hole of diameter 360 nm.

DIRECT NUMERICAL SOLUTION

We perform a DNS of phonon transport on a 3-D periodic domain of dimensions as described above. The boundary conditions are applied as shown in Figure 35. The mesh is generated using CUBIT. The solution is verified for mesh and **K**-space independence as before. The converged mesh has 1,471,500 cells. The rest of the parameters and solution procedure are the same as previously stated.

VOLUME-AVERAGED BTE MODEL

The simulation domain and boundary conditions for the model are similar to those in the previous section on spherical inclusions. Hence we use the converged physical and **K**-space meshes as before. The input solid volume fraction is $\alpha = 0.79$, corresponding to the DNS solution. The scattering phase function, $\Phi_{kk'}$, is determined using the ray tracing method for a cylinder of the same aspect ratio as in the DNS problem. We determine the model parameters τ and τ_B from the Fourier and ballistic limit solutions of the DNS as earlier. We verify the model as described in previously.

We compare the non-dimensional effective thermal conductivity obtained from the volume-averaged model with that of the DNS. The solution is plotted as a function of the bulk Knudsen number in Figure 40. The Knudsen based on interface scattering Kn_{τ_B} is held constant at 0.7. In the Fourier and ballistic limits we observe excellent agreement between DNS and volume-averaged model because the volume-averaged model parameters were calibrated to these two limiting solutions, as before. For Knudsen

numbers in between, we observe an average error of 3.25% and a maximum error of 10.2% in the effective thermal conductivity relative to the DNS solution.

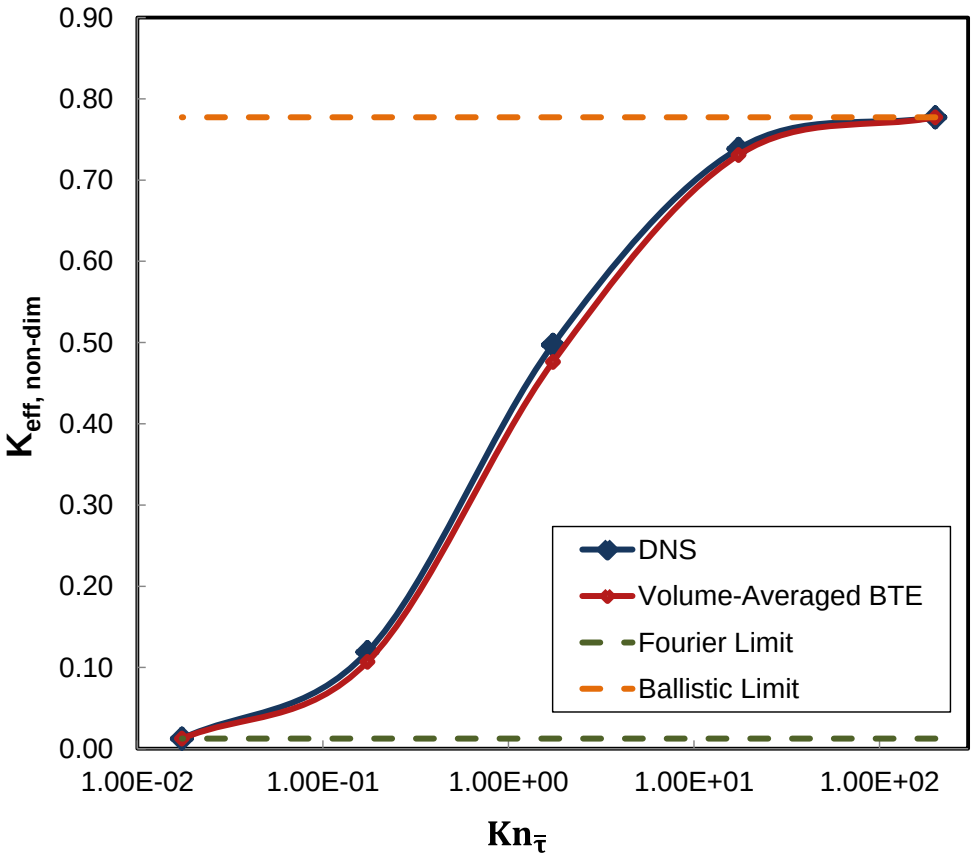

Figure 40: Comparison of volume-averaged BTE model with DNS for varying Knudsen number for periodic domain with cylindrical inclusions and solid volume fraction $\alpha = 0.79$, $\mathrm{Kn}_{\tau_B} = 0.7$

We now investigate the accuracy of the volume-averaged BTE model for varying porosities over a range of Knudsen numbers. The range of porosities considered and the number of cells in the physically converged mesh for the DNS solution are shown in Table 1. The boundary conditions are applied as previously stated.

Thickness (nm)	Width (nm)	Diameter (nm)	Porosity (ϕ)	Number of Cells
500	700	209	0.07	1239840
500	500	213.6	0.14	1327761
500	700	360.5	0.21	1471500
500	500	303.3	0.29	854832
500	700	486.5	0.38	1657854

Table 1: Geometries considered for cylindrical inclusions for studying the effect of porosity on effective thermal conductivity.

The Knudsen numbers based on the calibrated values of volume-averaged bulk and interface scattering relaxation times are shown in Table 2. The Knudsen numbers are calculated based on pore separation, L. The model parameters are documented for all the porosities considered.

Solid Volume Fraction, α	$Kn_{\bar{\tau}}(=\frac{v_g\bar{\tau}}{L})$	$Kn_{\tau_B}\left(=\frac{v_g\tau_B}{L}\right)$
0.93	7.89E-03	1.76
0.86	7.44E-03	1.05
0.79	7.05E-03	0.71
0.71	6.57E-03	0.75
0.62	6.19E-03	0.92

Table 2: Knudsen numbers based on calibrated volume-averaged BTE model parameters for varying porosities

Figure 41 shows the comparison of the effective thermal conductivity predicted by the volume-averaged BTE model with that from the DNS solution for different porosities for cylindrical inclusions. Comparisons are shown at ballistic and Fourier limits and at $\mathrm{Kn}_{\bar{\tau}} = 1.7$ and 0.17. The effective thermal conductivity is non-dimensionalized by the effective thermal conductivity obtained from DNS for porosity=0.07 for the corresponding $\mathrm{Kn}_{\bar{\tau}}$. The Knudsen numbers based on the interface scattering relaxation time Kn_{τ_B} for the different porosities in Figure 36 are shown in Table 2.

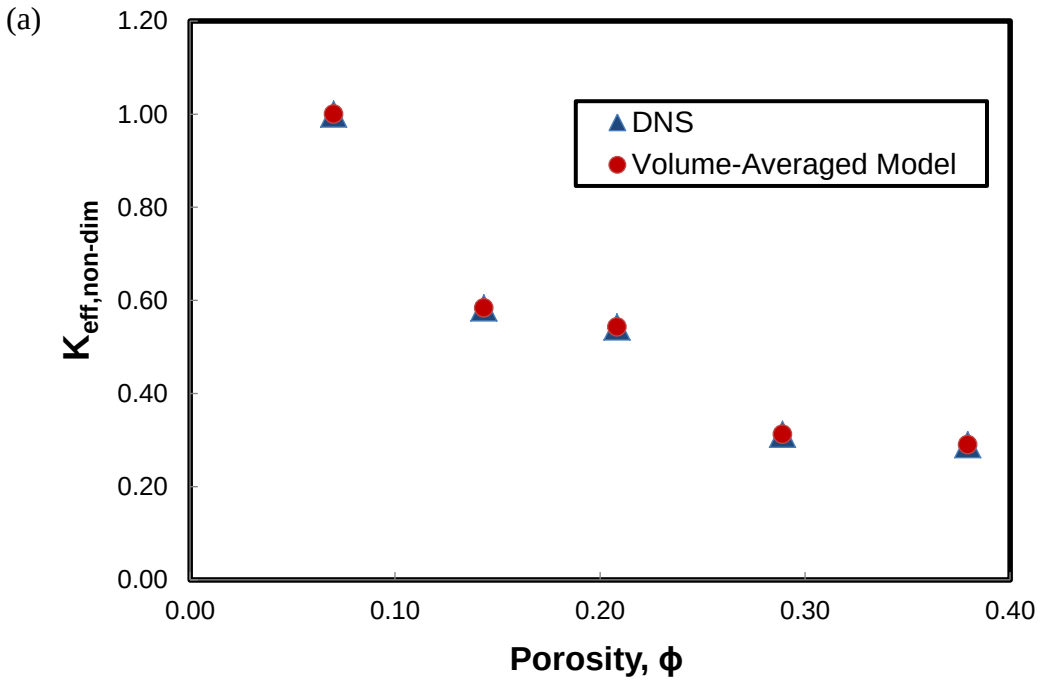

Figure 41 (a): Comparison of volume-averaged BTE model with DNS at ballistic limit

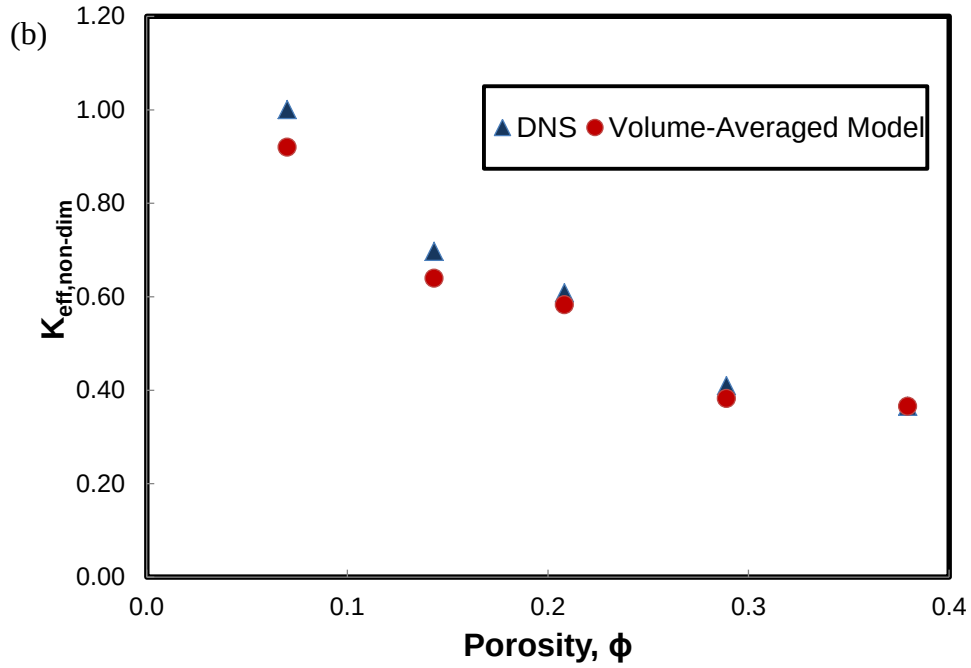

Figure 41 (b): Comparison of volume-averaged BTE model with DNS at $Kn_{\bar{\tau}} = 1.7$

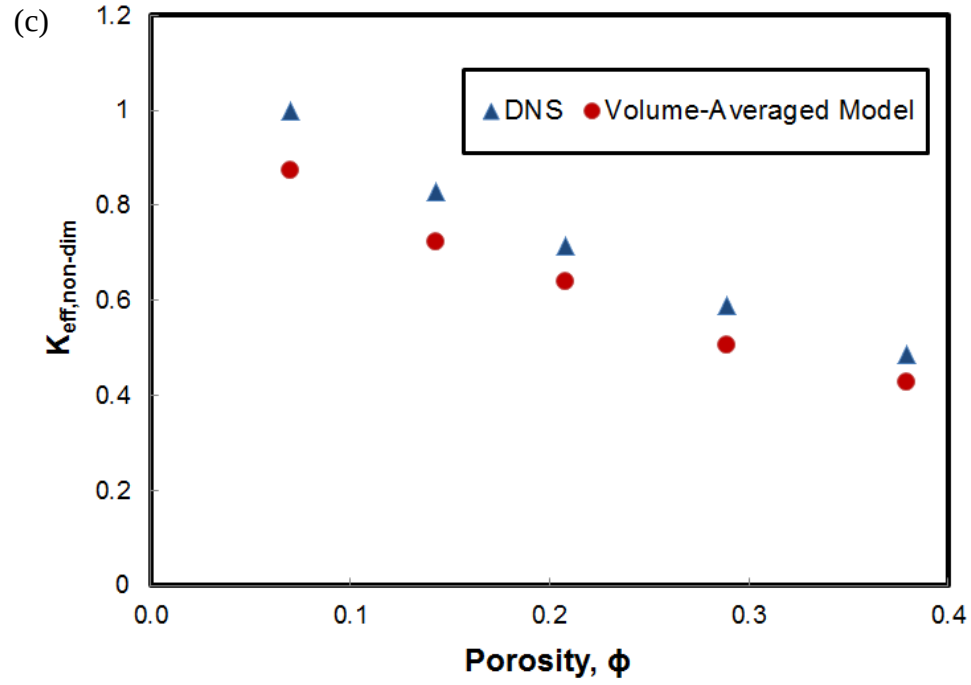

Figure 41 (c): Comparison of volume-averaged BTE model with DNS at $Kn_{\bar{\tau}} = 0.17$

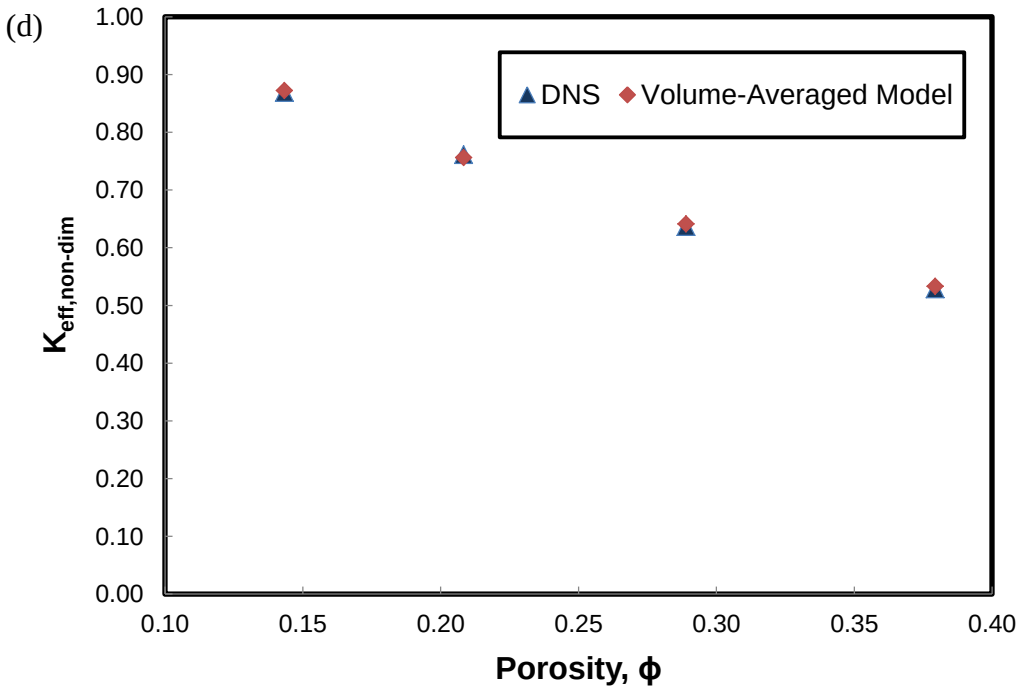

Figure 41 (d): Comparison of volume-averaged BTE model with DNS at the Fourier limit

The volume-averaged theory compares well with the DNS for all the porosities considered at the low Kn and ballistic limits [Figures 41 (a) and 41 (d)], as expected, since the volume averaged model was calibrated to the DNS at these limits. For mid-range Knudsen numbers, the maximum relative error with respect to the DNS solution is 14% [Figures (41 (b) and 41 (c)].

6.3 NON-GRAY VOLUME AVERAGED BTE MODEL FOR NANOPOROUS COMPOSITE

In this section we consider the same nanoporous silicon geometry as earlier [71], but under a non-gray approximation. We assume an isotropic spherical Brillouin zone for silicon. Phonon dispersion curves are obtained using lattice dynamics [98] using the

environment-dependent interatomic potential (EDIP) [34]. We use the dispersion curves corresponding to the [1 0 0] direction in bulk silicon as shown in Figure 42.

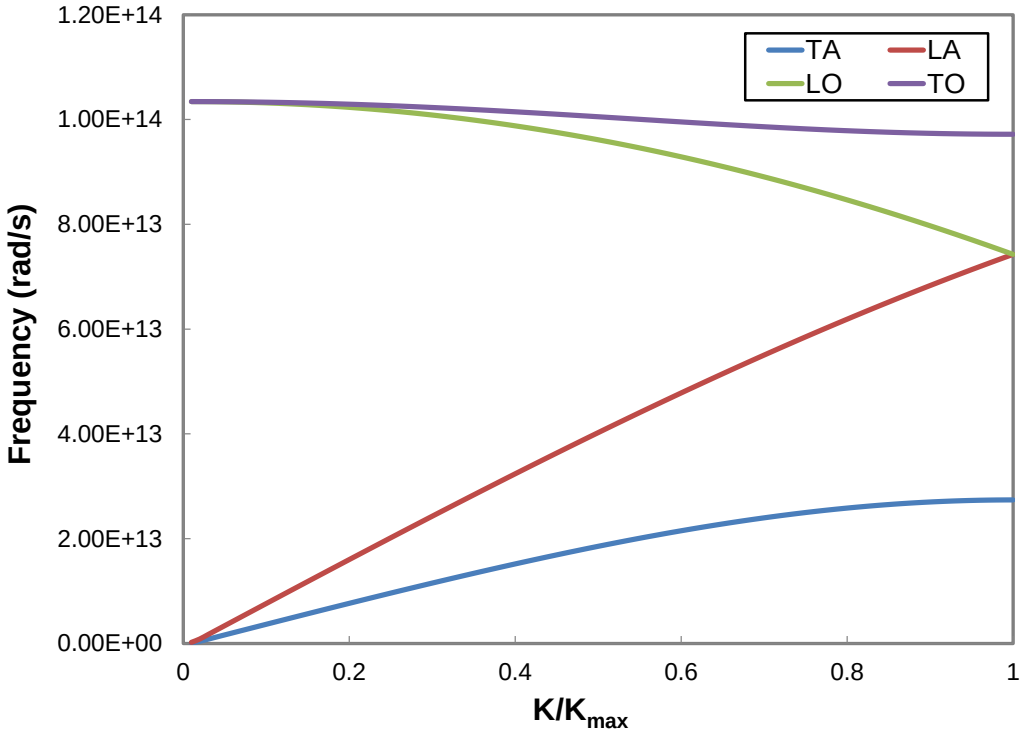

Figure 42: Dispersion relation for silicon in the [100] direction at 300 K [34]

The lattice constant a for the spherical Brillouin zone is adjusted to attain the correct specific heat for silicon [54]. It is the diameter of the approximated spherical Brillouin zone. A conceptual representation is shown in Figure 43.

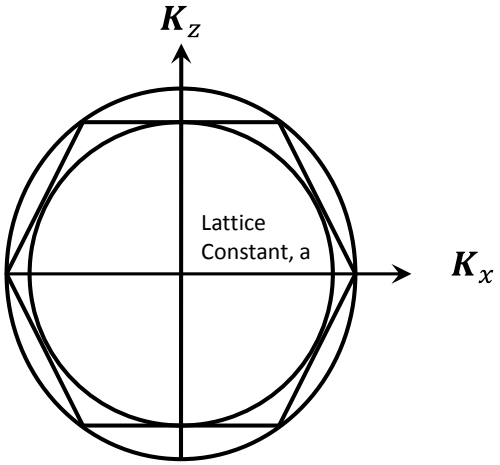

Figure 43: Representation of lattice constant, a, with respect to the Brillouin zone volume

Four different polarizations corresponding to the longitudinal acoustic (LA), transverse acoustic (TA), longitudinal optical (LO) and transverse optical (TO) modes are considered as shown in Figure 42. In this high symmetry direction [1 0 0], the two transverse modes are degenerate [99]. The relaxation times are found using the relations below [100].

$$\frac{1}{\tau_{\mathrm{im}}} = \mathrm{A}\omega^4$$

$$\frac{1}{\tau_{\mathrm{u}}} = \mathrm{BT}\omega^2 \mathrm{e}^{-\mathrm{C/T}}$$

$$\frac{1}{\tau_{eff}} = \frac{1}{\tau_{im}} + \frac{1}{\tau_u} \quad (90)$$

The impurity scattering relaxation time τ_{im} and the Umklapp scattering relaxation time τ_u yield the effective relaxation time using Matthiessen's rule [76]. Here the values of the constants A, B and C are $1.32\text{x}10^{-45}$ s^3, $1.73\text{x}10^{-19}$ s/K and 137.36 K respectively [100]. These constants are determined from curve-fits to bulk properties found

experimentally [100]. In the present work, relaxation times used are determined at 300K. In general, for non-gray problems, there is a range of Knudsen numbers, one for each K point. For reporting purposes, following [54], we define an average Knudsen number defined as follows:

$$Kn = \frac{1}{L}\frac{\sum_p \sum_{BZ} |v| \tau_{eff} \Delta^3 \mathbf{K}}{\sum_p \sum_{BZ} \Delta^3 \mathbf{K}} \qquad (91)$$

Here L is the characteristic length of the domain, $|v|$ is the magnitude of the group velocity of the phonon mode, $\tau_{eff}$is computed as above. The sum is over all polarizations p and the spherical Brillouin zone, BZ.

We orient the unit vectors $(\mathbf{K_x}, \mathbf{K_y}, \mathbf{K_z})$ for the wave vector space along the physical space unit vectors$(\mathbf{x}, \mathbf{y}, \mathbf{z})$. Figure 44 shows a schematic of the discretization of the Brillouin zone for a non-gray phonon dispersion [54]. The wave vector space is discretized in the angular and radial directions. For all our non-gray problems, we will be using an angular discretization of $(N_\theta, N_\phi) = (2x8)$ and a radial discretization of the wave vector magnitude of $(N_k = 8)$. The discretization of the **K**-space along with the four polarizations yield (2x8x8x4 =) 512 discrete algebraic equations in each physical cell in the computational domain.

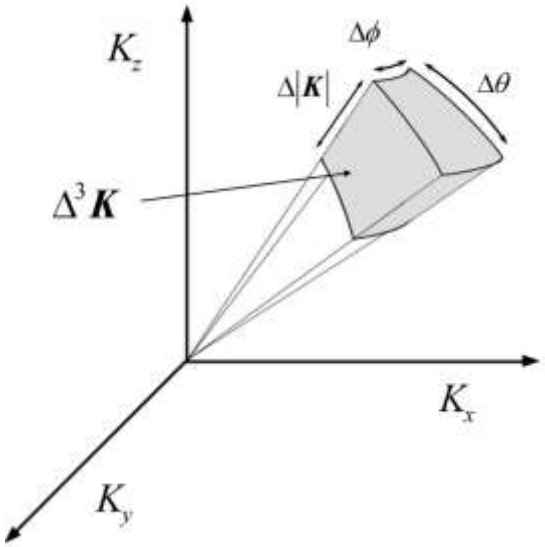

Figure 44: Discretization of the Brillouin zone for a non-gray dispersion [54]

For the non-gray problem, we consider a nanoporous silicon film with cylindrical through holes, as before. An REV is shown in Figure 45 (a). To reduce computational expense, our non-gray DNS simulations employ one quarter of the actual REV and apply the boundary conditions appropriately as shown in Figure 45 (b).

(a)

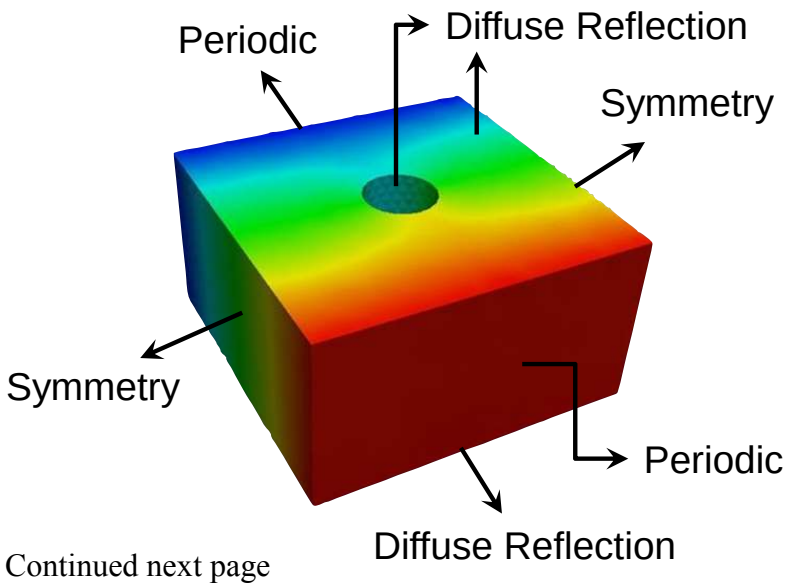

Figure 45: Continued next page

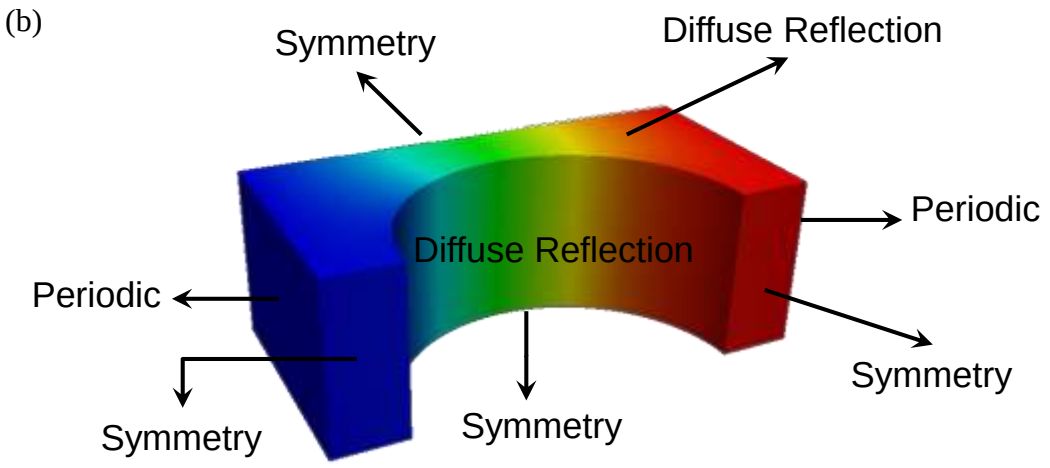

Figure 45: Problem domains for DNS. (a) Geometry of the REV with boundary conditions, and (b) quarter geometry with appropriate boundary conditions

For the DNS, we first chose a domain with a cylindrical inclusion of porosity, $\phi = 0.38$ and determine the exponent, d in equation (31). We consider a block of dimension 700 nm x 700 nm x 500 nm with a cylindrical hole of radius 243 nm; this yields a porosity of 0.38. The meshing is done in CUBIT and the domain has a physical mesh size of 92,208 cells. The **K**-space discretization used is $N_\theta x N_\phi x N_k = 2x8x8$. The silicon bulk thermal conductivity used is $K_{bulk} = 135 \frac{W}{m} - K$ and the specific heat, $C_v = 1.63x10^6 \frac{J}{m^3} - K$.

First we solve for Fourier conduction in the REV geometry volume-averaged bulk relaxation times, $\overline{\tau_k}$ for the volume averaged model. For the Fourier-limit solution, we use temperature boundary conditions and compute the effective thermal conductivity of the composite structure. The procedure is described in detail in chapter 3. Next we perform DNS in the ballistic limit. We use the effective thermal conductivity so computed to calibrate the interface scattering relaxation time, $\tau_{B,k}$. We determine the

anisotropic scattering phase function $\Phi_{\mathbf{KK'}}$ using the ray tracing algorithm discussed in chapters 2 and 3. We use the corresponding diameter of the cylindrical inclusion as an input to the ray tracing algorithm.

CALIBRATION AT THE BALLISTIC LIMIT

Two distinct approaches are undertaken to calibrate the interface scattering relaxation time at the ballistic limit. One involves employing constant values of $\tau_{B,k}$ for all **K**-points. The other requires calibration of the individual $\tau_{B,k}$s at the ballistic limit to the DNS solution using the Newton-Raphson method described in chapter 3.

CONSTANT $\tau_{B,k}$ APPROACH

We first compare the effective thermal conductivity predictions obtained from volume-averaged theory with that using DNS using the constant $\tau_{B,k}$ approach. We calibrate the volume-averaged BTE model using a single value of $\tau_{B,k}$ for all **K**-points. Then we investigate how the non-gray volume-averaged BTE model compares with the DNS for the same geometry for Knudsen numbers in between the ballistic and Fourier limits.

Figure 46 shows a comparison of the overall thermal conductivity comparison with DNS for three different porosities and Knudsen numbers. The effective thermal conductivity is non-dimensionalized using the effective thermal conductivity at the ballistic limit, as defined in equation (29).

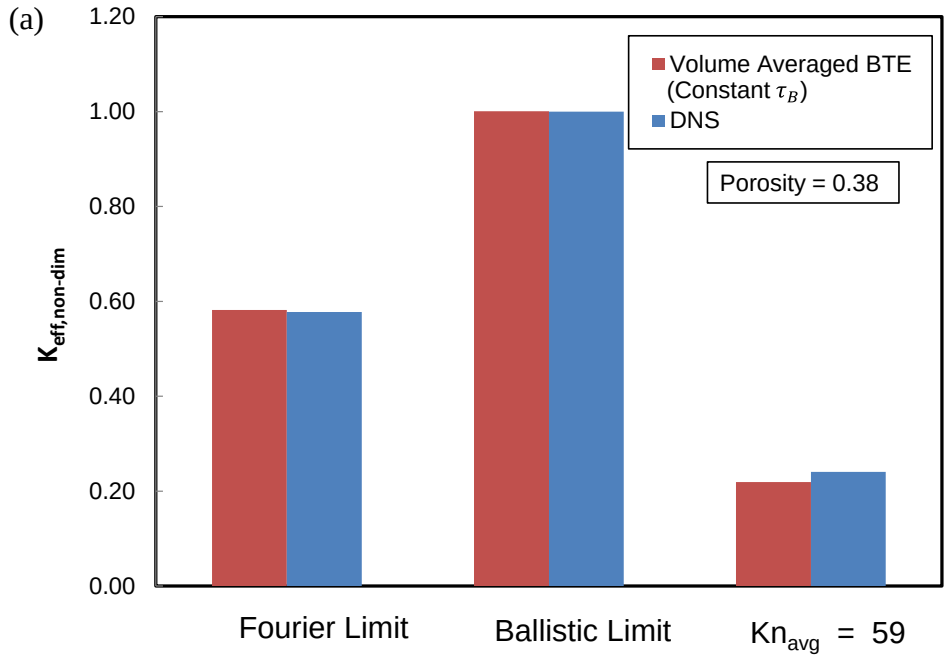

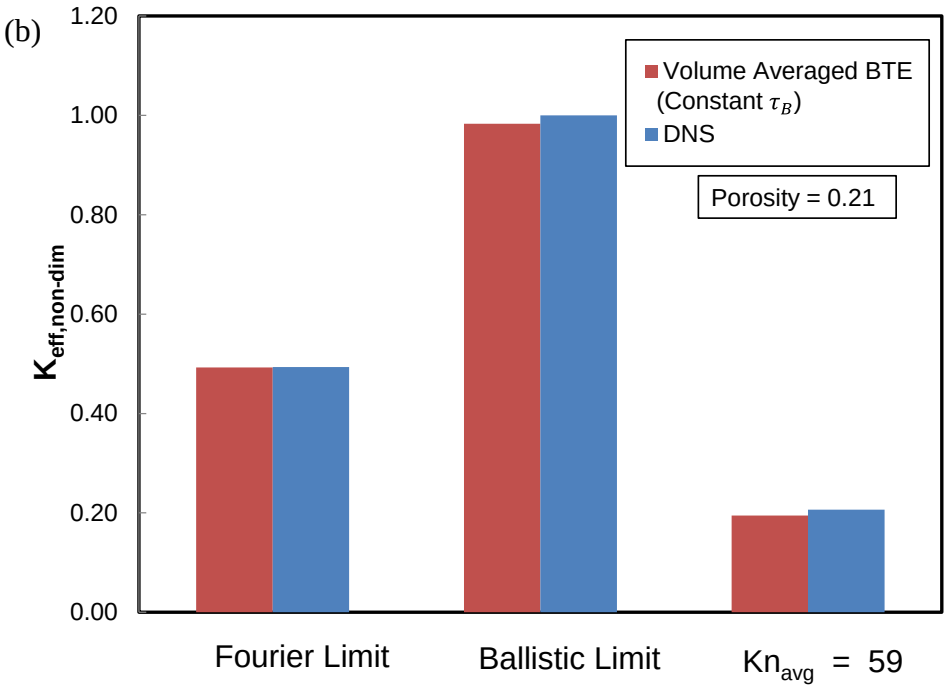

Figure 46: Continued on next page

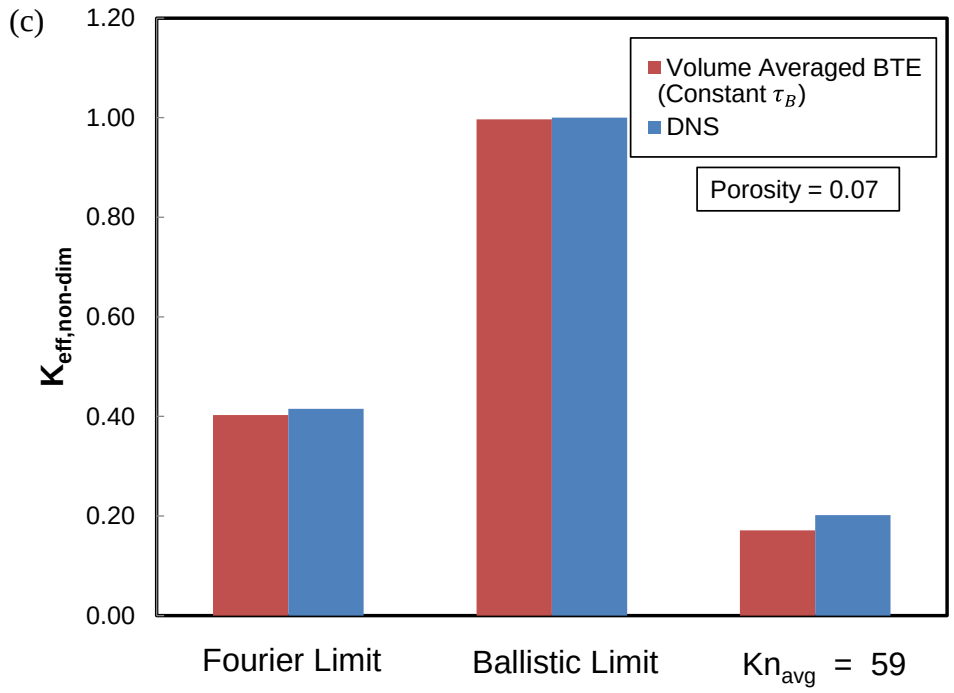

Figure 46: Comparison of effective thermal conductivity for DNS and non-gray volume-averaged BTE model with a constant $\tau_{B,k}$ calibration for porosity (a) $\phi = 0.38$ (b) $\phi = 0.21$, and (c) $\phi = 0.07$

The maximum error in the predicted effective thermal conductivity with respect to the DNS is 11.9%. However, the individual heat rate contribution of the phonon modes is not captured accurately. We compare the mode-wise heat rates obtained using both constant and variable $\tau_{B,k}$ approach in the next section.

VARIABLE $\tau_{B,k}$ APPROACH

The constant $\tau_{B,k}$ approach does not predict the individual contributions accurately. An alternative is to calibrate for individual $\tau_{B,k}$s at the ballistic limit using the Newton Raphson method as described in chapter 3. We determine ($N_{pol}xN_k = 4x8 = 32$) different values of the interface scattering relaxation time $\tau_{B,k}$.

To verify that the Newton-Raphson calibration procedure is working well, we compare the heat rate contribution of each phonon polarization for the DNS and the volume-averaged BTE in the ballistic limit. The maximum absolute error in the total heat rate is 0.19%. The maximum and minimum error in the modewise heat rate is 1.8% and 0.03% respectively. The calibrated solution is presented in Figures 47 (a)-(d). The heat rate is normalized using the net heat rate.

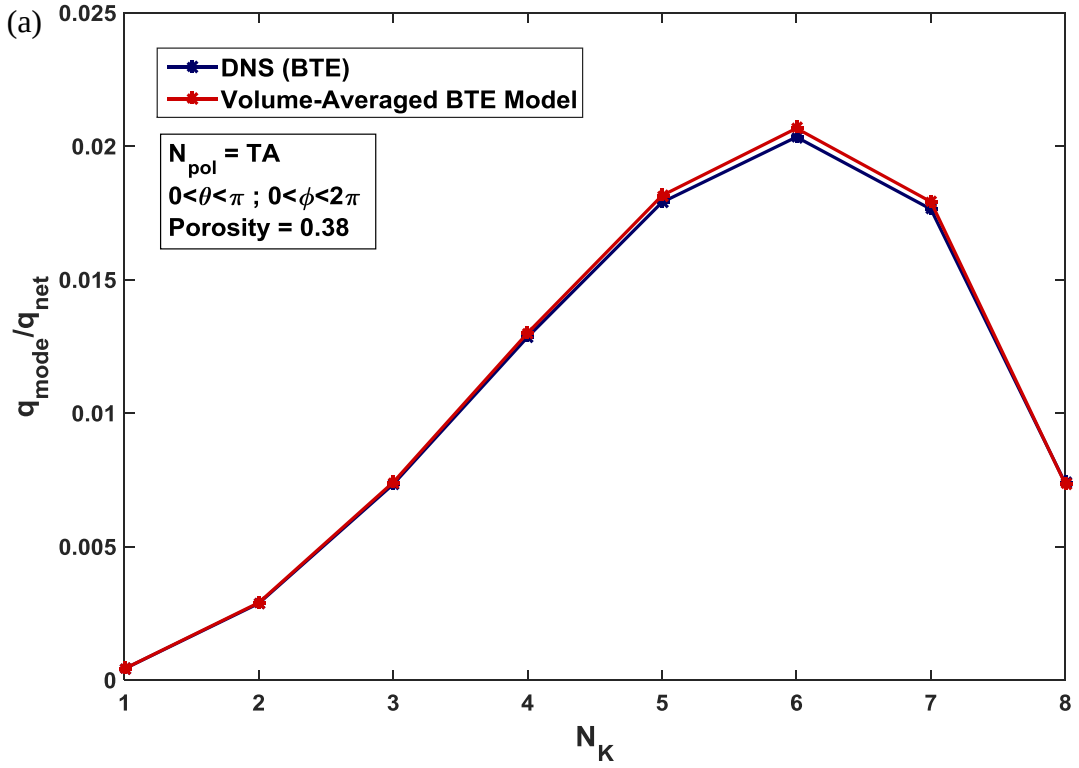

Figure 47: Continued on next page

(b)

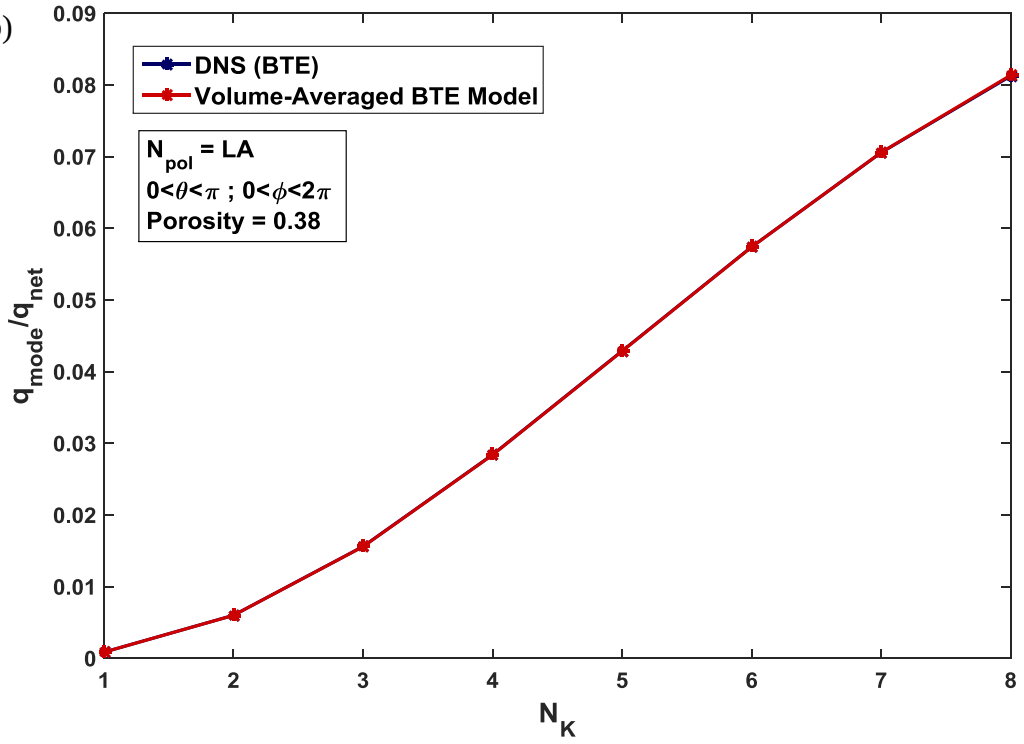

(c)

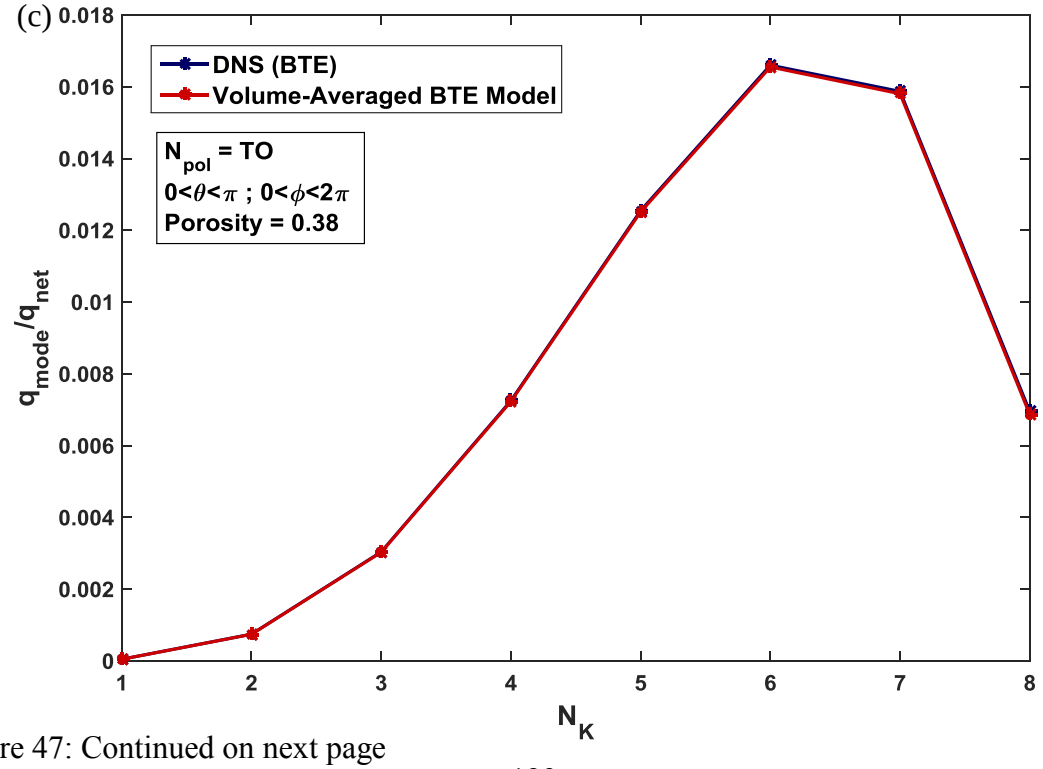

Figure 47: Continued on next page

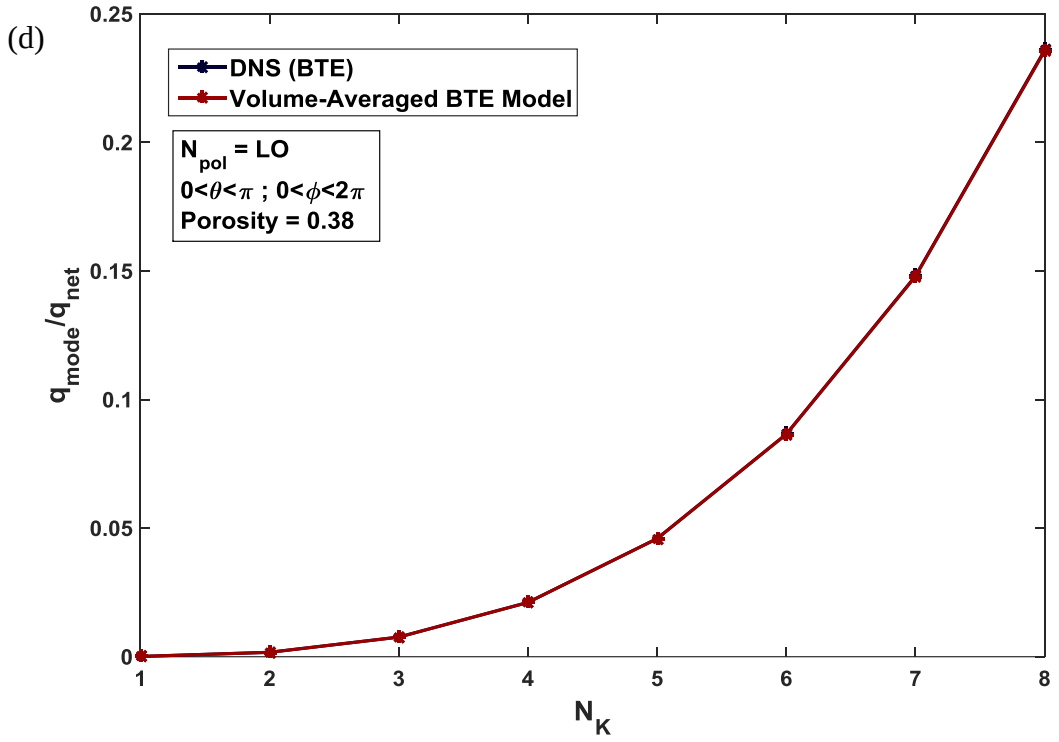

Figure 47: Comparison of DNS and volume-averaged BTE model at the ballistic limit for heat rate contribution of (a) TA modes, (b) LA modes, (c) TO modes, and (d) LO modes.

In Figure 48 we compare the mode-wise heat rate contributions of the above two approaches with the DNS at the ballistic limit for a porosity of 0.38. The green line represents the volume-averaged BTE model with the constant $\tau_{B,k}$ approach. The red dotted line represents the volume-averaged BTE model with the variable $\tau_{B,k}$ approach and the blue dots represent the DNS. The DNS and the variable $\tau_{B,k}$ approach match very well as expected. Although the overall heat rate matches with the DNS, the mode-wise heat rate contributions obtained using the constant $\tau_{B,k}$ approach do not match the DNS. In order to capture the physics accurately, contributions of different phonon modes towards the overall heat rate is of significance along with the overall thermal conductivity

match. Therefore, we will be using the variable $\tau_{B,k}$ approach to predict mode-wise and overall heat rates for different porosities.

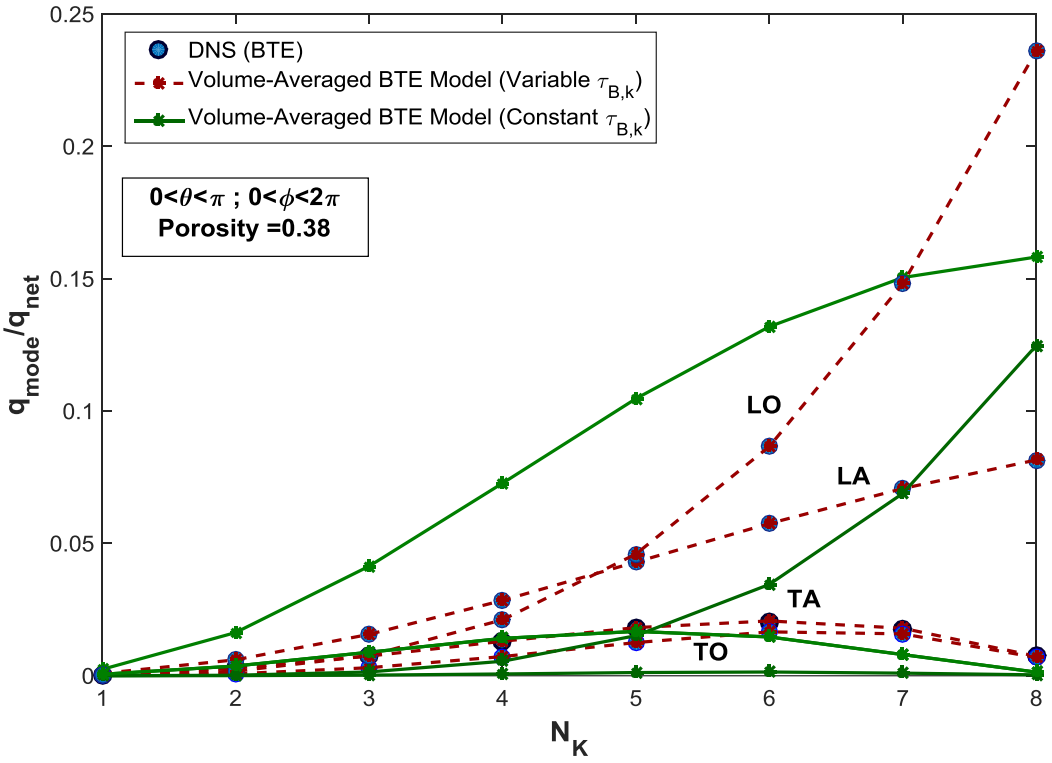

Figure 48: Comparison of DNS and volume-averaged BTE model with constant and variable $\tau_{B,k}$ approach at the ballistic limit for heat

VERIFICATION AT ISOTROPIC SCATTERING LIMIT

For verification, we compare the volume-averaged BTE model with the calibrated $\tau_{B,k}$ values at the isotropic scattering limit with the analytical expression for isotropic scattering:

$$K_{eff} = \sum_{BZ} \left(\frac{de_0}{dT}\right)_k v_k . v_k \alpha^2 \tau_{B,k} \Delta^3 K \qquad (3)$$

The calculation assumes that bulk scattering is absent. The solution matches within 2% of the analytical formulation at the isotropic scattering limit. Figure 49 shows a comparison

of the isotropic scattering solution to the isotropic analytical formulation and the anisotropic scattering results. The black line represents the heat rate computed using equation (3) for the calibrated values of $\tau_{B,k}$. The blue line represents the volume-averaged BTE solution using an isotropic scattering phase function. The red line represents the volume-averaged BTE solution using the anisotropic $\Phi_{KK'}$ at the ballistic limit.

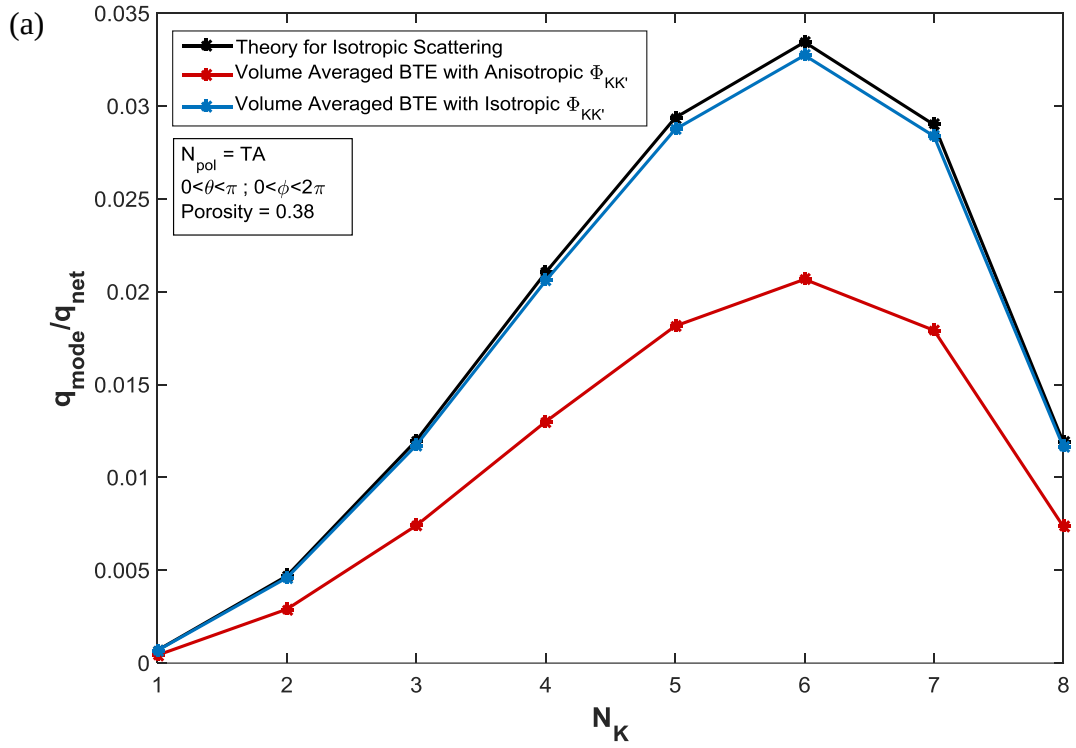

Figure 49: Continued on next page

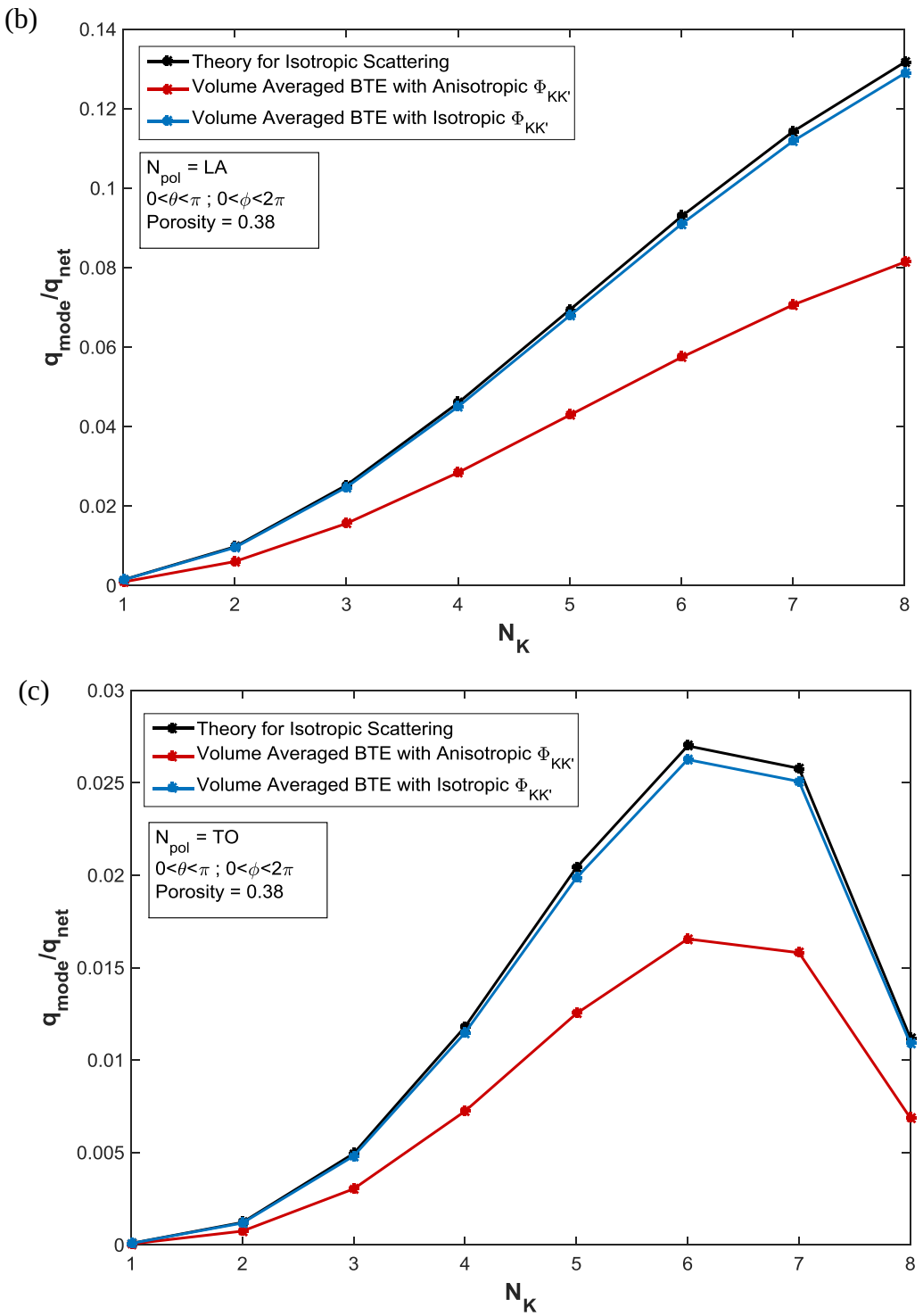

Figure 49: Comparison of volume-averaged BTE solution at the ballistic limit using isotropic and anisotropic $\Phi_{KK'}$ with the isotropic theory at the ballistic limit for different phonon modes: (a) TA, (b) LA, (c) TO and (d) LO.

Next we compare the DNS and the volume-averaged BTE model using this approach to compare at an average Knudsen number of 59. The Knudsen number in the domain ranges from 0.4 to 14×10^3. There is a significant spread in the Knudsen number due to the different scales of the relaxation times and group velocities in the silicon dispersion. We use the calibrated values of the volume-averaged bulk relaxation times, $\overline{\tau_k}$ and interface scattering relaxation times, $\tau_{B,k}$. The scattering phase function $\Phi_{\mathbf{KK'}}$ corresponding to the geometry is used.

Using the solution of the DNS, we compute the heat rate contributions of each phonon polarization and compare that with solution obtained from the volume-averaged BTE model. In Figure 50 (a)-(d) we compare the solution obtained from the variable $\tau_{B,k}$ approach with the DNS. In the ballistic limit, calibrating $\tau_{B,k}$ at each mode, yields better results at individual modes than assuming a constant value of the interface scattering relaxation time. We compare the DNS and the volume-averaged BTE with variable $\tau_{B,k}$ for three different porosities. The maximum error in the overall prediction is 26%. Although the overall heat rate match is better with the constant $\tau_{B,k}$ approach, the variable $\tau_{B,k}$ approach gives a more accurate depiction of the individual phonon mode contributions. Figures 51 and 52 show a condensed form of the comparison between the DNS and volume-averaged BTE model for the four different phonon modes.

In general, the match with the DNS solution at intermediate Kn is poorer than in the gray case. The reason is likely the large spread in Kn in non-gray calculations. This means that our DNS simulations are not equally resolved at all K-points, especially with

the coarse mesh we are using for these non-gray calculations. Thus, there may be significant discretization error in the low Kn calculations. The volume-averaged BTE is likely far better resolved than the DNS, and these differences in resolution add to the uncertainty in the calibrated parameters. Unfortunately, further spatial resolution of the non-gray DNS problem is not possible with available computational power.

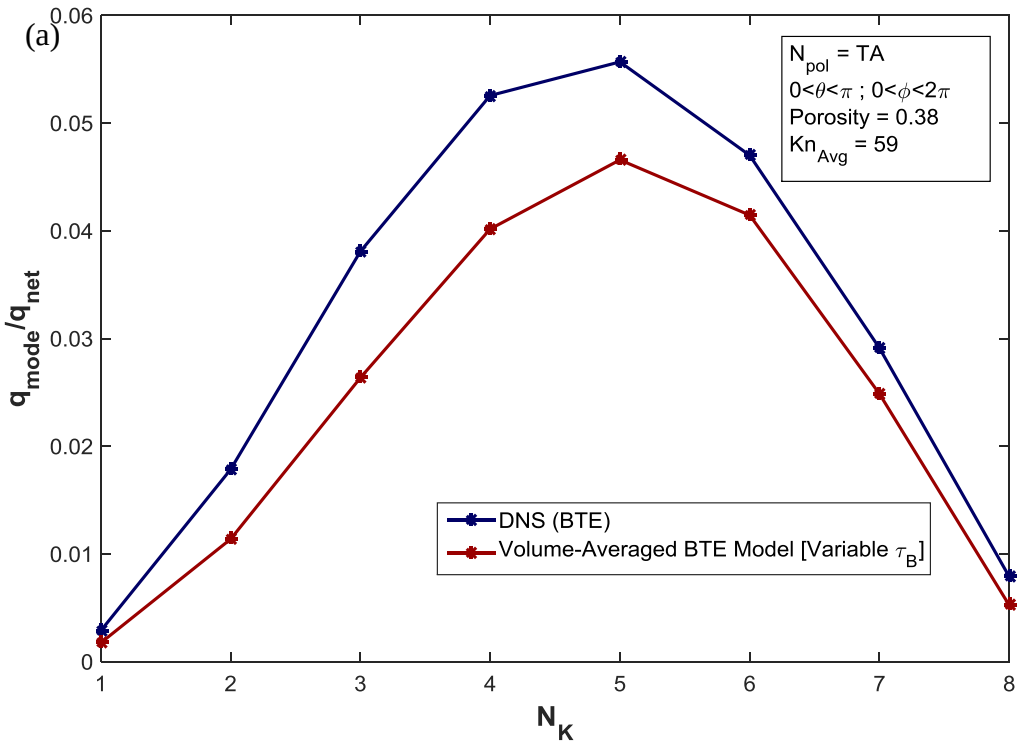

Figure 50: Continued on next page

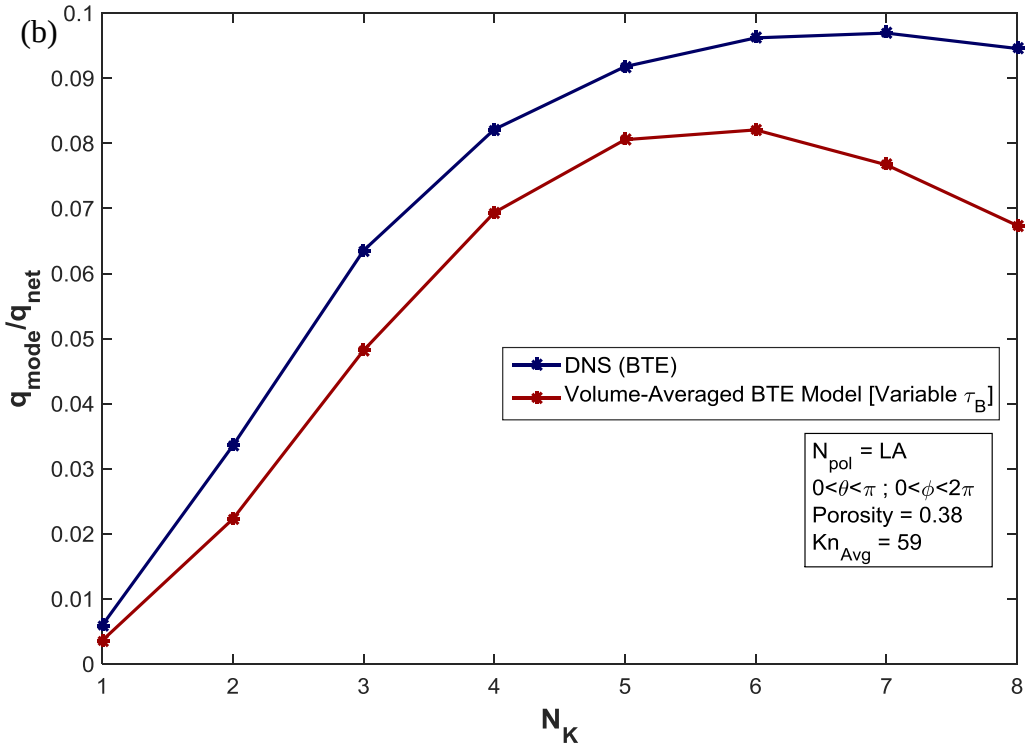

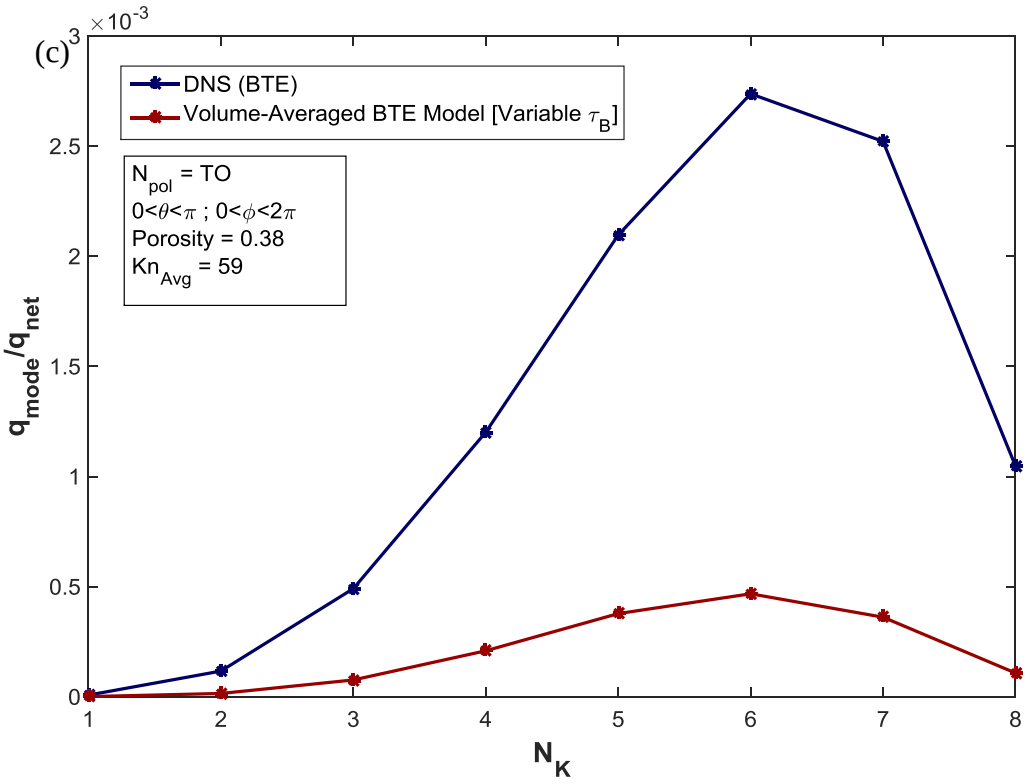

Figure 50: Continued on next page

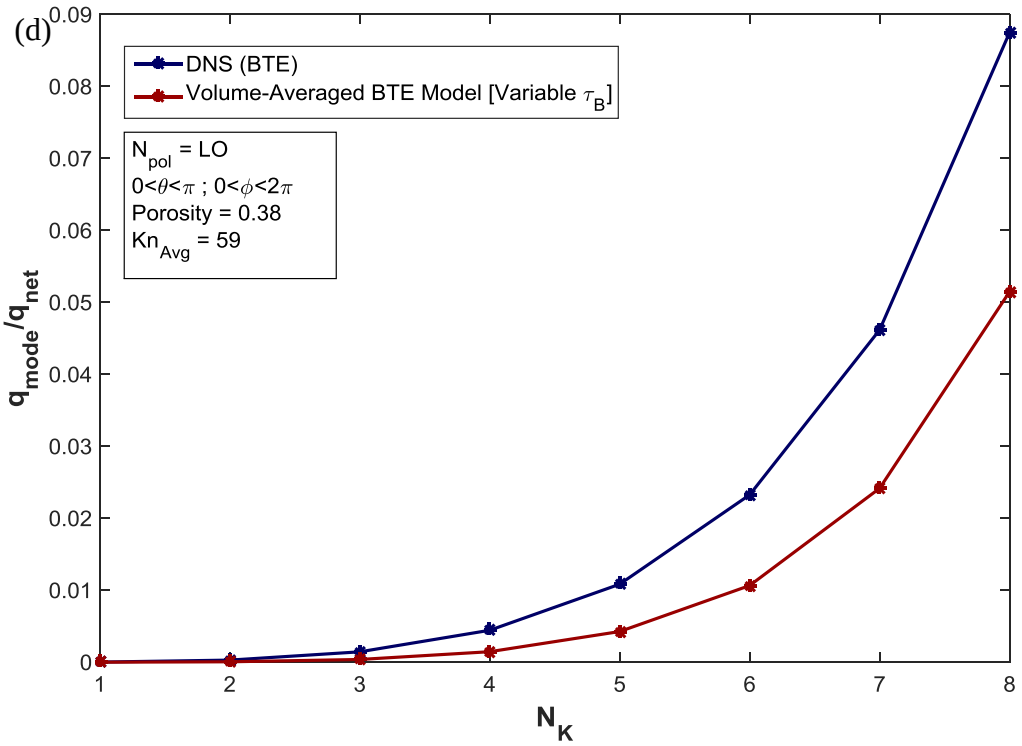

Figure 50: Comparison of volume-averaged BTE with DNS at a porosity of 0.38 for different phonon modes: (a) TA (b) LA (c) TO (d) LO

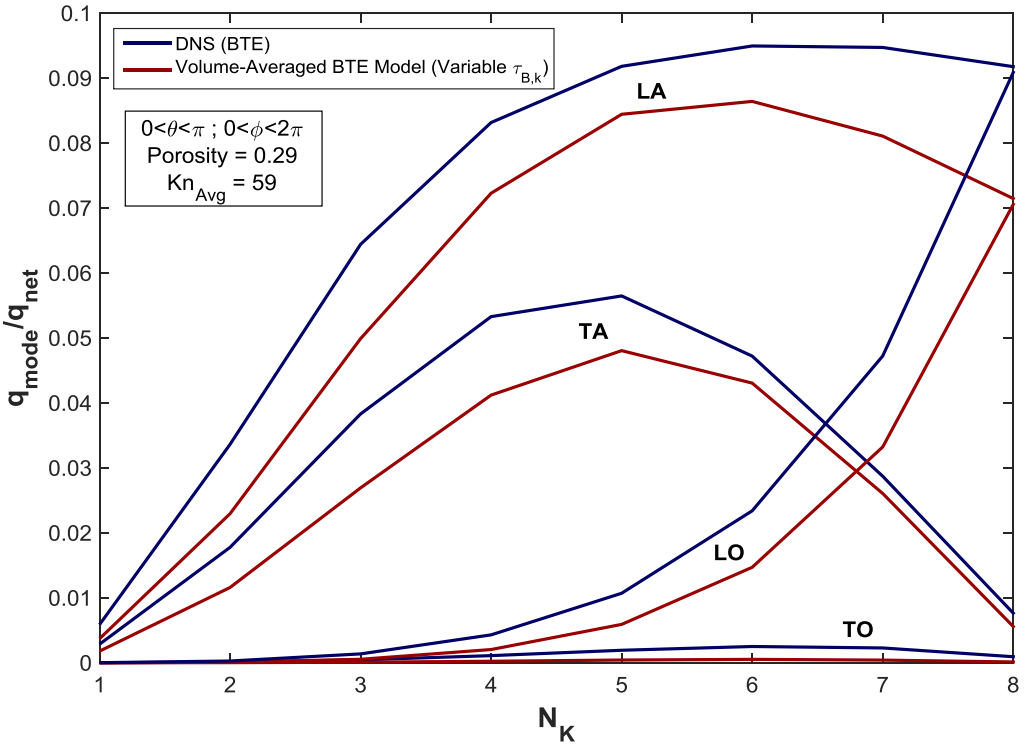

Figure 51: Comparison of volume-averaged BTE with DNS at a porosity of 0.29 for different phonon modes

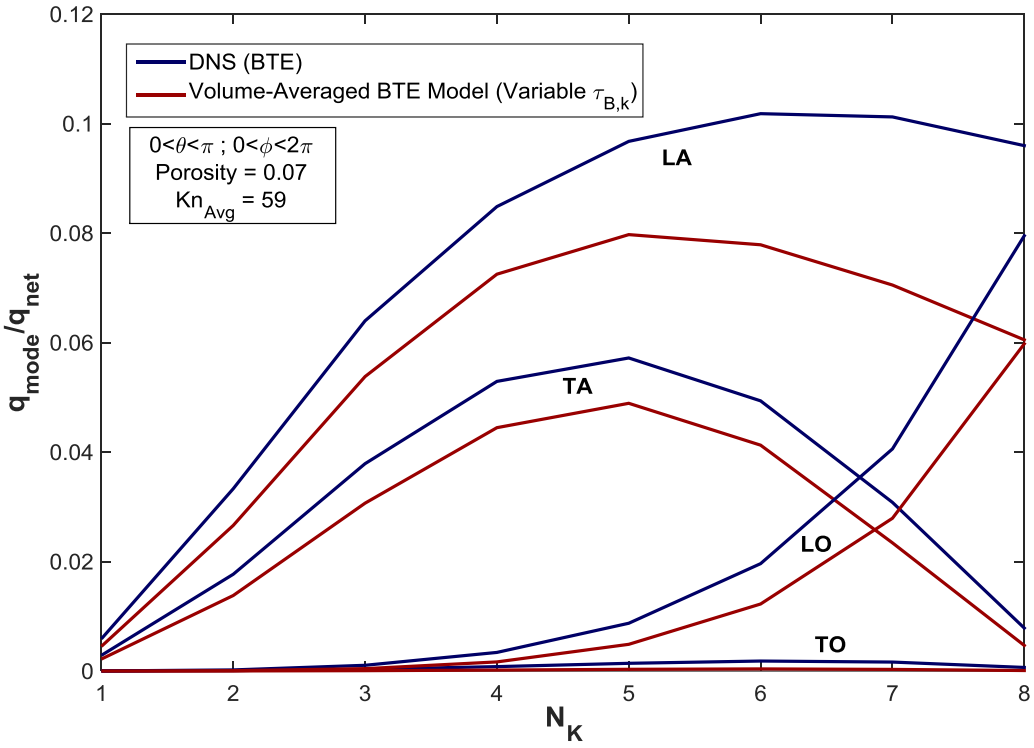

Figure 52: Comparison of volume-averaged BTE with DNS at a porosity of 0.07 for different phonon modes

6.4 VOLUME AVERAGED BTE MODEL FOR TWO-MATERIAL NANOCOMPOSITE

We consider silicon medium with a spherical germanium particle. We solve equation (57) in the domain for a spherical particle of diameter 5 nm. We vary the porosity by increasing the length scale of the outer domain. The geometries considered are listed in Table 3.

The results presented are for the gray limit with a phonon group velocity of 5843 m/s, frequency of 2e12 rad/s and a constant specific heat of $1.6\text{x}10^6$ J/m^3-K for the matrix material, in this case silicon. The bulk relaxation time for the matrix material is computed based on a bulk thermal conductivity of 137W/m-K using $Cv_g^2\tau/3$. The material

properties of the particle need to be considered for computing the scattering phase function. Additionally, the thermal properties of the particle material are considered in calculating the effective thermal conductivity of the composite at the Fourier limit. The Fourier limit solution is used to calibrate the volume-averaged bulk relaxation time, $\overline{\tau}$. Thus, both the silicon host material and the germanium particles contribute to the model parameters.

Film Dimension (nm x nm)	Particle Volume Fraction (ϕ)	$\mathbf{Kn}_{\overline{\tau}}$	$\mathbf{Kn}_{\tau_B}$
10x10	0.065	9.21	2.69
11x11	0.049	7.34	2.18
12x12	0.038	6.62	2.33
14x14	0.024	5.12	2.27

Table 3: Geometries and Knudsen numbers at calibrated model parameters for volume-averaged model simulation

The list of different properties [89] used for this computation is provided in Table 4. The velocity of the wave in Germanium is computed using Eq. 66 in Chapter 4. The discretization of the **K**-space used for the solution is $\left(N_\theta x N_\phi\right) = (8x16)$. The boundary

conditions are applied as earlier. At the composite interface we have a diffuse reflection condition. A temperature jump of 1K is applied between the right and left walls.

Properties	Silicon	Germanium
Thermal Conductivity, K $(\mathrm{W/m-K})$	137	60.2
Lamé Constant, λ $(\mathrm{N/m^2})$	$6.39x10^{10}$	$4.83x10^{10}$
Lamé Constant, μ $(\mathrm{N/m^2})$	$7.956x10^{10}$	$6.71x10^{10}$
Density, ρ $(\mathrm{Kg/m^3})$	2332	5322
Frequency, ω $(\mathrm{rad/s})$	$3x10^{12}$	$2x10^{12}$

Table 4: Material properties for two-material volume-averaged BTE composite model

For Fourier limit, the actual REV composite geometry is solved, considering a background silicon matrix with germanium particles. The Fourier conduction equation is solved in this composite, and the value of $\overline{\tau}$ is calibrated to effective thermal conductivity of the composite. To determine the value of τ_B, we consider a nanoporous material with pores equal in size to the particles. The DNS is performed on nanoporous geometry in the ballistic limit to determine τ_B. The boundary conditions for the DNS at the ballistic limit are the same as for the nanoporous domain DNS. Figure 53 shows the boundary conditions as applied on the Si-Ge composite domain under consideration.

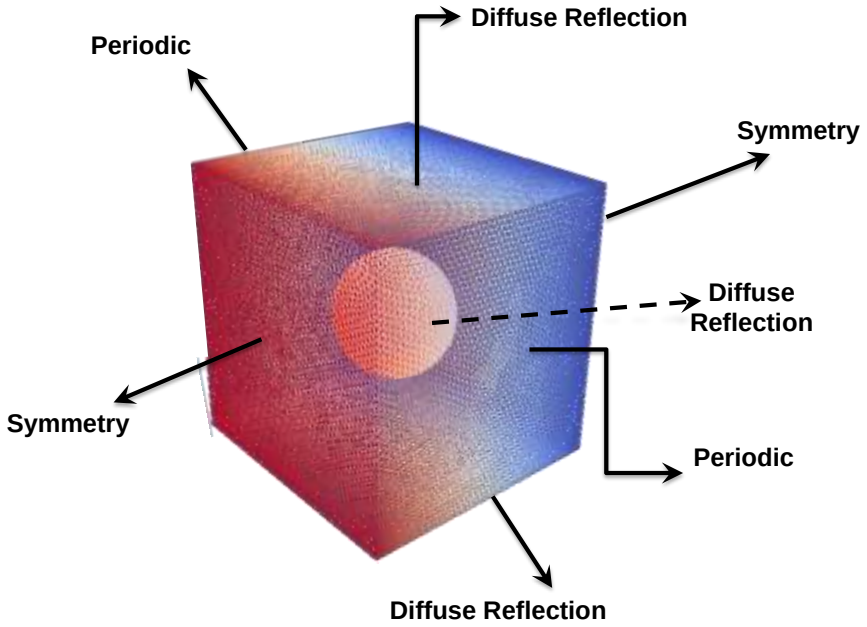

Figure 53: Boundary conditions on a composite domain of Si host with Ge particle for DNS

From these DNS, the volume-averaged bulk relaxation time and the interface scattering relaxation time are determined as previously done for the gray model. Such a treatment is justified because the particles are much smaller than the length scale of the bulk material, and may be considered point particles. Thus, the interface scattering time τ_B is determined primarily by the travel time of the phonon between particles, and this is captured by the computation in the nanoporous domain.

We determine the scattering phase function using Mie scattering theory as discussed in chapter 4. The volume-averaged model is solved on physical mesh consisting of 1000 cells. The volume-averaged BTE is solved on a corresponding 2D domain using the boundary conditions as stated previously. A periodic boundary

condition is applied with a positive temperature gradient of 1K from left wall to right wall.

The DNS cannot be used as a benchmark to the volume-averaged BTE at these limits because the wave nature of the transport in the vicinity of the particle cannot be captured by the DNS. We therefore present the effective thermal conductivity for a range of Knudsen numbers for varying porosities.

The following porosities are considered: 0.06, 0.024, 0.038, and 0.049 as shown in Table 4. The Knudsen numbers are calculated based on pore separation. The resulting volume-averaged BTE solutions are shown below in Figure 54. In each of the figures below, the Knudsen number based on τ_B, i.e., $v_g\tau_B/L$, is held constant, and the Knudsen number based on bulk scattering, $\overline{\tau}$, is varied from the Fourier to the ballistic limit. When bulk scattering is small, i.e., high $\mathrm{Kn}_{\overline{\tau}}$, the ballistic solution is recovered; in this limit, scattering is purely due to the presence of the particle. As $\mathrm{Kn}_{\overline{\tau}}$ is decreased, bulk scattering increases in dominance, and the effective thermal conductivity falls. Ultimately, bulk scattering dominates over particle scattering, and the Fourier limit for the composite is recovered.

(a)

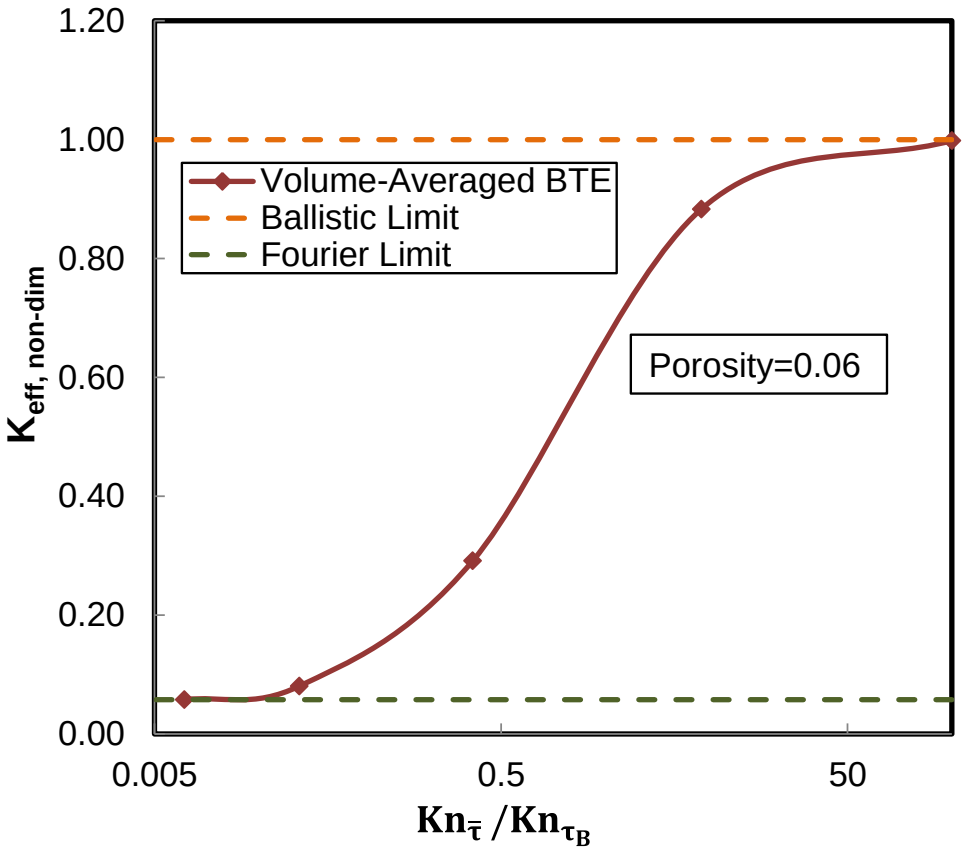

Figure 54: Continued on next page

(b)

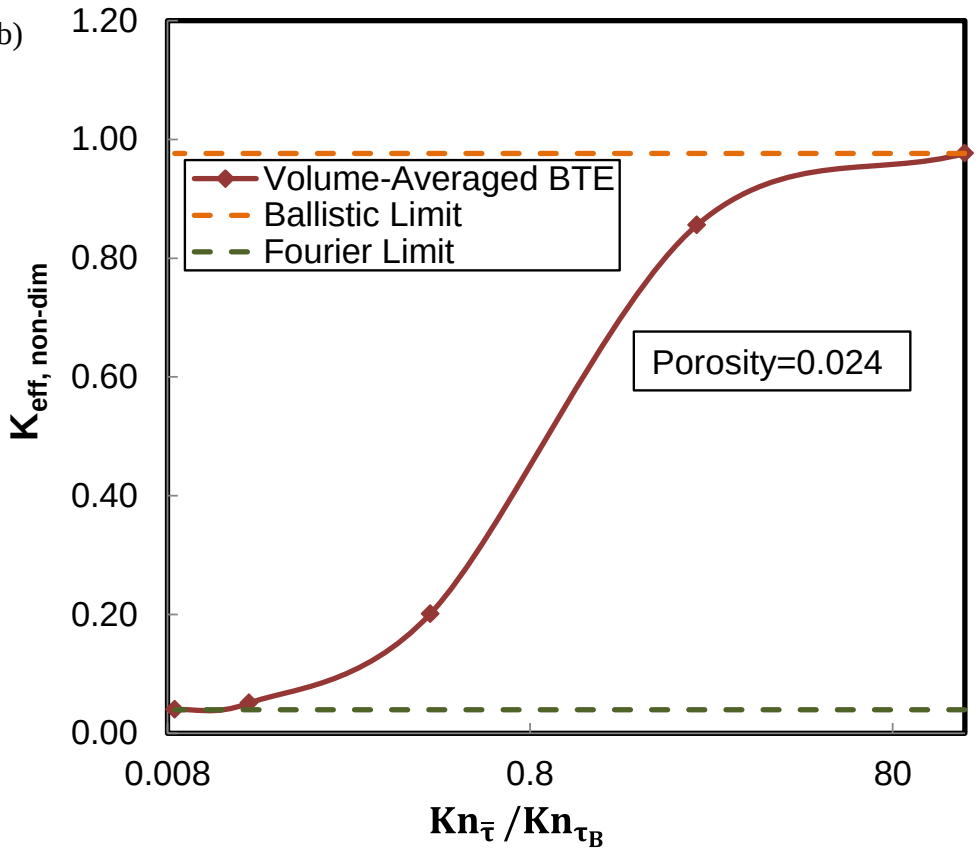

Figure 54: Continued on next page

(c)

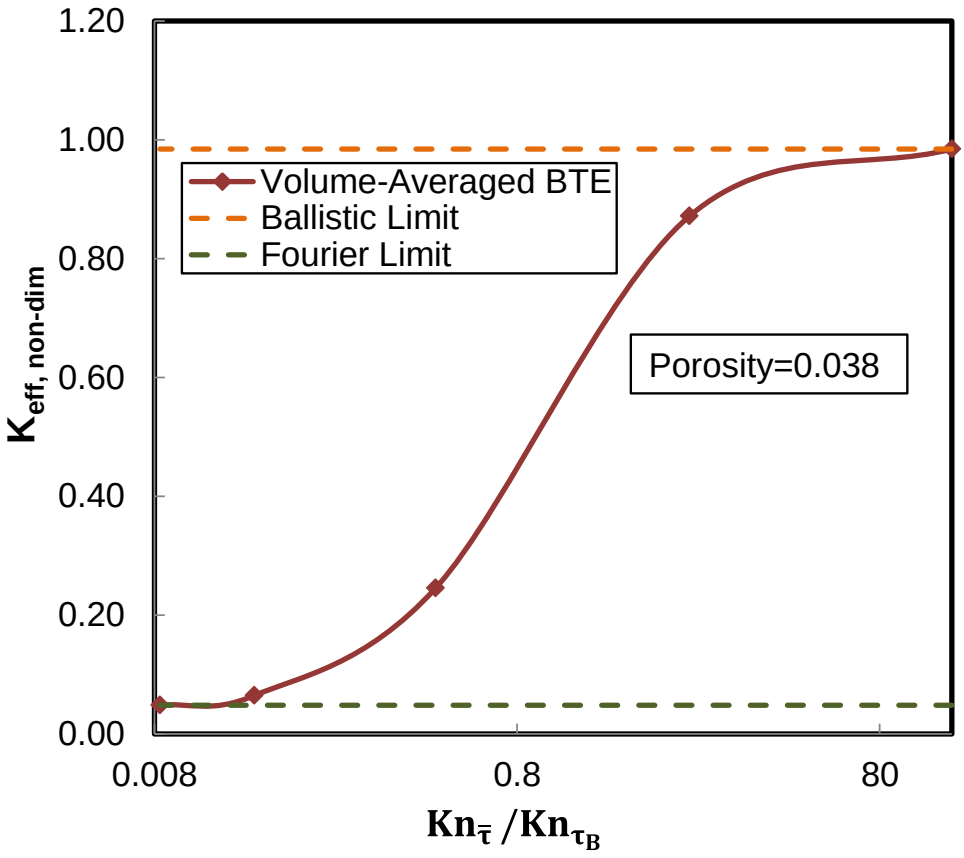

Figure 54: Continued on next page

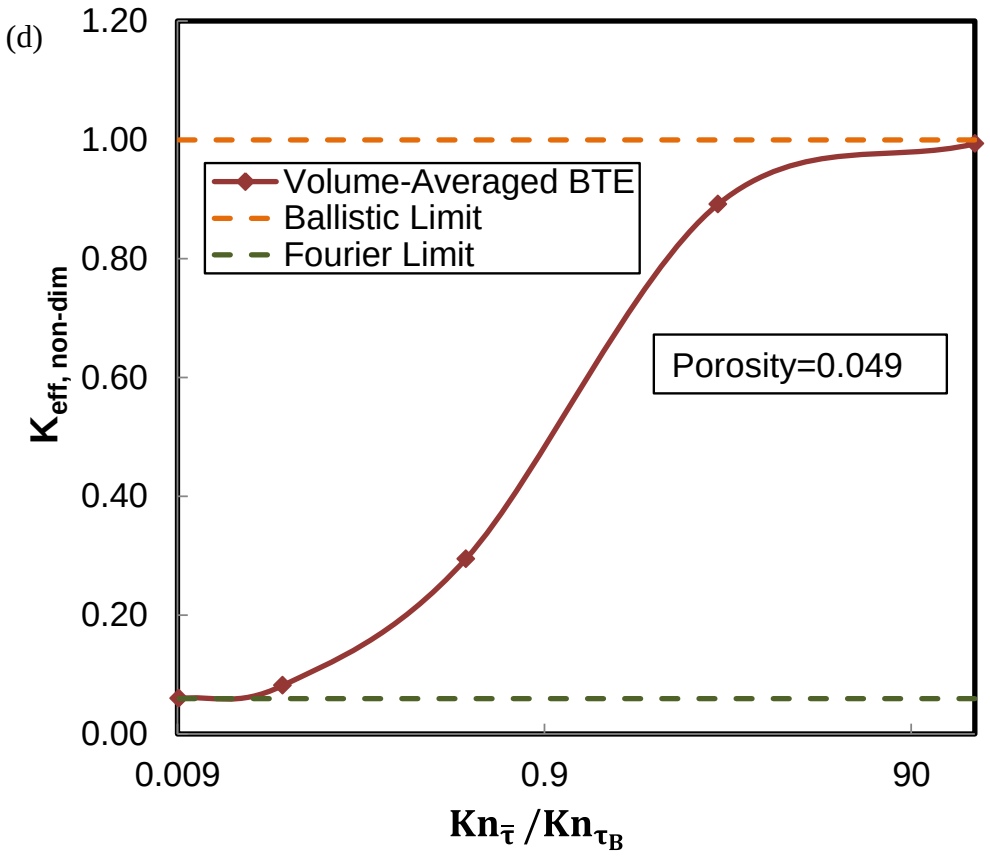

Figure 54: Volume-Averaged BTE model for a two material composite for varying Knudsen number for periodic domain with a spherical particle (a) $\phi = 0.06$ (b) $\phi = 0.024$ (c) $\phi = 0.038$ (d) $\phi = 0.049$

6.5 CLOSURE

In this chapter we presented the verification, validation and results for the different volume-averaged BTE model developed in previous chapters. We considered the gray model for nanoporous silicon geometries with two different inclusion shapes. We computed the effective thermal conductivity of the porous medium for a range of Knudsen numbers for varying porosities. The gray nanoporous volume averaged BTE model predicted the DNS benchmark thermal conductivity solution to within a maximum

error of 14%. For the gray model, we compared the heat rate contributions of different K-space points in the Brillouin zone with the DNS solution, and good agreement was obtained. In the non-gray model, we considered realistic phonon dispersions and geometries for our simulations. We considered two different approaches to calibrate the interface scattering relaxation time. The constant interface scattering term approach yielded better overall thermal conductivity predictions within 11.9% but the contributions of individual phonon modes was not captured accurately. The multiple interface scattering relaxation time approach yielded better comparison with the individual phonon mode heat rate contributions but overall thermal conductivity was under predicted by 26%. The volume-averaged BTE model in the two-material composite was demonstrated for a silicon host with germanium spherical particles. Solutions were presented for varying porosities and Knudsen numbers.

Chapter 7: Summary and Future Work

7.1 SUMMARY

In this chapter we summarize the main contributions of the dissertation and discuss future directions for this research. The semi-classical phonon Boltzmann Transport equation (BTE) is proven to be an effective predictive tool for nanocomposites due to its ability to describe the quasi-particle nature of the phonons at length scales comparable to phonon mean free path [6]. Due to its computational expense, the direct numerical simulations of the BTE can be limiting for complex nanocomposite domains. In this work, we have developed for the first time volume-averaged models for the phonon BTE to simulate heat transfer in nanocomposites. These models can be used in arbitrary geometries, accounting for both bulk scattering and boundary scattering effects across the range of Knudsen numbers. The model is demonstrated for gray and non-gray approximations in nanoporous composites in the geometric scattering limit. For two-material composites we solve the model in the Mie scattering limit for composites with small nanoparticulate inclusions. Significant speed ups are achieved over direct numerical simulation (DNS) by using the volume-averaged BTE models. The major contributions of this work are summarized below.

7.1.1 Volume-Averaging for Gray Phonon Boltzmann Transport Equation (BTE) in Nanoporous Materials

We developed a volume-averaged formulation for nanoporous domains by formally averaging the phonon BTE over a representative elemental volume (REV) of a

nanoporous material. We modeled the additional terms resulting from the volume-averaging as in-scattering and out-scattering terms. The in-scattering term is written as a function of a scattering phase function, $\Phi_{\mathbf{KK'}}$, and a new parameter, τ_B. This new parameter τ_B is interface scattering relaxation time and captures the scattering effects due to the presence of inclusions in the domain. Both τ_B and $\Phi_{\mathbf{KK'}}$ are functions of the interface geometry and the phonon wave vector space. We developed a generalized ray tracing algorithm to compute the phase function in the geometric scattering limit, analogous to that used in radiative transport [63] [64]. We further take in to consideration the effects of pores on the effective thermal conductivity of the composite by calibrating the volume-averaged bulk scattering relaxation time, $\overline{\tau}$ using a Fourier limit solution of the nanoporous domain.

We write the volume-averaged BTE in terms of the intrinsic average of the phonon energy density over the solid volume of the composite. The model parameter $\tau_B$is calibrated using a direct numerical solution of the phonon BTE at the ballistic limit. For domain sizes satisfying $Kn = (\frac{v_g \tau_B}{L}) \ll 1$ in the gray, isotropic limit, the interface scattering relaxation time can be predicted using equation (29) and the effective thermal conductivity obtained from the ballistic limit solution of the phonon BTE.

We solve the volume-averaged BTE for a nanoporous domain under the gray approximation using a finite volume method. We employ the MEMOSA framework and the COMET algorithm to promote convergence. We implemented a periodic boundary condition to model transport through a composite consisting of regularly repeating units.

We solve for two types of nanopores: spherical and cylindrical. We demonstrate that the model predicts effective thermal conductivity well by comparing with a benchmark direct numerical solution of the BTE for the full range of Knudsen numbers. We further compare the contributions of the discrete K points for DNS and volume-averaged BTE models. The average relative error in effective thermal conductivity prediction of the volume-averaged BTE with respect to the DNS is 3.25% for spherical inclusions and the maximum relative error is 10.2%. We conduct the study over varying range of porosities for cylindrical inclusions and observe an average relative error of 5% and a maximum relative error of 14% accounting the full range of Knudsen numbers. The accuracy of the model is higher closer to the Fourier and ballistic limits, as expected.

For cylindrical inclusions, the gray volume-averaged BTE model requires 16 times less CPU time than the DNS computation at a Knudsen number of 0.17. This is due to the high physical mesh requirement by the DNS for the actual REV geometry. The advantage of volume-averaging is in solving a effectively 1-D problem in a homogenized domain versus the full detailed 3-D problem in a DNS.

7.1.2 Non-Gray Volume-Averaged Theory for Phonon Boltzmann Transport Equation (BTE) in Nanoporous Materials

We implemented a non-gray version of the volume-averaged BTE model for nanoporous composites. We considered realistic non-gray phonon dispersions in silicon. The non-gray BTE when discretized in the **K**-space yield a large number of phonon BTEs to be solved, one for each discrete K point. We determine the interface scattering relaxation time parameter in this model using two different approaches. In the first

method, a constant value of τ_B is calibrated to match the DNS in the ballistic limit. In the second approach, a number of boundary scattering relaxation times $\tau_{B,k}$ s corresponding to the Brillouin zone discretization are determined, along with a number of bulk relaxation times, $\overline{\tau_k}$. The non-gray BTEs are coupled using the conservation of energy equation. Therefore, we use a Newton Raphson method to calibrate the $'k'$ number of unknown $\tau_{B,k}$s. The scattering phase function matrix is extended to the non-gray model assuming elastic scattering. The model is solved for varying porosities of nanoporous silicon film with cylindrical inclusions.

The constant interface scattering relaxation time approach predicts effective thermal conductivity within 12% accuracy of the corresponding benchmark DNS. However, the contribution of individual phonon modes was not captured accurately in this approach. The second approach with multiple values interface scattering relaxation time, $\tau_{B,k}$ underpredicted effective thermal conductivity by 26% compared to the DNS solution. Although underpredicting significantly, this method resulted in better comparison in the form of the heat rates contributions of individual phonon modes. This reduced order model needs to be further improved to predict the DNS solution more accurately.

7.1.3 Volume-Averaged Theory for BTE in Nanocomposite Domain

We extended the volume-averaged model for nanoporous domains for gray phonon dispersions to two-material composites. We consider nanocomposite domains with particles of a second material embedded in a matrix. The scattering due to the

particle presence is modeled using a scattering term similar to the nanoporous domains employing a scattering phase function. We determined the scattering phase function for particle sizes comparable to the phonon wavelength using the Mie scattering theory for transverse phonons [66, 72]. The volume averaged bulk relaxation times and interface scattering relaxation times were determined using the established calibration procedure.

The volume-averaged BTE model for the domain was discretized using a finite volume approach using COMET algorithm. We compute the effective thermal conductivity for the two-material nanocomposite domain for a range Knudsen numbers for different particle volume fractions in the domain.

7.2 Future Work

We can build upon the volume-averaging theory for BTE developed in this dissertation to explore different problems as well as improve upon the current machinery.

7.2.1 Parallelization of Volume-Averaged BTE and DNS for Periodic Boundaries

The present software to apply periodic boundary conditions necessary to simulate periodic nanocomposites is currently only available on single processor platforms. A significant computational advantage can be attained if the software were parallelized. Although the volume-averaging approach involves reduced mesh sizes, the solution of the fully resolved BTE is a computationally intensive process. This is especially so when non-gray transport is considered.

7.2.2 Geometric Scattering for Two-Material Model Including Non-Gray Effects

The volume-averaged BTE for two-material composites is general and can be extended to include non-gray effects. The model for scattering considered in this thesis was Mie scattering, valid when the particle inclusions are comparable in length scale to the wavelength of phonons. An obvious extension is to consider the geometric scattering limit, where ray-tracing approaches can be employed. Such a ray tracing model would account for interface reflectivity and transmissivity by employing models such as the diffuse mismatch model (DMM). This will allow for comparison of the two-material volume-averaged BTE composite model with the direct numerical solution of the composite.

7.2.3 Mie and Rayleigh Scattering for Two-Material Model Including Non-Gray Effects

The generalized volume-averaged BTE for two-material composites can be extended to include non-gray effects in Mie and Rayleigh scattering limits. Using the analytical scattering phase functions for longitudinal and transverse phonon modes in this limit [65, 66, 101], a scattering phase function matrix can be generated to include these phonon modes. The available theory considers independent scattering. This will allow inclusion of non-gray dispersions in a two-material composite. Although, this model will be limited by absence of benchmark solutions, experiments using equivalent nanocomposite geometries can be used for validation.

7.2.4 Generalization of Calibrated Parameters

An important area to explore will be to develop calibration curves for the different model parameters for standard inclusion shapes. This will require benchmarking with the DNS solutions for the specific shapes, which will be a significant but achievable undertaking. This will allow the volume-averaged BTE model to be readily usable as a reduced order model for predicting effective thermal properties in composites.

7.2.5 Two BTE System for Two-Material Composite

In the presence of significant thermal disequilibrium between the two materials in the composite, it may be necessary to carry two different volume averaged BTEs for the two materials in a homogenized domain. They will be coupled through the interface condition using a diffuse mismatch model. Thus:

BTE for Material 1: $\left(\nabla \cdot \mathbf{v}e" = \frac{e_0 - e"}{\tau}\right)_1$ (94)

BTE for Material 2: $\left(\nabla \cdot \mathbf{v}e" = \frac{e_0 - e"}{\tau}\right)_2$ (95)

We have the following model equation for a nanoporous domain:

$$\alpha \nabla \cdot \mathbf{v}\langle e_k" \rangle = \alpha \frac{\langle e_0 \rangle - \langle e_k" \rangle}{\overline{\tau_k}} - \frac{\langle e_k" \rangle}{\tau_{B,k}} + \frac{1}{V_{BZ}} \frac{1}{\tau_{B,k}} \int_{\mathbf{K}'} \Phi_{kk'} \langle e_{k'}" \rangle d^3\mathbf{K}' \quad (96)$$

The transmission of energy between the two materials is represented through a transmission term, as shown below:

Material 1:

$$\alpha \nabla \cdot \mathbf{v_1}\langle e_k" \rangle_1 = \alpha \frac{\langle e_0 \rangle_1 - \langle e_k" \rangle_1}{\overline{\tau_{k,1}}} - \frac{\langle e_k" \rangle_1}{\tau_{B,k,1}} + \frac{1}{V_{BZ,1}} \frac{1}{\tau_{B,k,1}} \int_{\mathbf{K}'} \Phi_{kk'} \langle e_{k'}" \rangle_1 d^3\mathbf{K}' + \tau_{12}[\langle e_0 \rangle_1 - \langle e_0 \rangle_2] \quad (97)$$

Material 2:

$$\alpha\nabla\cdot\mathbf{v_2}\langle e_k{''}\rangle_2 = \alpha\frac{\langle e_0\rangle_2-\langle e_k{''}\rangle_2}{\overline{\tau_{k,2}}}-\frac{\langle e_k{''}\rangle_1}{\tau_{B,k,2}}+\frac{1}{V_{BZ,2}}\frac{1}{\tau_{B,k,2}}\int_{\mathbf{K}'}\Phi_{kk'}\langle e_{k'}{''}\rangle_2 d^3\mathbf{K}'+\tau_{21}[\langle e_0\rangle_2-\langle e_0\rangle_1] \quad (98)$$

7.2.6 Generalized Volume-Averaged BTE for Complex Composite Domains

A more generalized volume-averaged BTE model with more than two types of composite materials can be explored. Scattering phase functions involving multiple materials and geometries can be computed, while considering the mismatch in the phonon dispersions between the different composite materials. This will put the burden on the scattering phase function calculation. Models for anisotropic conduction for inclusions with pronounced asymmetries are another area of interest. Once resolved, these approaches can be valuable in predictive modeling of the thermal properties in interesting nanostructured geometries.

References

1. Lu, W. and C.M. Lieber, *Nanoelectronics from the bottom up.* Nature Materials, 2007. **6**(11): p. 841-850.

2. Joshi, G., Lee, H., Lan, Y. C., Wang, X. W., Zhu, G. H., Wang, D. Z., Gould, R. W., Cuff, D. C., Tang, M. Y., Dresselhaus, M. S., Chen, G., Ren, Z. F., *Enhanced Thermoelectric Figure-of-Merit in Nanostructured p-type Silicon Germanium Bulk Alloys.* Nano Letters, 2008. **8**(12): p. 4670-4674.

3. Dresselhaus, M.S., Chen, G., Ren, Z. F., Fleurial, J. P., Gogna, P., Tang, M. Y., Vashaee, D., Lee, H., Wang, X. W., Joshi, G., Zhu, G. H., Wang, D. Z., Blair, R., Bux, S., Kaner, R., *Nanocomposites to enhance ZT in thermoelectrics*, in *Thermoelectric Power Generation*, T.P. Hogan, *et al*., Editors. 2008. p. 29-41.

4. Poudel, B., Hao, Q., Ma, Y., Lan, Y. C. Minnich, A., Yu, B., Yan, X. A., Wang, D. Z., Muto, A., Vashaee, D., Chen, X. Y., Liu, J. M., Dresselhaus, M. S., Chen, G., Ren, Z. F., *High-thermoelectric performance of nanostructured bismuth antimony telluride bulk alloys.* Science, 2008. **320**(5876): p. 634-638.

5. Ziman, J.M., *Electrons and phonons: The theory of transport phenomena in solids*. 1960, New York: Oxford Univerity Press, Inc.

6. Chen, G., *Nanoscale Energy Transport and Conversion : A Parallel Treatment of Electrons, Molecules, Phonons, and Photons*. 2005: Oxford University Press. 560.

7. Matthiessen, A., Rep. Brit. Ass., 32, 1862**.** 144**.**

8. Swartz, E.T. and R.O. Pohl, *Thermal-Resistance At Interfaces.* Applied Physics Letters, 1987. **51**(26): p. 2200-2202.

9. Hashin, Z., *Assessment Of Self Consistent Scheme Approximation - Conductivity Of Particulate Composites.* Journal of Composite Materials, 1968. **2**(3): p. 284-&.

10. Singh, D., *Frequency And Polarization Resolved Phonon Transport In Carbon And Silicon Nanostructures*. 2011, Purdue University.

11. Kurti, N., B.V. Rollin, and F. Simon, *Preliminary experiments on temperature equilibria at very low temperatures.* Physica, 1936. **3**: p. 266-274.

12. Kapitza, P.L., *The study of heat transfer in helium II.* Journal of Physics-Ussr, 1941. **4**(1-6): p. 181-210.

13. Khalatni.Im and I.N. Adamenko, *Theory Of Kapitza Temperature Discontinuity At A Solid Body Liquid Helium Boundary.* Zhurnal Eksperimentalnoi I Teoreticheskoi Fiziki, 1972. **63**(3): p. 745-752.

14. Little, W.A., *The Transport Of Heat Between Dissimilar Solids At Low Temperatures.* Canadian Journal of Physics, 1959. **37**(3): p. 334-349.

15. Schelling, P.K., S.R. Phillpot, and P. Keblinski, *Phonon wave-packet dynamics at semiconductor interfaces by molecular-dynamics simulation.* Applied Physics Letters, 2002. **80**(14): p. 2484-2486.

16. Costescu, R.M., M.A. Wall, and D.G. Cahill, *Thermal conductance of epitaxial interfaces.* Physical Review B, 2003. **67**(5).

17. Hopkins, P.E., P.M. Norris, and R.J. Stevens, *Influence of inelastic scattering at metal-dielectric interfaces.* Journal of Heat Transfer-Transactions of the Asme, 2008. **130**(2).

18. Stevens, R.J., A.N. Smith, and P.M. Norris, *Measurement of thermal boundary conductance of a series of metal-dielectric interfaces by the transient thermoreflectance technique.* Journal of Heat Transfer-Transactions of the Asme, 2005. **127**(3): p. 315-322.

19. Stoner, R.J. and H.J. Maris, *Kapitza Conductance And Heat-Flow Between Solids At Temperatures From 50 To 300 K.* Physical Review B, 1993. **48**(22): p. 16373-16387.

20. Mingo, N. and L. Yang, *Phonon transport in nanowires coated with an amorphous material: An atomistic Green's function approach.* Physical Review B, 2003. **68**(24).

21. Zhang, W., T.S. Fisher, and N. Mingo, *Simulation of interfacial phonon transport in Si-Ge heterostructures using an atomistic Green's function method.* Journal of Heat Transfer-Transactions of the Asme, 2007. **129**(4): p. 483-491.

22. Zhang, W., T.S. Fisher, and N. Mingo, *The atomistic Green's function method: An efficient simulation approach for nanoscale phonon transport.* Numerical Heat Transfer Part B-Fundamentals, 2007. **51**(4): p. 333-349.

23. Tian, Z.T., K. Esfarjani, and G. Chen, *Enhancing phonon transmission across a Si/Ge interface by atomic roughness: First-principles study with the Green's function method.* Physical Review B, 2012. **86**(23).

24. Li, X.B. and R.G. Yang, *Size-dependent phonon transmission across dissimilar material interfaces.* Journal of Physics-Condensed Matter, 2012. **24**(15).

25. Jeong, C., S. Datta, and M. Lundstrom, *Full dispersion versus Debye model evaluation of lattice thermal conductivity with a Landauer approach.* Journal of Applied Physics, 2011. **109**(7).

26. Miao, K., Sadasivam, S., Charles, J., Klimeck, G., Fisher, T. S., Kubis, T., *Buttiker probes for dissipative phonon quantum transport in semiconductor nanostructures.* Applied Physics Letters, 2016. **108**(11).

27. Milton, G.W., *The Theory of Composites* 2002: Cambridge University Press, New York.

28. Maxwell-Garnett, J.C., *Colours in metal glasses and in metallic films.* Philosophical Transactions of the Royal Society of London, Series A, Containing Papers of a Mathematical or Physical Character, 1904. **203**: p. 385-420.

29. Hasselman, D.P.H. and L.F. Johnson, *Effective Thermal-Conductivity Of Composites With Interfacial Thermal Barrier Resistance.* Journal of Composite Materials, 1987. **21**(6): p. 508-515.

30. Benveniste, Y. and T. Miloh, *On The Effective Thermal-Conductivity Of Coated Short-Fiber Composites.* Journal of Applied Physics, 1991. **69**(3): p. 1337-1344.

31. Every, A.G., Tzou, Y., Hasselman, D. P. H., Raj, R., *The Effect Of Particle-Size On The Thermal-Conductivity Of Zns Diamond Composites.* Acta Metallurgica Et Materialia, 1992. **40**(1): p. 123-129.

32. Nan, C.W., Birringer, R., Clarke, D. R., Gleiter, H., *Effective thermal conductivity of particulate composites with interfacial thermal resistance.* Journal of Applied Physics, 1997. **81**(10): p. 6692-6699.

33. Minnich, A. and G. Chen, *Modified effective medium formulation for the thermal conductivity of nanocomposites.* Applied Physics Letters, 2007. **91**(7).

34. Bazant, M.Z., E. Kaxiras, and J.F. Justo, *Environment-dependent interatomic potential for bulk silicon.* Physical Review B, 1997. **56**(14): p. 8542-8552.

35. Rossky, P.J., *Perspective on "Correlations in the motion of atoms in liquid argon" - Rahman A (1964) Phys Rev 136 : 405.* Theoretical Chemistry Accounts, 2000. **103**(3-4): p. 263-264.

36. Tersoff, J., *New Empirical-Approach For The Structure And Energy Of Covalent Systems.* Physical Review B, 1988. **37**(12): p. 6991-7000.

37. Stillinger, F.H. and T.A. Weber, *Computer-Simulation Of Local Order In Condensed Phases Of Silicon.* Physical Review B, 1985. **31**(8): p. 5262-5271.

38. Gonze, X. and C. Lee, *Dynamical matrices, born effective charges, dielectric permittivity tensors, and interatomic force constants from density-functional perturbation theory.* Physical Review B, 1997. **55**(16): p. 10355-10368.

39. Zhong, Z.R., X.W. Wang, and J. Xu, *Equilibrium molecular dynamics study of phonon thermal transport in nanomaterials.* Numerical Heat Transfer Part B-Fundamentals, 2004. **46**(5): p. 429-446.

40. MullerPlathe, F., *A simple nonequilibrium molecular dynamics method for calculating the thermal conductivity.* Journal of Chemical Physics, 1997. **106**(14): p. 6082-6085.

41. Schelling, P.K., S.R. Phillpot, and P. Keblinski, *Comparison of atomic-level simulation methods for computing thermal conductivity.* Physical Review B, 2002. **65**.

42. E. E. Lewis, W.F.M., *Computational methods of neutron transport*. 1984, United States: John Wiley and Sons, Inc.

43. Narumanchi, S.V.J., J.Y. Murthy, and C.H. Amon, *Submicron heat transport model in silicon accounting for phonon dispersion and polarization.* Journal of Heat Transfer-Transactions of the Asme, 2004. **126**: p. 946-955.

44. Murthy, J.Y. and S.R. Mathur, *Computation of sub-micron thermal transport using an unstructured finite volume method.* Journal of Heat Transfer-Transactions of the Asme, 2002. **124**: p. 1176-1181.

45. Murthy, J.Y. and S.R. Mathur, *An improved computational procedure for sub-micron heat conduction.* Journal of Heat Transfer-Transactions of the Asme, 2003. **125**(5): p. 904-910.

46. Narumanchi, S.V.J., J.Y. Murthy, and C.H. Amon, *Comparison of different phonon transport models for predicting heat conduction in silicon-on-insulator transistors.* Journal of Heat Transfer-Transactions of the Asme, 2005. **127**: p. 713-723.

47. Narumanchi, S.V.J., J.Y. Murthy, and C.H. Amon, *Boltzmann transport equation-based thermal modeling approaches for hotspots in microelectronics.* Heat and Mass Transfer, 2006. **42**(6): p. 478-491.

48. Chen, G., *Size and interface effects on thermal conductivity of superlattices and periodic thin-film structures.* Journal of Heat Transfer-Transactions of the Asme, 1997. **119**: p. 220-229.

49. Yang, R.G. and G. Chen, *Thermal conductivity modeling of periodic two-dimensional nanocomposites.* Physical Review B, 2004. **69**.

50. Jeng, M.S., Yang, R. G., Song, D., Chen, G., *Modeling the thermal conductivity and phonon transport in nanoparticle composites using Monte Carlo simulation.* Journal of Heat Transfer-Transactions of the Asme, 2008. **130**.

51. Tian, W.X. and R.G. Yang, *Thermal conductivity modeling of compacted nanowire composites.* Journal of Applied Physics, 2007. **101**.

52. Hsieh, T.Y. and J.Y. Yang, *Thermal conductivity modeling of circular-wire nanocomposites.* Journal of Applied Physics, 2010. **108**.

53. Singh, D., J.Y. Murthy, and T.S. Fisher, *Effect of Phonon Dispersion on Thermal Conduction Across Si/Ge Interfaces.* Journal of Heat Transfer-Transactions of the Asme, 2011. **133**.

54. Loy, J.M., *An Efficient Solution Procedure for Simulating Phonon Transport in Multiscale Multimaterial Systems*. 2013, The University of Texas at Austin.

55. Prasher, R., *Generalized equation of phonon radiative transport.* Applied Physics Letters, 2003. **83**(1): p. 48-50.

56. Travkin, V.S. and A.T. Ponomarenko, *Electrodynamic equations for heterogeneous media and structures on the length scales of their constituents.* Inorganic Materials, 2004. **40**: p. S128-S144.

57. Consalvi, J.L., B. Porterie, and J.C. Loraud, *A formal averaging procedure for radiation heat transfer in particulate media.* International Journal of Heat and Mass Transfer, 2002. **45**(13): p. 2755-2768.

58. Singh, B.P. and M. Kaviany, *Independent Theory Versus Direct Simulation Of Radiation Heat-Transfer In Packed-Beds.* International Journal of Heat and Mass Transfer, 1991. **34**(11): p. 2869-2882.

59. Singh, B.P. and M. Kaviany, *Modeling Radiative Heat-Transfer In Packed-Beds.* International Journal of Heat and Mass Transfer, 1992. **35**(6): p. 1397-1405.

60. Singh, B.P. and M. Kaviany, *Effect Of Solid Conductivity On Radiative Heat-Transfer In Packed-Beds.* International Journal of Heat and Mass Transfer, 1994. **37**(16): p. 2579-2583.

61. Quintard, M., M. Kaviany, and S. Whitaker, *Two-medium treatment of heat transfer in porous media: Numerical results for effective properties.* Advances in Water Resources, 1997. **20**(2-3): p. 77-94.

62. Moyne, C., *Two-equation model for a diffusive process in porous media using the volume averaging method with an unsteady-state closure.* Advances in Water Resources, 1997. **20**: p. 63-76.

63. Modest, M.F., *Radiative Heat Transfer*. 1993, New York, NY.

64. Glassner, A.S., *An Introduction to ray tracing*. 1989, San Francisco, CA: Morgan Kaufmann Publishers, Inc.

65. Prasher, R., *Transverse thermal conductivity of porous materials made from aligned nano- and microcylindrical pores.* Journal of Applied Physics, 2006. **100**.

66. Prasher, R.S., *Mie scattering theory for phonon transport in particulate media.* Journal of Heat Transfer-Transactions of the Asme, 2004. **126**(5): p. 793-804.

67. Song, D. and G. Chen, *Thermal conductivity of periodic microporous silicon films*. Applied Physics Letters, 2004. **84**(5): p. 687-689.

68. Dresselhaus, M., Chen, Gang, Tang, M. Y., Yang, R. G., Lee, H., Wang, D.Z., Ren, Z. F., Fleurial, J. P., Gogna, P., *New directions for nanoscale thermoelectric materials research*. in *MRS Proceedings*. 2005. Cambridge Univ Press.

69. *https://memshub.org/infrastructure/memosa*.

70. Loy J. M., Mathur S.R., and Murthy J. Y.,, *A Coupled Ordinates Method for the Convergence Acceleration of the Phonon Boltzmann Transport Equation.* J. Heat Transfer, 2013. **137**(1): p. 012402.

71. I. El-Kady, R.H.O.I., P. E. Hopkins, Z. C. Leseman, D. F. Goettler, B. Kim, C. M. Reinke, and M. F. Su, *Phonon Manipulation with Phononic Crystals*, P.r. SAND2012-0127, Editor. 2012: Sandia National Laboratories, California, CA.

72. Hulst, H.C.v.d., *Light Scattering by Small Particles*. 1981, New York: Dover Publications, Inc.

73. Hopkins, P.E., Reinke, C. M., Su, M. F., Olsson, R. H., Shaner, E. A., Leseman, Z. C., Serrano, J. R., Phinney, L. M., El-Kady, I., *Reduction in the Thermal Conductivity of Single Crystalline Silicon by Phononic Crystal Patterning.* Nano Letters, 2011. **11**(1): p. 107-112.

74. Kittel, C., *Introduction to Solid State Physics*. 1996, New York, NY: Wiley.

75. Pascual-Gutierrez, J.A., J.Y. Murthy, and R. Viskanta, *Thermal conductivity and phonon transport properties of silicon using perturbation theory and the environment-dependent interatomic potential.* Journal of Applied Physics, 2009. **106**.

76. Holland, M.G., *Analysis Of Lattice Thermal Conductivity.* Physical Review, 1963. **132**: p. 2461-&.

77. Thomas, J.A., Turney, J. E., Iutzi, R. M., Amon, C. H., McGaughey, A. J. H., *Predicting phonon dispersion relations and lifetimes from the spectral energy density.* Physical Review B, 2010. **81**(8).

78. Slattery, J.C., *Momentum, Energy, and Mass Transfer in Continua*. 1981, Huntington, N.Y: Robert Krieger Publishing.

79. DeVidts, P. and R.E. White, *Governing equations for transport in porous electrodes.* Journal of the Electrochemical Society, 1997. **144**: p. 1343-1353.

80. Vadakkepatt, A., Trembacki, Bradley, Mathur, Sanjay R., Murthy, Jayathi Y., *Bruggeman's Exponents for Effective Thermal Conductivity of Lithium-Ion Battery Electrodes.* Journal of the Electrochemical Society, 2016. **163**(2): p. A119-A130.

81. Doyle, M., T.F. Fuller, and J. Newman, *Modeling Of Galvanostatic Charge And Discharge Of The Lithium Polymer Insertion Cell.* Journal of the Electrochemical Society, 1993. **140**(6): p. 1526-1533.

82. Newman, J. and W. Tiedemann, *Porous-Electrode Theory With Battery Applications.* Aiche Journal, 1975. **21**(1): p. 25-41.

83. Bruggeman, V.D., *Berechnung verschiedener physikalischer konstanten von heterogenen substanzen. i. dielektrizit¨atskonstanten und leitf¨ahigkeiten der mischkorper aus isotropen substanzen.* Annalen der Physik, 1935. **416**(7): p. 636.

84. Chen, Z.G., Han, Guang, Yang, Lei, Cheng, Lina, Zou, Jin, *Nanostructured thermoelectric materials: Current research and future challenge*. Progress in Natural Science: Materials International, 2012. **22**(6): p. 535-549.

85. Morelli, D.T., Caillat, T., Fleurial, J. P., Borshchevsky, A., Vandersande, J., Chen, B., Uher, C., *Low-temperature transport properties of p-type CoSb3.* Physical Review B, 1995. **51**(15): p. 9622-9628.

86. Hsu, K.F., Loo, S., Guo, F., Chen, W., Dyck, J. S., Uher, C., Hogan, T., Polychroniadis, E. K., Kanatzidis, M. G., *Cubic AgPbmSbTe2+m: Bulk thermoelectric materials with high figure of merit.* Science, 2004. **303**(5659): p. 818-821.

87. Weathers, A., Shi, L., *Thermal transport measurement techniques for nanowires and nanotubes.* Annual Review of Heat Transfer, 2013. **16**: p. 101-134.

88. Henry, A.S. and G. Chen, *Spectral phonon transport properties of silicon based on molecular dynamics Simulations and lattice dynamics.* Journal of Computational and Theoretical Nanoscience, 2008. **5**(2): p. 141-152.

89. Auld, B.A., *Acoustic Fields and Waves in Solids*. Vol. 1. John Wiley & Sons.

90. Thornton, J.B.M.a.S.T., *Classical Dynamics of Particles and Systems*. 1995: Harcourt Brace.

91. Chai, J.C., H.S. Lee, and S.V. Patankar, *Finite-Volume Method For Radiation Heat-Transfer.* Journal of Thermophysics and Heat Transfer, 1994. **8**: p. 419-425.

92. Patankar, S.V., *Numerical Heat Transfer and Fluid Flow*. 1980, New York, NY: Taylor & Francis.

93. Livne, A.B.a.O.E., *Multigrid Techniques*. 2011, Philadelphia, PA.: SIAM.

94. Mathur, S.R. and J.Y. Murthy, *Coupled ordinates method for multigrid acceleration of radiation calculations.* Journal of Thermophysics and Heat Transfer, 1999. **13**: p. 467-473.

95. Heaslet, M.A. and R.F. Warming, *Radiative transport and wall temperature slip in an absorbing planar medium.* International Journal of Heat and Mass Transfer, 1965. **8**(7): p. 979-994.

96. *https://cubit.sandia.gov/.*

97. Jain, A., Y.J. Yu, and A.J.H. McGaughey, *Phonon transport in periodic silicon nanoporous films with feature sizes greater than 100 nm.* Physical Review B, 2013. **87**(19).

98. Born, M., and Huang, K., *Dynamical theory of crystal lattices*. 1954: Clarendon Press, Oxford.

99. de Gironcoli, S., *Phonons in Si-Ge systems: An ab initio interatomic-force-constant approach.* Physical Review B, 1992. **46**(4): p. 2412-2419.

100. Mingo, N., Yang, L., Li, D., Majumdar, A., *Predicting the thermal conductivity of Si and Ge nanowires.* Nano Letters, 2003. **3**(12): p. 1713-1716.

101. Prasher, R.S., *Thermal transport cross section and phase function of longitudinal phonons for scattering by nanoparticles and microparticles.* Journal of Applied Physics, 2004. **96**(9): p. 5202-5211.

Vita

Columbia is from Malda, India, and received her B.S. in Mechanical Engineering in 2006 from Jadavpur University, Kolkata, India, in 2006. She received her M.S. in Mechanical Engineering from Texas Tech University in 2008. Prior to joining the graduate program at The University of Texas at Austin, Columbia worked as an Analyst at Stress Engineering Services, Inc., in Houston, Texas. During graduate school she worked as intern at Apple, Inc., Cupertino, California. Columbia is the author of four peer-reviewed journal articles and three conference publications. Columbia is a recipient of the competitive 2014 Qualcomm Innovation Challenge Fellowship. She is a recipient of the Bruce J. Heim Foundation scholarship from American Society of Mechanical Engineers and Warren A. and Alice L. Meyer Endowed Scholarship in engineering from Cockrell School of Engineering. During her tenure as a graduate student, Columbia held several leadership roles on campus and served as president of the Graduate Engineering Council and the Graduate Student Assembly. She was awarded the Cockrell School of Engineering Student Leadership Award for her services to the graduate student community. Columbia will be joining the Research & Development team at Intel Corporation in Hillsboro, Oregon, upon graduation.

Permanent Email: columbia.mishra@gmail.com

This dissertation was typed by the author